The Slovak Biophysical Society

VIth. Slovak Biophysical Symposium

Program and Abstracts

Comenius University in Bratislava
Jessenius faculty of Medicine in Martin
11. – 13. 3. 2014

ISBN 978-80-89544-67-7

Scientific committee:

Prof. MUDr. Ján Jakuš, DrSc. (JLF UK Martin)
Prof. RNDr. Tibor Hianik, DrSc. (FMFI UK Bratislava)
Prof. RNDr. Pavol Miškovský, DrSc. (PF UPJŠ Košice)
RNDr. Karol Ondriaš, DrSc. (UMFG SAV, Bratislava)
Ing. Alexandra Zahradníková, DrSc. (UMFG SAV, Bratislava)
Doc. RNDr. Iveta Waczulíková, PhD. (FMFI UK Bratislava)
RNDr. Ivan Zahradník, CSc. (UMFG SAV, Bratislava)
RNDr. Dušan Chorvát, PhD. (ILC Bratislava)
Doc. RNDr. Ivan Poliaček, PhD. (JLF UK Martin)
Doc. RNDr. Martin Kopáni, PhD. (LF UK Bratislava)

Organizing committee:

Prof. MUDr. Ján Jakuš, DrSc. – predseda
RNDr. Michal Šimera, PhD. – zástupca
Doc. RNDr. Ivan Poliaček, PhD.
Mgr. NadeždaVišňovcová, PhD.
Ing. Marcel Veterník
Ing. Peter Macháč
Ing. Monika Somorová
Iveta Najšlová

Editors:

Doc. RNDr. Ivan Polaček, PhD
RNDr. Michal Šimera, PhD
Ing. Marcel Veterník
Ing. Peter Macháč
Prof. MUDr. Ján Jakuš, DrSc

”This abstracts book was supported by the Slovak Research and Development Agency under the contract No. APVV-0189-11” (prof. Jakuš)

Program

Tuesday, March 11, 2014

12.30 – 14.00 **Registration** (hotel lobby)

14.15 – 14.30

Opening ceremony (congress hall 1)

Chairs: **T. Hianik, J. Danko, J. Jakuš**

14.30 – 16.00

Tutorial lectures dedicated to 60th anniversary of prof. Ján Jakuš

Chairs: **T. Hianik, M. Šimera**

T1 **T. Hianik,** A. Poturnayová, M. Šnejdárková, I. Karpišová, M. Leitner, A. Ebner.: Application of molecular acoustics and atomic force spectroscopy for study of molecular interactions at surfaces

T2 **M. Kopáni,** R. Boca, M. Miglierini, M. Čaplovičová, R. Fiala, N. Žilka, T. Smolek, V. Šišovský, S. Galbavý, J. Jakubovský.: Histochemical, immunohistochemical, electron microscopy, Mössbauer spectroscopy and SQUID magnetometry study of iron biomineralization in human globus pallidus

T3 **M. Šimera**, I. Poliaček.: Institute of Medical Biophysics – yesterday and nowadays

T4 **I. Tonhajzerová**, Z. Višňovcová, M. Mešťaník, A. Čalkovská.: Electrodermal activity in psychophysiological research - yes or no?

16.00 – 16.30 **Coffee break and snack**

16.30 – 17.30

SKBS Young Researcher Prize Lecture

Chairs: **T. Hianik, I. Waczulíková**

T5 **K. Šipošová**.: Study of protein amyloid aggregation: focus on inhibitors

T6 **Z. Jurašeková**.: Across the world with Raman spectroscopy: From the research laboratory to the museum exposition, from the artworks to the organic molecules

18.00 **Dinner**

Wednesday, March 12, 2014

9.00 – 9.30 Establishment of posters

9.30 – 11.10

1. Proteins Structure and Stability

Chairs: **I. Záhradník, A. Záhradníková**

O1 **A. Antošová**, Z. Bednáriková, K. Šipošová, E. Demjen, J. Marek, Z. Gažová.: Structure of lyzozyme fibrils is determined by experimental conditions

O2 **Ľ. Borko**, V. Bauerová-Hlinková, J. Košťan, V. Pevala, L. Urbániková, J. Gašperík, E. Hostinová, A. Zahradníková, J. Ševčík.: Human cardiac Ryanodine receptor: Structural study of the N-terminal region

O3 **M. Fabian**, D. Jancura.: Electron-proton coupling at the catalytic center of cytochrome c oxidase

O4 **D. Jancura**, M. Fabian.: EPR detection of radical(s) in cytochrome c oxidase

O5 **E. Sedlák**.: Display technologies in evolving of new protein therapeutics

11.10 – 11.30 **Coffee break and snack**

11.30-13.30

2. Membrane Systems and Transport Processes

Chairs: **K. Ondriaš, K. Stroffeková**

O6 A. Faltinová, Ľ. Borko, V. Hlinková, J. Ševčík, **A. Zahradníková**.: Mechanism of the ryanodine receptor domain switch

O7 **M. Hoťka,** I. Zahradník.: Effect of cell electromotive potential on cell impedance in cardiac myocytes

O8 M. Hoťka, **I. Zahradník**.: Temperature and voltage dependence of membrane capacitance in cardiac myocytes

O9 **A. Musatov**.: Contribution of oxidatively modified cardiolipin to mitochondrial oxidative stress

O10 **Z. Naďová,** J. Joniová, M. Mišuth, F. Sureau, P. Miškovský.: The role of PKCα in cell death induced by photo-activated hypericin

O11 **I. Valent**.: Electrodiffusion kinetics of ionic transport in a simple model of membrane channel

13.30 – 14.45 **Lunch**

15.00 – 16.00

Poster session

Poster competition committee: **T. Hianik, J. Jakuš, K. Ondriaš, J. Staničová**

P1 **Z. Bednáriková**, V. Zavišová, M. Koneracká, K. Šipošová, I. Antal, A. Antošová, M. Kubovčíková, P. Kopčanský, Z. Gažová.: PLA nanoparticles are able to destroy insulin amyloid aggregates

P2 **D. Belej,** E. Sedlák, G. Fabriciová, D. Fedunová, D. Jancura.: Thermal stability of human serum albumin – DSC study

P3 **Ľ. Blaščáková,** J. Joniová, J. Kronek, Z. Naďová, F. Sureau, P. Miškovský, D. Jancura.: Construction and characterization of physico-chemical properties of drug delivery vehicle based on lipoproteins

P4 **D. Fedunová,** A. Antošová, J. Bágeľová, J. Marek, E. Demjén, Z. Gažová.: Imidazolium-based ionic liquids as amyloid-inducers of lysozyme fibrils

P5 **M. Grman,** K. Ondriaš, P. Nagy, M. Feelisch.: On the interaction of hydrogen sulfide with S-Nitroso-N-acetyl-DL-penicillamine – the involvement of polysulfides

P6 **H. Habiňáková,** D. Špigúthová, V. Jakušová, J. Jakuš.: Intensity of electric and magnetic fields at school environment

P7 **D. Horváth**, J. Uličný.: Simulated manifold learning for image analysis and visualization - exploration of the potential of Langevin Dynamics

P8 **M. Klacsová,** J. Karlovská, D. Uhríková, S.S. Funari, P. Balgavý.: Temperature study of the DOPE+DOPC+alkanol system

P9 **M. Maslaňáková**, L. Balogová, P. Miškovský, R. Tkáčová, K. Štroffeková.: Anti- and pro-apoptotic Bcl2 proteins distribution and metabolic profile in human aorta endothelial cells before and after HypPDT

P10 **S. Melikishvili,** K. Ciepluch, M. Ionov, Z. Garaiová, I. Waczulíková, T. Hianik, M. Bryszewka.: Carbosilane dendrimers complexes with HIV-derived peptides and their interactions with lipid monolayers and vesicles

P11 M.-M. Mocanu, C. Ganea, K. Šipošová, A. Filippi, E. Demjen, J. Marek, Z. Bednáriková, A. Antošová, I. Baran**, Z. Gažová**.: Correlation between polymorphism of amyloid fibrils and cytotoxicity in renal cells

P12 R. Varhač, **A. Musatov,** N.C. Robinson, E. Sedlák.: Factors affecting kinetic stability of cytochrome c oxidase

P13 **D. Špigúthová**, V. Jakušová, H. Habiňáková, J. Jakuš.: Mobile phone and adolescents - knowledge and efficiency of their education

P14 **Z. Jurašeková**, S. Sánchez-Cortés, P. Miškovský: What do we know about quercetin and other flavonoids from their Raman spectra?

P15 **K. Šipošová,** T. Kozár, P. Kutschy, Z. Krištofíková, A. Bartoš, D. Ripová, A. Antošová, Z. Bednáriková, D. Fedunová, Z. Gažová.: Anti-amyloid activity of indole-based compounds

Non-competitive posters

P16 **M. Šimera,** I. Poliaček, M. Veterník, B. Dobroľubov, H. Baráni, N. Višňovcová, J. Jakuš.: Effect of kainic acid medullary raphe lesions on cough in anesthetized rabbits

P17 **M. Veterník,** M. Šimera, J. Jakuš, I. Poliaček.: Effect of moving average window width on integration of EMG signal

P18 **I. Poliaček,** M. Šimera, M. Veterník, P. Macháč, H. Baráni, N. Višňovcová, J. Jakuš.: Medullary midline raphe contributes to phase duration control of tracheobronchial coughing - codeine trials in cat

16.00 – 16.30 **Coffee break and snack**

16.30 – 17.30

3. Modern Microscopic and Spectroscopic Techniques

Chairs: **D. Chorvát, A. Marček Chorvátová**

O12 **V. Huntošová**, P. Miškovský, G. Wagnières.: Highly sensitive in vivo pO_2 detection by luminescence lifetime of photosensitive probes

O13 **D. Chorvát,** M Uherek, A. Mateašík, A. Marček Chorvátová.: Perspectives of nonlinear optical imaging in cardiovascular research

O14 **P. Žiak, K. Lucká**.: Femtosecond laser use in ophthalmology

O15 J. Varchola, V. Huntošová, P. Miškovský, G. Wagnieres**,** **G. Bánó**.: Singelt oxygen production by photo-excited RuPhen

17.30 – 18.30 **Assembly of the Slovak Biophysical Society**

19.00 **Symposium dinner**

Thursday, March 13, 2014

9.00 – 10.30

4. Biophysics and Medical Biophysics

Chairs: **K. Kozlíková, J. Jakuš**

O16 **M. Šimera**, I. Poliaček, B. Dobroľubov, M. Veterník, J. Plevková, J. Jakuš: Cough and sneeze, differences and their mutual interactions

O17 **N. Višňovcová**, N. Višňovcová jr.: Our study of unwanted side effects during radiotherapy treatment

O18 **B. Dobroľubov,** M. Šimera, M. Veterník, J. Jakuš, I. Poliaček.: GABA-ergic inhibition in the medullary raphe modulates coughing in cats

O19 **M. Veterník,** M. Šimera, J. Jakuš, I. Poliaček.: Modulation of tonic and phasic activity of respiratory neurons - computer modeling

10.30 – 10.45 **Coffee break and snack**

10.45 – 13.00

Chairs: **J. Staničová, I. Poliaček**

O20 **Z. Garaiová,** M. Ionov, K. Ciepluch, S. Melikishvili, I. Waczulíková, T. Hianik, M.A. Muñoz-Fernandez, J.F. de la Mata, R. Gomez-Ramirez, M. Bryszewska.: Study of interactions between lipid membranes and HIV-derived peptides complexed with carbosilane dendrimers

O21 **J. Horilová,** A. Mateašík, I. Cavarga, P. Mlkvý, M. Cagalinec, A. Kaasik, D. Chorvát, A. Marček Chorvátová.: Multimodal fluorescence detection of cancer

O22 **J. Staničová**, V. Verebová.: Implementation of computer technology into biophysical lessons at University of Veterinary Medicine and Pharmacy

O23 **K. Kozlíková,** M. Trnka.: Analysis of the Electrical Activity of the Heart Atria Using Autocorrelation Maps at Time Normalization

O24 **K. Kozlíková**.: The application of the isointegral QRST maps

O25 **K. Ondriaš,** F. Kristek, L. Tomášová, L. Máleková, A. Mišák, M. Tomášek, M. Whiteman.: Effects of H2S donor AP39 on rat blood pressure and membrane channels

O26 **K. Štroffeková,** L. Balogová, M. Maslaňáková, P. Miškovský.: Anti- and pro-apoptotic Bcl2 proteins distribution and metabolic profile in U87 MG cells before and after HypPDT

General discussion

13.30 Closing ceremony

14.00 Lunch

Structure of lyzozyme fibrils is determined by experimental conditions

A. Antosova[1], Z. Bednarikova[1, 2], K. Siposova[1], E. Demjen[1], J. Marek[1], Z. Gazova[1]

[1]Department of Biophysics, Institute of Experimental Physics SAS, Kosice, Slovakia
[2]Department of Biochemistry, Faculty of Science, P. J. Safarik University, Kosice, Slovakia
email: antosova@saske.sk

Most proteins form supramolecular amyloid aggregates *in vivo* associated with several localized or systemic amyloidosis. Although various pathways of amyloid aggregation have been postulated, a general mechanism of fibrillization is still missing. Hen egg white lysozyme (HEWL) is a globular protein of 14.5 kDa homologous to human lysozyme, which is responsible for systemic lysozyme amyloidosis and [1]. Mature amyloid fibrils of lysozyme are straight and often contain several protofilaments in a periodic twist. The number of protofilaments and the period of fibril twisting are determined by experimental conditions of protein fibril self-assembly [2].

The fibrillization and morphology of HEWL amyloid fibrils prepared *in vitro* at two different experimental conditions were studied. Lysozyme fibrils were formed at i) pH 2.7, 65 °C in the presence of a saline solution (80 mM NaCl) after 2 h of intensive stirring (LF-NaCl) and at ii) pH 2.5, 65 °C in ultrapure water after 48 h of intensive stirring (LF-UPW). The kinetics of HEWL aggregation was investigated by Thioflavin-T (ThT) fluorescence assay and atomic force microscopy (AFM). The shape of both growth curves retains the typical sigmoidal profile of amyloid fibrillization with lag phase of about 1 h for LF-NaCl fibrils and 20 h for LF-UPW fibrils. The differences were observed also for time at which the values of fluorescence intensities achieved the steady-state values; namely, 2 h for LF-NaCl fibrils and 45 h for LF-UPW fibrils.

AFM and image analysis [3, 4] were used to characterize the morphology of obtained lysozyme fibrils. As it is apparent from Figure 1, the morphology of the LF-NaCl and LF-UPW fibrils is significantly different. Fibrils prepared in presence of salt (LF-NaCl) are shorter and have higher tendency to associate into the bundles (Figure 1A) compared to fibrils prepared in ultrapure water (LF-UPW) (Figure 1B). The twisting typical for amyloid fibrillarstructures is observed for both types of fibrils.

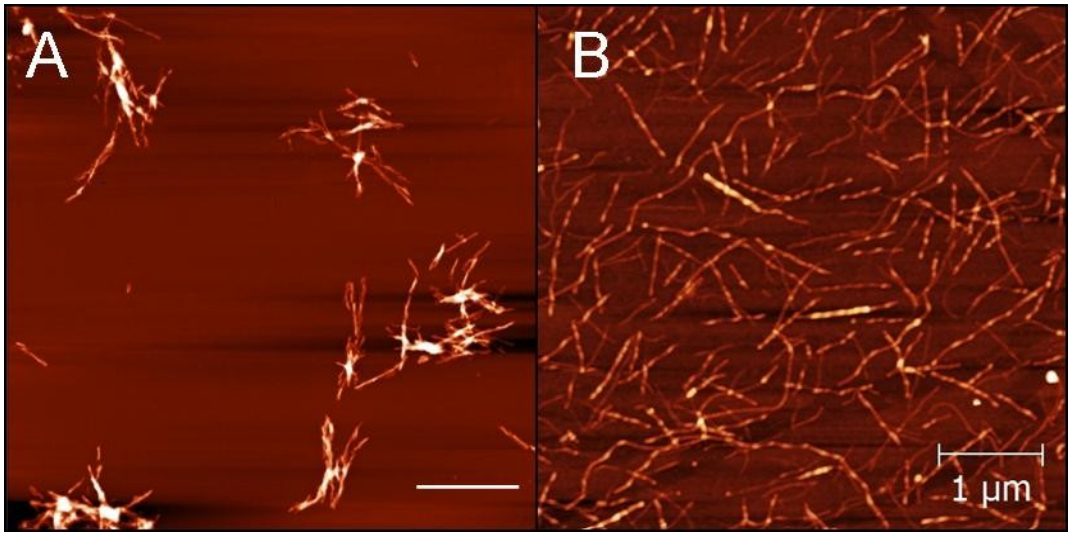

Figure 1. AFM images of mature lysozyme fibrils LF-NaCl (A) and LF-UPW (B).

Far UV-CD spectroscopy was used to examine the secondary structure f of prepared fibrils (LF-NaCl and LF-UPW). The CD spectra detected for LF-NaCl and LF-UPW were substantially different from those detected for native lysozyme. In case of both types of fibrils the content of β–sheet increased to 33% (LF-NaCl) or 27% (LF-UPW) compare to native lysozyme (16%).

The obtained data clearly indicate that experimental conditions influence the kinetic of lysozyme amyloid fibrillization and morphology of mature fibrils. Lysozyme protein aggregation was facilitated in presence of salt (LF-NaCl), the fibrils are shorter compare to those prepared in ultrapure water (LF-UPW), which are longer and more separated. The obtained results may contribute to a better understanding of the processes of amyloid self-assembly of globular proteins.

Acknowledgement: This work was supported by the research grant from the Slovak Grant Agency VEGA 0181, 0175, 0176 and the project ESF 26110230061**,** and 26110230097and APVV 0526-11.

References

[1] C. Lara, J. Adamcik, S. Jordens, R. Mezzenga, Biomacromolecules 12 (2011) 1868-1875 and references therein.
[2] R. Kodali, R. Wetzel, Current Opinion in Structural Biology 17 (2007) 48-57.
[3] J. Marek, E. Demjenova, Z. Tomori, J. Janacek, I. Zolotova, F. Valle, M. Favre, G. Dietler, Cytometry Part A 63 (2005) 87-93.
[4] J. Matas, Z. Shao, J. Kittler, J. Lecture Notes in Computer Science 974 (1995) 83-88.

PLA nanoparticles are able to destroy insulin amyloid aggregates

Z. Bednarikova[1, 2], V. Zavisova[1], M. Koneracka[1], K. Siposova[1], I. Antal[1], A. Antosova[1], M. Kubovcikova[1], P. Kopcansky[1],Z. Gazova[1, 3]

[1]Department of Biophysics, Department of Magnetism, Institute of Experimental Physics SAS, Kosice, Slovakia,
[2]Department of Biochemistry, Faculty of Science, P. J. Safarik University, Kosice, Slovakia
[3]Department of Medical and Clinical Biochemistry and LABMED, Faculty of Medicine, Safarik University, Kosice, Slovakia
E - mail: bednarikova@saske.sk

Self-assembly of native proteins into insoluble highly-ordered protein deposits of amyloid fibrils is a pathological feature of many degenerative diseases such as Alzheimer's disease (AD), Parkinson's disease (PD), type II diabetes mellitus, and some types of cancers [1]. Amyloid fibril deposits of insulin are observed in patients with type II diabetes after long-term treatment with insulin injection. Insulin aggregation is also a major problem in production, storage, and delivery of this important pharmaceutical compound. Currently, great efforts have been made to understand the pathogenesis of these diseases but mechanism of amyloid fibrillization is still not fully resolved [2]. However, recent data suggest that inhibition of the formation of amyloid aggregates or destruction of amyloid structures have been beneficial for cell cultures and animal models [3].

We have investigated interaction of insulin amyloid fibrils (IF) with three types of PLA (Poly(D,L-lactide)) nanoparticles (PLA-NPs), namely i) PLA nanoparticles alone (PLA); ii) PLA nanoparticles modified by various amount of bovine serum albumin (PLA_{BSA}) and iii) PLA nanoparticles loaded with magnetite nanoparticles modified by different amount of albumin (PLA_{FeBSA}). PLA nanoparticles were chosen due to their biocompatible and biodegradable properties.

The properties of all types of studied PLA-nanoparticles were characterized by several independent methods. The analysis of images obtained with scanning electron microscopy showed almost spherical shape of studied PLA-NPs in all cases. Hydrodynamic diameters of PLA-NPs determined by dynamic light scattering (DLS) method are summarized in Table 1.

The ability of studied PLA-nanoparticles to interfere with insulin amyloid fibrils was examined using Thioflavin T fluorescence assay. Our data demonstrate that all three types of PLA-NPs are able to destroy insulin amyloid fibrils. However, the extent of depolymerizing activity was significantly affected by the composition of studied PLA nanoparticles due to their different physico-chemical properties and size (Figure 1). In case of PLA_{FeBSA} the extent of fibril destruction depends on the amount of added PLA_{FeBSA}.The depolymerizing activity was only 10% for IF: NPs ratio 10:1, however for higher ratios the decrease was very significant, namely about 70% and 90% for ratios 1:1 and 1:10. Nanoparticles made only from polylactic acid (PLA) and PLA_{BSA} nanoparticles have similar depolymerizing effect. Their ability to destroy insulin amyloid fibrils is low (about 40% and 50% respectively) even for higher IF: NPs ratios = 1:1 and 1:10. The different extent of fibril destruction was confirmed by transmission electron microscopy.

Importantly, the agent used for modification (BSA) showed no potential to affect insulin amyloid fibrils. The fluorescence intensities of BSA (at the same concentrations

occurring for depolymerizing experiments with PLA-NPs) were comparable to fluorescence intensity of insulin fibrils (Figure 1, pink star).

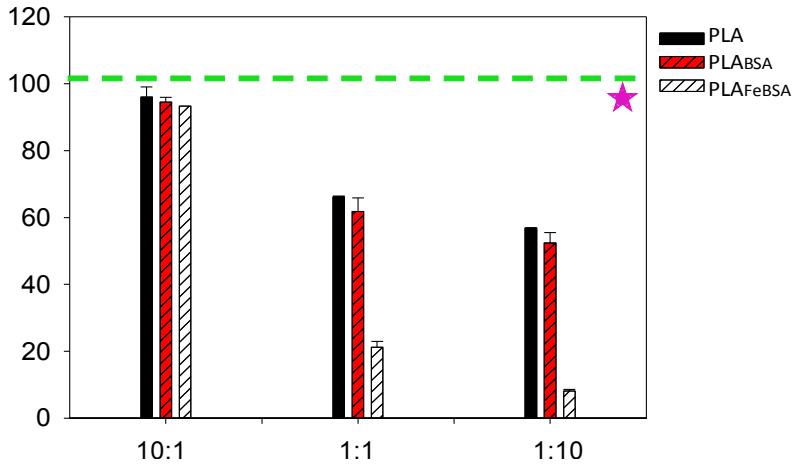

Figure 1. Fluorescence signals detected for insulin amyloid fibrils (IF) in the presence of all types ofPLA-NPs (black bars), PLA_{BSA} (red bars with pattern) and PLA_{FeBSA} (white bars with pattern) at IF: NPs ratios = 10:1, 1:1, 1:10 and in the presence of BSA alone (pink star) normalized to fluorescence intensity detected for untreated insulin amyloid fibrils (taken as100%, green dotted line).

Table 1. Hydrodynamic diameters of studied PLA nanoparticles.

type of nanoparticle	D_{hydr} (nm)
PLA	206
PLA_{BSA}	309
PLA_{FeBSA}	114

On the basis of our results we can conclude that all three types of PLA-nanoparticles, namely PLA, PLA_{BSA} and PLA_{FeBSA}, have ability to interfere with insulin amyloid fibrils which lead to the reduction of amount of amyloid fibrils. The most significant depolymerizing activity was observed for PLA_{FeBSA}. We suggest that this high activity is due to the presence of magnetite and smaller size of nanoparticles compare to other studied PLA-NPs. We assume that interaction of PLA_{FeBSA} with beta-sheets stabilizing insulin fibrils is more intensive because of smaller sterical barrier. The obtained results indicate that present of magnetite and size of the PLA nanoparticles are the main factors affecting the depolymerizing efficiency.

Acknowledgement: This work was supported by the research grant from the Slovak Grant Agency VEGA 0181, 0077, 0041, university grant VVGS-2013-98, the project ESF 26110230061and 26110230097and APVV 0171-10.

References

[1] Dobson, C.M., Karplus, M. In Curr.Opin.Struct. Biol. 9, (1999), p. 92-101
[2] Zhang, M., Yu, Y., Wang, Ch-X., Yang, Y-L., Wang, Ch. In Adv. Mater. 25(28), (2013), p. 3780-3801
[3] Khlistunova, I., Biernat, J., Wang, Y., Pickhardt, M., von Bergen, M., Gazova, Z., Mandelkow, E., Mandelkow, E. M. J. In Biol. Chemistry 28, (2006), p. 1205-1214.

Thermal stability of human serum albumin – DSC study

D. Belej[1], E. Sedlák[2,3], G. Fabriciová[1], D. Fedunová[4], D. Jancura[1,2]

[1]Department of Biophysics, Faculty of Science, Safarik University, Kosice, Slovak Republic
[2]Center for Interdisciplinary Biosciences, Faculty of Science, Safarik University, Kosice, Slovak Republic
[3]Department of Biochemistry, Faculty of Science, Safarik University, Kosice, Slovak Republic
[4]Institute of Experimental Physics, Slovak Academy of Science, Slovak Republic

Human serum albumin (HSA) is the most abundant protein in human plasma (concentration about 45 mg/ml) with ascribed ligand binding and transport properties, antioxidant functions, enzymatic and antioxidant activities [1,2]. This protein also contributes significantly to colloid-osmotic blood pressure. HSA is a non-glycosylated 65 kDa protein consisting of 585 amino acids having three homologous □-helical domains. Design of this molecule provides a variety of binding sites for many physiological important ligands, fatty acids, hemes, amino acids, bilirubin, steroids and metal ions, including a wide variety of drugs, helping thus in the transport, distribution and metabolism of these compounds. HSA has two primary binding sites named Sudlow site I and II located in IIA or IIIA subdomain, respectively, which serve as binding cavities for a variety of ligands [1,3].

Understanding the relationship between the structure of proteins and the energetics of their stability and binding with other biomolecules is very important in biotechnology and is essential to the engineering of stable proteins and to the structure-based design of pharmaceutical ligands [3]. From this point of view, the study of the thermal stability of HSA as well as the investigation of the influence of the formation of HSA-drug complex on this stability is an utmost importance for clinical and pharmaceutical practice. In the previous years, the thermal stability of HSA has been widely investigated mainly by differential scanning calorimetry (DSC) [4]. This technique enables direct determination of the thermodynamic parameters (calorimetric and van't Hoff enthalpies (ΔH_{cal} and ΔH_{vH}) and temperature (T_m)) of the denaturation as well as evaluation of entropy and Gibbs energy of the transitions between folded and unfolded states of the studied biopolymer.

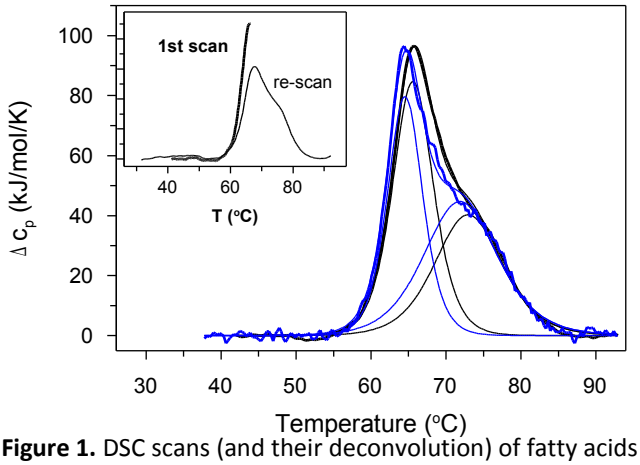

Figure 1. DSC scans (and their deconvolution) of fatty acids containing HSA at different scan rates: 0.5°C/min (blue line) and 1.5 °C/min (black line).

Inset: Reversibility of thermal transition of HSA in at the scan rate 1.5°C/min.

In this work we study by means of DSC the dependence of the thermal denaturation of HSA on the concentration, scan rate and presence of fatty acids. Deconvolution analysis suggests that DSC endotherms are well approximated as the sum of two independent two state transitions in both types of albumin, defatted as well as containing fatty acids (Fig. 1). Our results show that the presence of fatty acids in HSA significantly stabilizes the structure of this protein. Further, DSC curves exhibit a marked dependence on protein concentration in both fatty acid containing and fatty acids free HSA (Fig. 2). The increase of HSA stability with increasing of the concentration enables to determine oligomeric state of albumin at

denaturation process.From the linear dependence of $1/T_m$ on albumin concentration follows that HSA tends to form dimers.

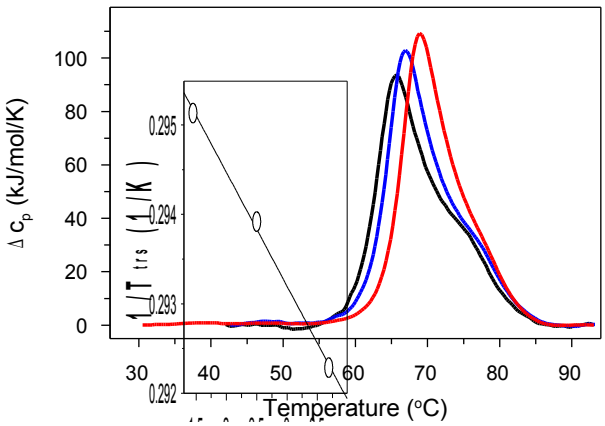

Figure 2. DSC curves at different concentration of HSA (black - $4.4x10^{-6}$ M, blue – $1.1x10^{-5}$M and red – $4.1x10^{-5}$M) in 10mM buffer, with pH 7.0 obtained by scanning up to 90°C at scan rate: 90°C/h.

Inset: Dependence of $1/T_m$ on logarithm of albumin concentration.

Our data show only a slight increase of T_m and ΔH_{cal} with a scan rate increase (Fig. 1). This finding is in accordance with the previous observations [5]. The reversibility of the transition of HSA molecule depends on the temperature at which the protein was heated. Reversibility of the thermal transition after heating of the sample to the temperature ~90°C and cooling up to ~20°C is negligible, however heating only up to the temperature of the thermal denaturation (~ 67°C in the case of fatty acids containing HSA) leads to 60% reversibility (inset Fig.1) .

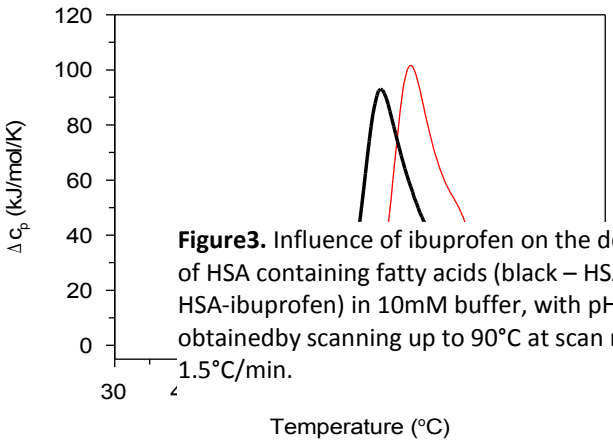

Figure3. Influence of ibuprofen on the denaturation of HSA containing fatty acids (black – HSA, red – HSA-ibuprofen) in 10mM buffer, with pH 7.0 obtainedby scanning up to 90°C at scan rate: 1.5°C/min.

This work contains also preliminary results about the influence of several drugs (ibuprofen, warfarin, emodin) on the thermal stability of HSA. Interaction of these molecules with HSA leads to a significant stabilization of the protein (higher temperature and enthalpy of the denaturation) (Fig. 3). This type of measurements may be beneficial for the easy determination of the binding site(s) of ligands to HSA.

Acknowledgements: This work was supported by the Structural funds of the EU (contracts: NanoBioSens (ITMS code: 26220220107), SEPO II (ITMS code: 26220120039), and CEVA II (ITMS code: 26220120040), by the contract APVV-0242-11, and the EU 7FP project CELIM (316310).

References:

[1] T.Peters, All about Albumin: Biochemistry, Genetics, and Medical Applications, Academic Press, 1995
[2] A. Varshney, P. Sen, E. Ahmad, M. Rehan, N. Subbarao, R.H. Khan, Chirality 22 (2010) 77-87.
[3] B. Elsadek, F. Kratz, J. Controlled Release 157 (2012) 4-28.
[4] G. Bruylants, J. Wouters, C. Michaux, Current Medicinal Chemistry 12 (2005) 2011-2020.
[5] A. Michnik, J. Thermal Analysis and Calorimetry 71(2003), 509-519.

Construction and characterization of physico-chemical properties of drug delivery vehicle based on lipoproteins

L. Blascakova[1], J. Joniova[1,2], J.Kronek[3], Z. Nadova[1], F. Sureau[2], P. Miskovsky[1,4], D. Jancura[1,4]

[1] Department of Biophysics, Faculty of Science, Safarik University, Kosice, Slovak Republic
[2] Laboratoire Jean Perrin, Université Pierre et Marie Curie, Paris, France
[3] Polymer Institute of the Slovak Academy of the Sciences, Bratislava, Slovak Republic
[4]Center for Interdisciplinary Biosciences, Faculty of Science, Safarik University, Kosice, Slovakia
e-mail: ludmila.blascakova@student.upjs.sk

Low-density lipoproteins (LDL) (Fig. 1a), a natural *in vivo* carrier of cholesterol in the vascular system, play a key role in the delivery of hydrophobic drug to tumor cells. LDL are viable nanocarriers for targeted delivery of therapeutic drugs since they have homogenous size (18-25 nm), functional capacity to transport hydrophobic and/or amphiphilic drugs, long circulation time in blood, excellent biocompatibility and customizable targeting capability [1-3]. Regarding their utilization in cancer chemotherapy an additional major advantage favoring LDL-based formulations is their vast targeting potential via mechanism mediated by LDL receptors that are over-expressed in several types of cancer cells versus normal cells [4, 5].

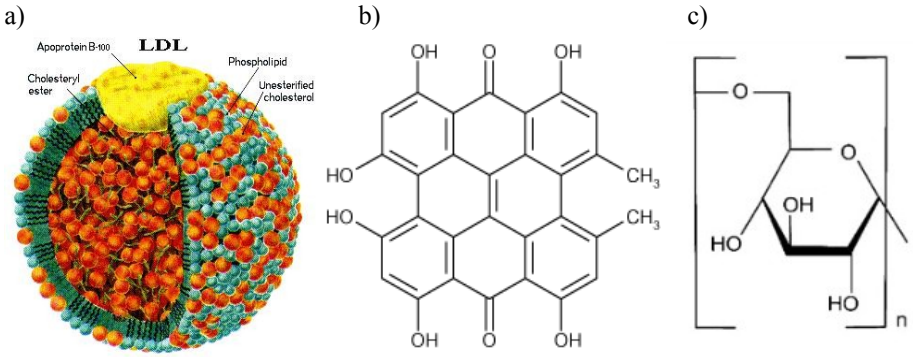

Fig. 1 Structure of a) LDL particle, b) hypericin, c) dextran

Our group has published in the recent years several articles about the properties of the complex of LDL with photosensitizer hypericin (Hyp) [8-13]. Hyp (Fig. 1b) is a natural photosensitizing pigment from plants of the genus *Hypericum*. Hyp under light illumination causes anti-proliferative and cytotoxic effects (necrosis as well as apoptosis) in many tumor cell lines. These properties, together with minimal dark toxicity, certain tumor selectivity and high clearance rate from the host body, make Hyp a promising agent for photodynamic therapy (PDT) of cancer as well as for tumor photo-diagnosis [6, 7].

In our studies was shown that high Hyp/LDL ratio (>30/1) leads to a significant decrease of quantum yield of Hyp fluorescence [8]. This decrease is caused by the formation of non-fluorescent Hyp aggregates inside LDL particles and by dynamic self-quenching of Hyp fluorescence. It was shown that only monomeric form of Hyp is able to produce the excited triplet state of Hyp in LDL, which in aerobic conditions leads to a singlet oxygen production [9]. The kinetics of association of Hyp with free LDL molecules and Hyp/LDL complex have been also thoroughly studied and described [10, 11]. We have demonstrated the important role of the LDL receptor pathway for Hyp delivery into U-87 MG cells in the presence of LDL: a substantial increase of Hyp uptake was observed after overexpression of LDL receptors on the cell surface [12]. It was also shown that overloading of LDL with Hyp (Hyp/LDL = 200/1) leads to a higher intracellular accumulation of Hyp molecules in

comparison with the situation when the same quantity of Hyp is accumulated in LDL, but with a lower Hyp⁄LDL ratio (20/1). Moreover, Hyp⁄LDL ratio seems to affect the subcellular distribution of Hyp [13] and consequently the mechanism of photodynamicallyinduced cell death. To make LDL-based delivery system even more efficient we have constructed adelivery vehicle bycoating of LDL surface by oligosaccharide dextran (Fig. 1c). Dextran serves as an element which modify surface of LDL particles. It was shown than the redistribution process of Hyp between LDL molecules (Fig. 2) is significantly suppressed (~40%) by dextran coating of LDL surface. The modification of LDL molecules by dextran does not inhibit their recognition by cellular LDL receptors and U-87 MG cellular uptake of Hyp loaded in LDL/dextran complex appears to be similar to that one observed for Hyp transported by unmodified LDL particles.

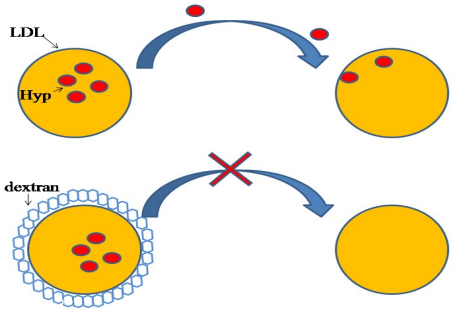

Fig. 2. Redistribution process of the drug between LDL molecules

In this work chemical modification of dextran is suggested to enhance the protective against drug redistribution from drug-modified dextran-LDLcomplexes to other plasma proteins. Moreover, thorough study of physico-chemical properties (size, stability, homogenity) of a new prepared drug delivery complex based on LDL is presented as well.

Acknowledgements: This work was supported by the Structural funds of the EU (contracts: NanoBioSens (ITMS code: 26220220107), SEPO II (ITMS code: 26220120039), and CEVA II (ITMS code: 26220120040), by the contract APVV-0242-11, the EU 7FP project CELIM 316310 and by the International Program for Scientific Cooperation (PICS N°5398) from the CNRS.

References:

[1] K.K. Ng, J.F. Lovell, G. Zheng, Accounts Chem, Res. 4 (2011) 1105-1113.
[2] H. Ji, J.E. Lovell, J. Chen, K. Ng, W. Cao, L. Ding, Z. Zhang, G. Zheng, Photochem. Photobiol. Sci. 10 (2011) 810-816.
[3] G. Zheng, J. Chen, H. Li, J.D. Glickson, Proc. Natl. Acad. Sci. USA 102, 17757-17762 (2005).
[4]M.S. Brown, J.L. Goldstein, Science 191 (1976) 150-154.
[5]S. Vitols, C. Peterson, O. Larsson, P. Holm, B. Aberg, Cancer Res. 52 (1992) 6244-6247.
[6]T. Kiesslich, B. Krammer, K. Plaetzer, Current Medical Chemistry 13 (2006) 2189-2204.
[7] P. Miskovsky, Current Drug Targets 3 (2002) 55-84.
[8]S. Kascakova, M. Refregiers, D. Jancura, F. Sureau, J.C. Maurizot, P. Miskovsky. Photochem. Photobiol. 81 (2005) 1395–1403.
[9]P. Gbur, R. Dedic, D. Chorvat jr., P. Miskovsky, J. Hala, D. Jancura, Photochem. Photobiol. 85 (2009) 816-823.
[10]L. Buriankova, D. Buzova, D. Chorvat jr., F. Sureau, D. Brault, P. Miskovský, D. Jancura, Photochem. Photobiol. 87 (2011) 56–63.
[11] S. Kascakova, Z. Nadova, A. Mateasik, J. Mikes, V. Huntosova, M. Refregiers, F. Sureau, J.C. Maurizot, P. Miskovsky, D. Jancura. Photochem. Photobiol. 84 (2008) 120–127.
[12] V. Huntosova, L. Alvarez, L. Bryndzova, Z. Nadova, D. Jancura, L. Buriankova, S. Bonneau, D. Brault, P. Miskovsky, F. Sureau. Int. J. Pharmaceut. 389 (2010) 32–40.
[13] V. Huntosova, D. Buzova, D. Petrovajova, P. Kasak, Z. Nadova, D. Jancura, F. Sureau, P. Miskovsky. Int. J. Pharmaceut. 436 (2012) 463-471.

Human cardiac Ryanodine receptor: Structural study of the N-terminal region

Ľ. Borko[1], V. Bauerová-Hlinková[1], J. Košťan[2], V. Pevala[1], L. Urbániková[3], J. Gašperík[1], E. Hostinová[1], A. Zahradníková[1], J. Ševčík[1]

[1]Biochemistry and Structural Biology department, Institute of Molecular Biology SAS, Dubravská cesta 21, Bratislava, 84551, Slovakia
[2]Biochemistry & Biophysics, Structural & Computational Biology department, Max F. Perutz Laboratories, Dr. Bohr-Gasse 9 (VBC 5), Vienna, 1030, Austria
[3]Genomics and Biotechnology department, Institute of Molecular Biology SAS, Dubravská cesta 21, Bratislava, 84551, Slovakia

Human ryanodine receptor (hRyR2) is a cardiac calcium ion channel present in sarcoplasmatic membrane . It mediates the calcium ions release in response to electrical stimulation during excitation-contraction coupling. Human RyR2 is a large homotetramer, composed of four subunits with a molecular weight of ≈ 560 kDa . N-terminal (aa ≈ 1-655) and central (aa ≈ 2100-2500) region are believed to be involved in channel gating allosteric regulation . Mutations located in these two regions are linked with several hearth diseases . To properly understand hRyR2 gating mechanism and prevent malfunction, it is of high importance to know the atomic structure of the key regions as well as of entire molecule.

Here we report structural study of $hRyR2^{1-606}$ region. This region is involved in an allosteric regulation mechanism known as domain switch and, as a mutation hotspot, it encompasses 23 substitution and two deletion mutations connected to several diseases (CPVT, ARVD2). We analyzed the $hRyR2^{1-606}$ by X-ray crystallography as well as by small angle X-ray scattering (SAXS). Samples for crystallization and SAXS analysis were prepared through IMAC and size exclusion chromatography. Quality of the samples was tested *via* SDS and native PAGE and stability was analyzed with DLS. After a successful crystallization diffraction data to 2.4 Å were obtained. The phase problem was solved by molecular replacement using rabbit RyR1 structure (2XOA) . For refinement and building the structure of the $hRyR2^{1-606}$ the CCP4 software package was used. The corresponding SAXS model was built using software package ATSAS 2.5.

The significant similarity of the N-terminal three-domain structure was confirmed by comparison of the $hRyR2^{1-606}$ structure with related structures (rabbit RyR1, 2XOA and inositol 1,4,5-triphosphate receptor, 3UJO). However there were regions not determined in the X-ray structure. SAXS analysis led to a low-resolution model, which involved the whole $hRyR2^{1-606}$ molecule. The regions visible in the low-resolution SAXS model, but not in the X-ray structure were built using the I-TASSER structure prediction server.

The structure of $hRyR2^{1-606}$ is the first structure from human protein containing ≈ 600 amino acids. It has a great potential for further study of allosteric channel regulation and mutation analysis.

Acknowledgements
This work was supported by the research grants from the Slovak Grant Agency VEGA No. 2/0131/10 and Slovak research and development agency APVV-0628-10. The authors thank to Dr. Jacob A. Bauer and Dr. Eva Kutejová for helpful discussions.

References

[1] Meissner, G., *Regulation of mammalian ryanodine receptors.* Front Biosci, 2002. **7**: p. d2072-80.
[2] Meissner, G., *Molecular regulation of cardiac ryanodine receptor ion channel.* Cell Calcium, 2004. **35**(6): p. 621-8.
[3] Otsu, K., et al., *Molecular cloning of cDNA encoding the Ca2+ release channel (ryanodine receptor) of rabbit cardiac muscle sarcoplasmic reticulum.* J Biol Chem, 1990. **265**(23): p. 13472-83.
[4] Ikemoto, N. and T. Yamamoto, *Regulation of calcium release by interdomain interaction within ryanodine receptors.* Front Biosci, 2002. **7**: p. d671-83.
[5] Yano, M., et al., *Mechanisms of Disease: ryanodine receptor defects in heart failure and fatal arrhythmia.* Nat Clin Pract Cardiovasc Med, 2006. **3**(1): p. 43-52.
[6] Tung, C.C., et al., *The amino-terminal disease hotspot of ryanodine receptors forms a cytoplasmic vestibule.* Nature, 2010. **468**(7323): p. 585-8.
[7] Winn, M.D., et al., *Overview of the CCP4 suite and current developments.* Acta Crystallogr D Biol Crystallogr, 2011. **67**(Pt 4): p. 235-42.

GABA-ergic inhibition in the medullary raphe modulates coughing in cats

B. Dobrolubov, M. Simera, M. Veternik, J. Jakus, I. Poliacek

Comenius University in Bratislava, Jessenius Faculty of Medicine in Martin, Institute of Medical Biophysics, Mala Hora 4, 03601 Martin, Slovakia
E-mail contacts: borissvk@gmail.com, poliacek@jfmed.uniba.sk

GABA acts in the CNS primarily as the mediator of inhibitory synapses providing substantial portion of active neuronal inhibition in the brain. We microinjected this inhibitory neuromediator in the area of medullary raphe where neurons essential for appropriate generation of coughing are placed in cat [1,2]. We hypothesised that increased GABA-ergic inhibition in the medullary midline will reduce the strength and alter the timing of tracheobronchial coughing.

Fourteen pentobarbitone anesthetized spontaneously breathing cats were used (3,54±0,27 kg). Six microinjections of 1 mM GABA dissolved in artificial cerebrospinal fluid were made during one protocol (203±12 nl per all 6 microinjections) at the depths (2 injections at each) of approximately 1.1, 2.2, and 3.3 mm below the dorsal medullary surface. These microinjections were placed at four separated rostro-caudal positions: approximately 1 mm caudal (n=5), 1 mm (n=7), 2.5 mm (n=5), and 4 mm (n=7) rostral to the obex. Cough was induced mechanically by a soft catheter in the tracheobronchial area.

Blood pressure, esophageal pressure and electromyograms (EMGs) of the diaphragm and the abdominal muscles were recorded. Diaphragm and abdominal muscles EMGs as well as esophageal pressure values were normalized to their mean amplitudes during control pre-microinjection coughs. ANOVA and paired t-test were employed in statistical analysis.

GABA microinjections 4 mm rostral to the obex reduced the number of coughs during 10s stimulation (CN) from 4.48±0.30 to 3.17±0.24 ($p<0,01$; 4.20±0.45 coughs in recovery more than 6 min after microinjections, $p<0,01$ vs. post-microinjection value), amplitudes of cough abdominal EMG to 50±10% ($p<0.05$; recovery 85±24%, $p>0.05$ vs. post-microinjection value), and of cough expiratory esophageal pressure maxima to 61±9% ($p<0.01$; recovery 83±9%, $p<0.05$ vs. post-microinjection value). Temporal analysis of coughing showed a prolongation of dipahragmatic activity (by 23%; $p<0.05$) and inspiratory phase (by 22%; $p<0.05$) during coughing due to GABA microinjections 4 mm rostral to the obex.

Cough expiratory efforts were also reduced by GABA microinjections 1 mm rostral to the obex: amplitudes of abdominal EMG to 49±9% ($p<0.001$; recovery 82±9%, $p<0.01$ vs. post-microinjection values) and of cough expiratory esophageal pressure to 64±11% ($p<0.05$; recovery 102±13%, $p<0.01$ vs. post-microinjection value).

CN and the parameters of coughing were not altered significantly by GABA microinjections 1 mm caudal and 2.5 mm rostral to the obex.

Our data confirmed a contribution of active GABA-related inhibition in medullary raphe in generation (and inhibition) of cough reflex. Markedly different efficiency and diversity of effects at different rostro-caudal raphe positions were seen. In accordance with

our previous data, raphe neurons significantly contribute to control of phase duration during coughing [3].

Acknowledgements: We gratefully acknowledge Iveta Najslova and Ing. Peter Machac for the excellent technical assistance. This work was supported by the VEGA 1/0126/12. „This work was supported by the Slovak Research and Development Agency under the contract No. APVV-0189-11"

[1] Jakuš J, Stránsky A, Poliaček I, Baráni H, Bošeľová Ľ. Effects of Medullary Midline Lesions on Cough and Other Airway Reflexes in Anaesthetized Cat. Physiol Res 1998; 47(3): 203-213.
[2] Baekey DM, Morris KF, Nuding SC, Segers LS, Lindsey BG, Shannon R. Medullary raphé neuron activity is altered during fictive cough in the decerebrate cat. J Appl Physiol 2003; 94:93–100.
[3] Poliacek I, Simera M, Veternik M, Machac P, Barani H, Visnovcova N, Halasova E, Jakus J. Contribution of medullary raphé to control of coughing-Codeine trials in cat**.** Respir Physiol Neurobiol 2012; 184(1): 106-112.

Electron-proton coupling at the catalytic center of cytochrome c oxidase

M. Fabian[1,2], D. Jancura[1,3]

[1] Center for Interdisciplinary Biosciences, Faculty of Science, Safarik University, Kosice, Slovakia (e-mail: fabian@rice.edu)
[2] Department of Biochemistry & Cell Biology, Rice University, Houston, USA
[3] Department of Biophysics, Faculty of Science, Safarik Unversity, Kosice, Slovakia

The principal biological function of respiratory oxidases is a generation of transmembrane proton gradient. The energy required for the proton translocation by cytochrome c oxidases is released from the downhill electron transport to molecular oxygen. On average, cytochrome oxidases are able to uptake 2 protons from mitochondrial matrix by each electron transferred from ferrocytohrome *c* to oxygen. One of these protons is used for water formation in the course of oxygen reduction. The second one is pumped through the membrane from the matrix domain into the intermembrane space of mitochondria [1].

Mammalian cytochrome oxidases contain 4 redox active centers involved in the electron transfer and the reduction of oxygen. These centers are denoted as Cu_A, heme *a*, heme a_3 and Cu_B. Cu_A is the dinuclear copper center and serves as the first electron acceptor from cytochrome c. From Cu_A electrons flow to heme *a* and then to the binuclear heme a_3-Cu_B site. At the catalytic heme a_3-Cu_B center O_2 is reduced to water. This catalytic center is also the site where the known inhibitors of respiration (e.g. cyanide, carbon monoxide) are bound.

Available X-ray structures of oxidases [2-4] substantially contributed in understanding of their function. However, in spite the structural information and the large pool of accumulated data on the coupling of electron and proton transfer, the results and their interpretation are highly controversial or even still missing. One site that is difficult to investigate experimentally is the catalytic heme a_3-Cu_B site. Yet, there are many indications that this center may play a key role not only in the reduction of oxygen and formation of water but also in the proton translocation. Because of the close proximity of iron of heme a_3 and Cu_B (~5Å) and especially the very weak spectroscopic features of Cu_B, the direct investigation of Cu_B imposes the challenge. To reveal the properties of Cu_B relevant for the electron-proton coupling it is necessary to design some indirect methods.

In this work we present the approach that enables us to determine the reduction potential of Cu_B under the conditions when all other three redox centers (Cu_A, heme *a*, heme a_3) are oxidized. For this study the purified cytochrome c oxidase from bovine heart mitochondria was employed. We show here that midpoint potential of Cu_B exhibits the strong dependence on pH with the slope of – 60 mV/ pH unit in the range between pH 6 and 9.0. This dependence indicates that the one-electron reduction of Cu_B is associated with an uptake of one proton. In addition we have confirmed that the reduction potential of heme *a* shows weaker dependence on pH. It is increased about 30 mV with the decrease of pH by one unit. Data indicated that ligands like cyanide and formate are bound to the Cu_B site. The binding of these ligands results in the decrease of the reduction potential relative to that of the unligated Cu_B. The affinity of Cu_B to ligands shows the pH dependency and it is increased with the pH decrease. The coupling stoichiometry of one proton with one electron requires at least one protolytic, acid-base group that responds to the charge changes at Cu_B. However, the identity of this group remains to be established.

Acknowledgement
This work was supported by the project CELIM (316310) funded by7FP EU (REGPOT).

References

[1] M. Wikstrom, Biochim. Biophys. Acta 1817(2012) 468-475.
[2] T. Tsukihara, H. Aoyama, E. Yamashita, T. Tomizaki, H. Yamaguchi, K. Shinzawa-Itoh, R. Nakashima, R. Yaono, S. Yoshikawa, S. *Science* 269 (1995) 1069-1074.
[3] S. Iwata, C. Ostermeier, B. Ludwig, H. Michel, Structure at 2.8 Å resolution of cytochrome c oxidase from *Paracoccus denitrificans*, Nature 376 (1995) 660-669.
[4] J. Abramson, S. Riistama, G. Larsson, A. Jasaitis, M. Svensson-Ek, L. Laakkonen, A. Puustinen, S. Iwata, M. Wikström, The structure of the ubiquinol oxidase from *Escherichia coli* and its ubiquinone binding site, Nature Struct. Biol. 7 (2000) 910-917.

Mechanism of the ryanodine receptor domain switch

A. Faltinová[1], Ľ. Borko[2], V. Hlinková[2], J. Ševčík[2], A. Zahradníková[1,2]

[1] Department of Muscle Cell Research, Institute of Molecular Physiology and Genetics, Slovak Academy of Sciences, Vlárska 5, 833 34 Bratislava, Slovakia.
[2] Department of Biochemistry and Structural Biology, Institute of Molecular Biology, Slovak Academy of Sciences, Dúbravská cesta 21, 845 51 Bratislava, Slovakia, e-mail: alexandra.zahradnikova@savba.sk

Ryanodine receptors (RyRs) are large homotetrameric calcium-permeant ion channels in the membrane of the endo/sarcoplasmic reticulum (ER/SR). Cardiac RyR2 channels open in response to electrical stimulation during systole and the resulting massive release of calcium ions from the SR lumen into the cytosol mediates excitation-contraction coupling. During diastole, a small diastolic calcium leak occurs due to the very low but non-zero RyR2 activity. Mutations linked to several heart diseases and causing an increase of the calcium leak are clustered within N-terminal (1-655) and central (2100-2500) regions, as well as in the channel pore-containing C-terminal regions [1]. Activation of calcium release by a peptide from the central region of the skeletal RyR (aa 2442-2477) is suppressed by the N-terminal peptide DP3 (aa 324-351) [2]. Therefore it has been proposed that in RyR channels the N-terminal region allosterically regulates channel activity by interacting with the central part of the protein. Indeed, it has been shown that in agreement with this hypothesis, a peptide corresponding to amino acids 163-195 of RyR2 (in which 5 disease-causing mutations are found) binds to RyRs and activates diastolic calcium release [3], and a domain peptide from the central domain, DPc10, increases the open probability of the RyR [4].

Here we tested this hypothesis for a peptide from the central region that contains an unusually high density of mutations (DP_{cpvtC}, $RyR2^{2380-2411}$). Our experimental strategy was based on the fact that the interaction between the examined RyR2 domains can be suppressed (i.e., channel can be activated) by adding a peptide with amino acid sequence identical to a part of the "domain switch" [4]. The effect of DP_{cpvtC} on the activity of ryanodine receptors isolated from rat heart was examined in planar lipid bilayers. At a zero holding potential and at 100 nM cytosolic and 8 mM luminal Ca^{2+} concentration, DP_{cpvtC} induced concentration-dependent activation of the ryanodine receptor that led up to 20-fold increase of open probability at saturating DP_{cpvtC} concentrations. The effect of the peptide appeared within 30 s after addition to the experimental chamber. At all DP_{cpvtC} concentrations RyR2 channels displayed large variability in open probability, open time and opening frequency. DP_{cpvtC} prolonged RyR2 openings up to 8 times and increased RyR2 opening frequency by up to 100%. With increasing DP_{cpvtC} concentration, the fraction of high open probability records increased up to 5 times, and their open time increased up to four times. The closed times did not depend on DP_{cpvtC} concentration either in low- or high-open probability records. The DP_{cpvtC} concentration dependence of all gating parameters had EC_{50} of 20 µM and a Hill slope of 2. Comparison of the effects of DP_{cpvtC} with those of ATP [5] and cytosolic Ca^{2+} [6] suggests that activation does not involve luminal feed-through and is not caused by modulation of the cytosolic activation A-site. The data suggest that although "domain unzipping" by DP_{cpvtC} occurs in both modes of RyR activity, it affects RyR gating only when the channel resides in the H-mode of activity. Based on these results we propose that domain unzipping leads to increase in RyR activity by two mechanisms – by increased occurrence of the channel in the H-mode of activity, and by slowing down transitions of the channel from open to closed states.

To obtain structural insight into our single-channel results, models of the N-terminal region (aa 1-606, [7-8], the central domain (aa 2333-2700) and the RIH-2 domain (aa 2121-2332) were constructed using the I-TASSER server [9]. The N-terminal region consists of domains A and B with a beta-trefoil fold and of domain C with armadillo fold. The central and RIH-2 domains were predicted to consist solely of armadillo repeats. Docking of the N-terminal region and the central domain into the cryo-EM map of the skeletal RyR (EMD-1606, [10]) showed that the sequences corresponding to DP_{cpvtC} and DPc10 in the central domain as well as those corresponding to the N-terminal domain peptides are accessible from the cytosol, which explains their easy replacement by domain peptides. Binding of the domain peptides can occur only upon changes in the tertiary structure of RyR. However, the N-terminal region and the central domain, although located close to each other, cannot directly interact. A model that incorporates the RIH-2 domain as the mediator of the "domain switch" can explain our data, as well as those previously published [2-4, 11].

Acknowledgement

This work was supported by the Slovak Grant Agency VEGA, projects No. 2/0197/11and 2/0148/14 and by the Slovak Research and Development Agency under the contracts No. APVV-LPP-0441-09, APVV-0721-10 and APVV-0628-10.

References

[1] L.M. Blayney, F.A. Lai, Pharmacol. Ther. 123 (2009) 151-177
[2] Yamamoto T, El-Hayek R, Ikemoto N, J Biol Chem. 275 (2000) 11618-11625
[3] H. Tateishi, M. Yano, M. Mochizuki, T. Suetomi, M. Ono, X. et al., Cardiovasc. Res. 81 (2009) 536-545
[4] D.R. Laver, B.N. Honen, G.D. Lamb, N. Ikemoto, Eur. Biophys. J. 37 (2008) 455-467
[5] Tencerova B, Zahradnikova A, Gaburjakova J, Gaburjakova M. J Gen Physiol 140 (2012) 93-108
[6] Gaburjakova J, Gaburjakova M. J Membr Biol 212 (2006) 17-28
[7] L. Borko, J. Kostan, A. Zahradnikova, V. Pevala, et al.. Protein Pept Lett 20 (2013) 1211-1216
[8] V. Bauerova-Hlinkova, L. Borko, A. Zahradníková, J. Gasperik, E. Hostinova, J. Kostan, J. Sevcik, In: Book of Abstracts, Applied Natural Sicences 2013, Novy Smokovec, Slovak Republic, 2.-4.10.2012, Ed. M. Ondrejovic, P. Nemecek, p. 94.
[9] A. Roy, A. Kucukural, Y. Zhang, Nat Protoc. 5 (2010) 725-738
[10] M. Samso, W. Feng, I.N. Pessah, P.D. Allen, PLoS Biol 7 (2009) e85
[11] T. Suetomi, M. Yano, H. Uchinoumi, M. Fukuda, et al., Circulation 124 (2011) 682-694

Imidazolium-based ionic liquids as amyloid-inducers of lysozyme fibrils

D. Fedunová, A. Antošová,J. Bágeľová, J. Marek, E. Demjén, Z.Gažová

Department of Biophysics, Institute of Experimental Physics, Slovak Academy of Sciences, Kosice, Slovakia
e-mail:fedunova@saske.sk; bagelova@saske.sk

The study of processes responsible for formation of amyloid fibrils is of interest in several decades, since they are associated with various diseases, such as Alzheimer's and Parkinson's, diseases, type II diabetes or hereditary systemic amyloidosis [1]. Finding that the ability to form amyloid fibrils is generic property of polypeptide chain [2] has extended the focus also on other proteins not related to any diseases. Recently, the amyloid fibrils have been tested as novel biomaterials due to their properties such as elasticity and stability [3]. The specific conditions have been established for direct growth of amyloid fibrils *in vitro* for wide range of proteins pointing out that solvent properties play an important role in controlling of fibrillization process. Recently, novel class of solvents – ionic liquids (ILs) has been used for variety of processes. ILs are organic salts consisting only from ions with melting point below 100 °C. The major advantage of ILs is that their physicochemical properties (density, viscosity, melting point, polarity, etc.) can be tuned by appropriate combination of cations and anions in order to obtain solvent with desired properties [4].

In this work we have studied the effect of two ionic liquids with 1-ethyl-3-methylimidazolium as cation combined with two different anions – tetrafluoroborate (as chaotropic) [$EMIMBF_4$] and acetate (as kosmotropic) [EMIMac] - on kinetics of lysozyme amyloid fibrillization and morphology of formed fibrils. The kinetics of amyloid fibril formation has been monitored by Thioflavin T fluorescence assay and CD spectroscopy. The morphology of lysozyme fibrils were visualized by AFM and analyzed by using modified live-wire algorithm for image analysis [5]. We have found that lysozyme at 2 mg/ml concentration dissolved in acidified water, pH 2.5 and incubated at 65 °C with intensive stirring doesn't transform into fibrils during long time period (more than 8 days). Addition of $EMIMBF_4$ at concentrations from 0.5 % to 5% (v/v) to lysozyme solution (2 mg/ml) leads to formation of amyloid fibrils. The growth curves at all studied concentrations have sigmoidal profile. The lag time decreases with increasing ILs concentrations with simultaneous increase of curve steepness. At the highest ILs concentration (5%) the steady-state fluorescence intensity value is reached at 20 min corresponding to formation of mature fibrils. At the presence of EMIMac, the kinetics pattern is broader with lesser steepness, larger lag phase and longer time needed for achievement of steady-state intensity comparing with $EMIMBF_4$, except for 5% ILs. At this concentration, similar kinetics is observed for both ILs pointing out that at this high concentration probably the ionic strength plays more important role in fibrillization process than ionic liquid character of solvent.

The obtained lysozyme fibrils have been visualized by AFM. For both types of fibrils the twisting typical for amyloid fibrilarstructures is observed. The presence of different types of fibrils was deduced from the height distribution of fibril ridges. Fibrils obtained at 1% the $EMIMBF_4$ at themiddle stage of fibrillation present the widest spectrum of fibril sizes, the filament ridge heights attain 15 nm. Populations of mature fibrils occur in the interval 3-15nm (Fig.1). At the presence of 1% EMIMac, the significant fraction is in the shorter range 3-10nm.

In this work we have found that both used ILs are able to trigger lysozyme fibrillization at low protein concentration at various concentration of ILs. Different nature of used anions has only slight effect manifested by elongated kinetics profile, higher abundance of β-sheet structures for $EMIMBF_4$ and variation of apparent high. Comparing to tetrafluoroborate anion, presence of acetate anion is partially slowing down the process of fibrillization.

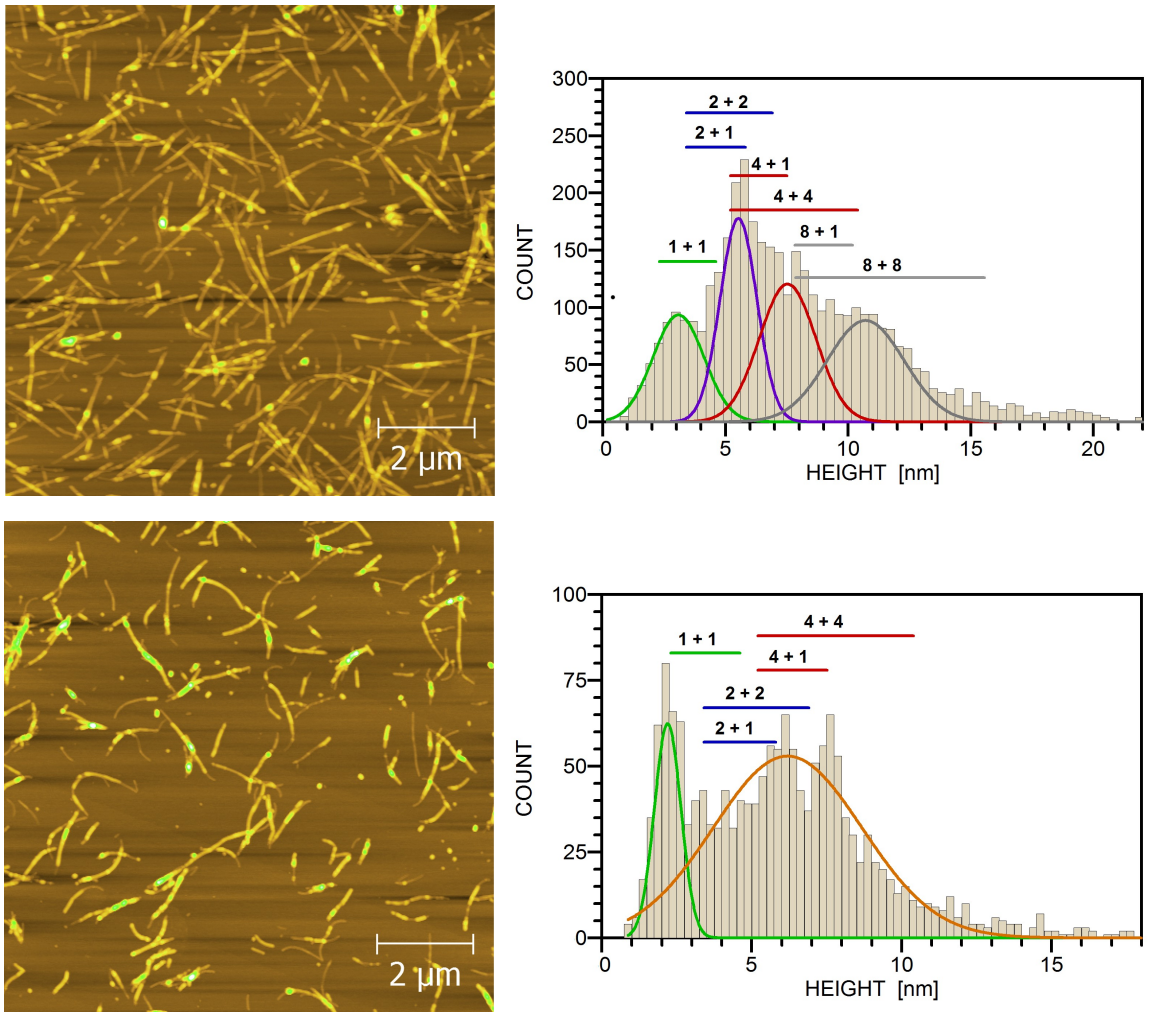

Fig. 1. AFM images of lysozyme fibrils and fibril ridges height distributions at 1% $EMIMBF_4$ (up) and EMIMac (down) (using ~3900 and ~1600 cross sections, respectively). Horizontal lines represent regions of individual fibril types, the numbers above the lines correspond to given assembly model type. Conditions for fibrillization: 2 mg/ml lysozyme pH 2.5, intense shaking, 65°C, and one of ILs.

The induction of fibrillization process is of importance not only for screening of potential therapeutic compounds against amyloid-related diseases, but also for preparation of novel biomaterials.

Acknowledgement

This work was supported by the Slovak Grant Agency VEGA, projects Nos. 2/0176/14, 2/0181/13, 2/0175/14, bythe Slovak Research and Development Agency under the contract No. APVV-0171-10, APVV-0526-11 and ESF projects 26110230061 and 26110230097.

References

[1] D. H. Small, S. S. Mok, J. C. Bornstein, Nat. Rev. Neurosci. 2 (2001) 595–598.
[2] M. Fändrich, C. M. Dobson. EMBO J 21 (2002) 5682 – 5690.
[3] I. Cherny, E. Gazit, Angew. Chem. Int. Ed 47 (2008) 4062-4069.
[4] G. A. Baker, S. Baker, S. Pandey, F.V. Bright, Analyst 130 (2005) 800–808.
[5] J. Marek, E. Demjenova, Z. Tomori, J. Janacek, I. Zolotova, F. Valle, M. Favre, G. Dietler, G. Cytometry Part A 63 (2005) 87-93

Study of interactions between lipid membranes and HIV-derived peptides complexed with carbosilane dendrimers

Z. Garaiová[1], M. Ionov[2], K. Ciepluch[2],S. Melikishvili[1], I. Waczulíková[1], T. Hianik[1], M.A. Muñoz-Fernandez[3], J.F. de la Mata[4], R. Gomez-Ramirez[4], M. Bryszewska[2]

[1] Department of Nuclear Physics and Biophysics, FMFI UK, Mlynska dolina F1, 842 48 Bratislava, Slovakia, e-mail: zuzana.garaiova@fmph.uniba.sk
[2] Department of General Biophysics, Faculty of Biology and Environmental Protection, University of Lodz, Pomorska 141/143, 90-236 Lodz, Poland
[3] Immunomolecular Biology Laboratory, Hospital Gregorio Marañon, Dr. Esquerdo 46, 28007 Madrid, Spain
[4] Inorganic Chemistry Department, University Alcala de Henares, 28871 Alcala de Henares, Spain

Human immunodeficiency virus (HIV) is the retrovirus responsible for AIDS disease which still remains the serious illness worldwide. The AIDS research is currently focused to development of immunovaccines based on dendritic cells (DCs). It has been shown that DCs possess imunostimulatory potential and their application as a vaccine adjuvant holds many promises in the treatment of HIV-1 infection . In order to achieve a therapeutic effect, the antigen – HIV derived peptide should be transported into DCs. However, an efficient carrier is required for delivery the antigen into the cell across the plasma membrane. In this context, highly branched molecules of nanoscopic size - dendrimers are studied .

We have proposed to use carbosilane dendrimers (CBD) of second generation as suitable vehicles for HIV peptide delivery to DCs . We used CBD of two types: CBD of either carbon-silicon bonds (CBD-CS, BDBR0011) or oxygen-silicon bonds (CBD-OS, NN16). Three types of HIV-derived peptides were selected: Nef, P24, Gp160. These peptides complexed with CBDs dendrimers (dendriplexes) were then studied for interactions with membranes of various lipid compositions that model plasma membrane of DCs.

We prepared large unilamellar vesicles (LUVs) composed of zwitterionic dimyristoylphosphatidylcholine (DMPC) and negatively charged dipalmitoylphosphatidyl glycerol (DPPG). Interactions between LUVs and HIV-derived peptides alone or those complexed with CBDs were studied by means of size and zeta potential measurements.

HIV-derived peptides itself in the concentration range of 0.3μM - 6 μMdid not change the size of DMPC LUVs, while the zeta potential slightly decreased upon the exposure of all peptides. In the case of DMPC/DPPG LUVs, HIV-derived peptides did not cause any significant changes in the measured parameters.

HIV-derived peptides complexed with CBD-CS dendrimers moved the zeta potential of zwitterionic DMPC LUVs and negatively charged DMPC/DPPG LUVs towards the positive values. The hydrodynamic diameter of negatively charged DMPC/DPPG LUVs started to significantly increase at CBD-CS dendriplex/lipid molar ratio 0.06. Interactions between HIV-derived peptides complexed with CBD-OS dendrimers and LUVs had similar character to those of CBD-CS dendriplexes. However, the presence of CBD-OS caused more pronounced changes in the measured parameters for both the pure DMPC as well as DMPC/DPPG LUVs.

Acknowledgement
This work was supported by Slovak Research and Development Agency, projects No. SK-PL-0070-12, APVV-0410-10, by Science Grant Agency VEGA (project No. 1/0785/12) and Polish Ministry of Science and Higher Education (Polish-Slovak bilateral grant).

References

[1] M. Pion, M. J. Serramia, L. Dia., M. Bryszewska, T. Gallart, F. Garcia, R. Gomez, F. J. de la Mata, M. A. Munoz-Fernandez.Biomaterials, 31(33) (2010) 8749-58.
[2] J. Peng, Z.Wu, X. Qi, Y. Chen, X. L Molecules, 18(7) (2013) 7912-7929.
[3] M. Ionov, K. Ciepluch, B. Klajnert, S. Glińska, R. Gomez-Ramirez, F. J. de la Mata, M. A. Munoz-Fernandez, M. Bryszewska, Colloids and Surfaces B: Biointerfaces, 101(0) 2013 236-242.

On the interaction of hydrogen sulfide with S-Nitroso-N-acetyl-DL-penicillamine – the involvement of polysulfides

M. Grman[1, 2], K. Ondriaš[2], P. Nagy[3], M. Feelisch[4]

[1] Department of Nuclear Physics and Biophysics, FMFI UK, Mlynská dolina F1, 842 48 Bratislava, Slovak Republic
[2] Institute of Molecular Physiology and Genetics, Slovak Academy of Sciences, Vlárska 5, 833 34 Bratislava, Slovak Republic
[3] Department of Molecular Immunology and Toxicology, National Institute of Oncology, Ráth György utca 7-9, Budapest, Hungary, 1122
[4] Clinical & Experimental Sciences, Faculty of Medicine, University of Southampton, Southampton General Hospital, Tremona Road, Southampton, United Kingdom

e-mail: grman.marian@gmail.com

Hydrogen sulfide (H_2S) and nitric oxide (NO) are two gasotransmitters involved in many (patho)physiological processes [1, 2]. Interaction of NO with thiol groups leads to formation of S-nitrosothiols (RSNOs), which may serve as a bioreservoir for NO [3]. Further, the interaction between H_2S and S-nitrosothiols leads to decomposition of RSNO and formation of "new" product – S-nitrosopersulfide ($ONSS^-$) [4, 5].

In the first part we investigated the effect of polysulfides on the kinetics of S-nitroso-N-acetyl-DL-penicillamine (SNAP) decomposition and of the $ONSS^-$ formation. We studied it under two different conditions – the effect of increasing concentration of polysulfides on the interaction of 200 µM SNAP with 2 mM H_2S and on the interaction of 200 µM SNAP with decreasing H_2S concentration. The experiments were done at physiological pH in the 175 mM Tris/HCl buffer. We found, in both cases, that increasing concentration of polysulfides leads to higher "yield" of $ONSS^-$ and that polysulfides accelerate the $ONSS^-$ formation. We assume that polysulfides are crucial in the formation of $ONSS^-$, they serve as intermediate in RSNO-H_2S interaction and they are the "starting point" for the formation of $ONSS^-$.

In the second part we studied the decomposition of $ONSS^-$ in time. We found (by cold cyanolysis, by the monobromobimine based method and reverse phase chromatography and by the methylene blue method) that this decomposition leads mainly to generation of polysulfides coming from the decomposed $ONSS^-$ and a small concentration of H_2S. Presented results can contribute to better understanding of the biological effect of $ONSS^-$ in the living organisms.

Acknowledgement
This work was supported by the Slovak Grant Agency VEGA 2/0050/13, by the Slovak Research and Development Agency under the contract No. APVV-0074-11 and by UK/524/2014.

References

[1] Z. Tomaskova, A. Bertova, K. Ondrias, Curr. Pharm. Biotechnol. 12(9) (2011) 1394-1405.
[2] G.K. Kolluru, X. Shen, C.G. Kevil, Redox Biol. 1(1) (2013) 313-318.
[3] J.S. Stamler, O. Jaraki, J. Osborne, D.I. Simon, J. Keaney, J. Vita, D. Singel, C.R. Valeri, J. Loscalzo, Proc. Natl. Acad. Sci. U. S. A. 89(16) (1992) 7674-7677.
[4] K. Ondrias, A. Stasko, S. Cacanyiova, Z. Sulova, O. Krizanova, F. Kristek, L. Malekova, V. Knezl, A. Breier, Pflugers Arch. 457(2) (2008) 271-279.
[5] F. Seel, M. Wagner, Z. Naturforsch. 40(6) (1985) 762-764.

Intensity of Electric and Magnetic Fields at School Environment

H. Habiňáková[1], D. Špigúthová[1], V. Jakušová[2], J. Jakuš[1]

[1] Institute of Medical Biophysics, Jessenius Faculty of Medicine in Martin, Slovakia
[2] Institute of Public Health, Jessenius Faculty of Medicine in Martin, Slovakia

Assessment of a level of electromagnetic smog at school environment becomes more important due to a growing number of technical equipments which are employed at schools (e.g. Wi - Fi routers, computers , mobile phones etc.).

In a period of Nov. - Dec. 2013 we recorded the level of intensity of electric field **E** (V / m) and magnetic field **H** (A / m) at school environment in the Grammar School of V. Pauliny-Toth in Martin. Using RadMan XT ESM-30 device we performed 45 dosimeter measurements during the working days with a length of each measurement being 30 minutes in 10-second intervals. Frequency range of electromagnetic field (EMF) of the dosimeter for**E** was 1 MHz - 40 GHz and for **H**: 27 MHz - 1 GHz. We observed the main characteristics of the EMF during elevated exposures (23 measurements), and when measured the exposure under standard conditions (22 measurements).The average measured value for **E** was 6.125 ± 0.017 (%) and for **H** 5.463 ± 0.016 (%) of the standard law value. The statistical evaluation proved an increase in intensity of the EMF for the group of higher exposure compared to a group with standard exposure. This is presented as a graphical evaluation of the maximum, average and minimum intensities of both EMFs. However, our results showed that all our measured values were lower than the law limit values given for exposure to EMF valid for population [1]. As given by law No 325/2006 non-harmfull power density of EMF is accepted up to 10 W/m^2.

The results of our dosimetric measurements at school environment confirm that level of electromagnetic radiation increases with an increase of the radiofrequency operated devices. Detection and comparison of EMF parameters can anticipate a potential health risk for young people taking a quite long time in a space polluted by electromagnetic smog [2].

Acknowledgement
This work was supported by the Slovak Research and Development Agency under the contract No. APVV-0189-11"(prof. Jakuš)

References

[1] Law no. 325/2006 Z.z. from the Collection of Laws of the Slovak Republic of 31 May 2006 specifying requirements for sources of electromagnetic fields and limits of the exposure of inhabitants to electromagnetic fields in the environment.
[2] WHO / IARC, 2011. *International Agency for Research on Cancer classifies radiofrequency electromagnetic fields as possibly carcinogenic to humans.* [online] [2012-10-5] Available at: http://www.iarc.fr/en/mediacentre/pr/2011/pdfs/pr208_E.pdf

Application of molecular acoustics and atomic force spectroscopy for study of molecular interactions at surfaces

T. Hianik[1], A. Poturnayová[1,2], M. Šnejdárková[2], I. Karpišová[1], M. Leitner[3], A. Ebner[3]

[1] Department of Nuclear Physics and Biophysics, FMFI UK, Mlynska dolina F1, 842 48 Bratislava, Slovakia, e-mail: tibor.hianik@fmph.uniba.sk
[2] Institute of Animal Biochemistry and Genetics, Slovak Academy of Sciences, 900 28 Ivanka pri Dunaji, Slovakia
[3] Institute of Biophysics, Johannes Kepler University, A-4020 Linz, Austria

The study of molecular interactions at surfaces is important for solution of many biophysical problems. It is for example the study of the mechanisms of recognition processes between the ligands (for example hormones) and their cell receptors or the mechanisms of interaction nanoparticles with cell membranes, which is important for targeted drug delivery. This is also important for optimization recognition properties of biosensors, which are based on receptors immobilized at the surfaces. Among powerful techniques allowing to study of these processes are molecular acoustic based on analysis of thickness shear oscillation of quartz crystal (TSM) modified by biolayer at its surface. The interaction of the molecules of interest with receptors immobilized on the surface of TSM transducer resulted in changes of oscillation frequency. However, due to interaction of the biolayer with surrounding solvent also surface viscosity contributes to the changes of oscillation frequency. Therefore special technique is required for analysis of these processes [1]. Currently the molecular imaging techniques, such as atomic force microscopy (AFM) are commonly used for characterization of surfaces with atomic resolution. This technique in combination with TSM allowing to obtain more complex picture of the mechanisms of molecular interactions at surfaces. In addition the single molecule force spectroscopy (SMFS) [2] gives possibility to study with high precision the molecular forces between the receptor immobilized at AFM tip and the molecules of interest immobilized at the surfaces. The molecular forces in pN scale can be measured. In this contribution several examples of application of TSM, AFM and SMFS methods for analysis of the interactions between receptors and ligands at various surfaces will be presented. Special focus will be on the interaction between DNA aptamers or calixarenes immobilized at surfaces and the proteins added to the surfaces or immobilized at the AFM tip.

Acknowledgement
This work was supported by Slovak Research and Development Agency, projects No. SK-AT-0009-12, APVV-0410-10 and by Science Grant Agency VEGA (project No. 1/0785/12)

References

[1] T. Hianik, I. Grman, I. Karpisova, Chem. Commun. 41 (2009) 6303-6305.
[2] I Neundlinger, A. Poturnayova, I. Karpisova, C. Rankl, P. Hinterdorfer, M. Snejdarkova, T. Hianik, A. Ebner, Biophys. J. 101 (2011) 1781–1787.

Multimodal fluorescence detection of cancer

J. Horilova [1,2], A. Mateasik [1], I. Cavarga [3], P. Mlkvy [3], M. Cagalinec [4] , A. Kaasik [4], D. Chorvat[1], A. Marcek Chorvatova[1]

[1] Dep. of Biophotonics, International Laser Centre, Ilkovicova 3, 841 04 Bratislava, Slovakia
[2] Dep. of Biophysics, Faculty of Science, P. J. Safarik University, Jesenna 5, 04154 Kosice, Slovakia
[3] Oncology Institute of st. Elisabeth, Heydukova 10, 81250 Bratislava, Slovakia
[4] Dep. of Pharmacology, University of Tartu, Ravila 19, 50411 Tartu, Estonia
e-mail: j.horilova@gmail.com

Introduction. Early cancer detection is crucial for its successful diagnostics and treatment. Multimodal optical imaging of suspected tissues is showing to be a very promising method. Combination of steady-state spectroscopic methods with time-resolved approach provides more precise insight into native metabolism, when focused on tissue autofluorescence [1]. Cancer is linked with increased metabolic activity, higher demand for nutrients and thus increased accumulation of metabolites. In this work, endogenous fluorescence of protoporphyrin IX (PpIX) was induced with administration of aminolevulinic acid (δ-ALA). δ-ALA is the first compound needed for porphyrin synthesis leading to heme production [2]. In clinical diagnosis, δ-ALA is used in photodynamic diagnosis (PDD) of neoplastic tissue that exhibit increased accumulation of PpIX after δ-ALA administration (Fig. 1). However, similar fluorescence pattern is often observed also in inflammatory processes, so new approaches are needed to be adopted in measurement and analysis of PpIX fluorescence to make PDD more sensitive in cancer detection [3].

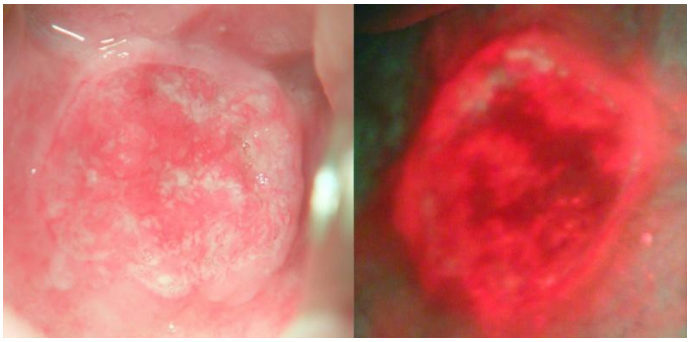

Fig. 1: Photodynamic diagonosis of neoplastic tissue in oral cavity – (left) neoplastic tissue in white light, (right) the PpIX fluorescence of tissue 1h after δ-ALA administration

Materials and methods. Homozygous female nude mice (Hsd:AthymicNude-Foxn1nu (Harlan), 8 weeks old), bearing U87-MG tumor xenografts subcutaneously. 1×106 U87-MG cells were resuspended in 100 µl of fresh DMEM medium (Gibco Invitrogen), without serum and antibiotics. The xenografting was performed by implanting the cell suspension subcutaneously in the left flank region. 250 mg/kg of 50 mg/ml δ-ALA (Sigma) solution in PBS was injected into mice intraperitoneally. Mice were anesthetized with 3% isoflurane and maintained in anesthesia with 1.75 – 2% isoflurane up to 1 hour. Scans were performed before injection as a baseline, 5 min, 1.5 hour and 3 hours after injection using time-resolved tomography MX3 system (ArtOptix) detecting PpIX with 480 nm excitation and detection window 600 – 650 nm [1].

Results. Immediately after injection, δ-ALA–induced PpIX synthesis begins to accumulate in tumor up to cca 180 min, when PpIX concentration in tissues reaches maximal levels, as it can be seen on the graph. Values of fluorescence intensity were obtained from regions of interest in respect to tumor topography.

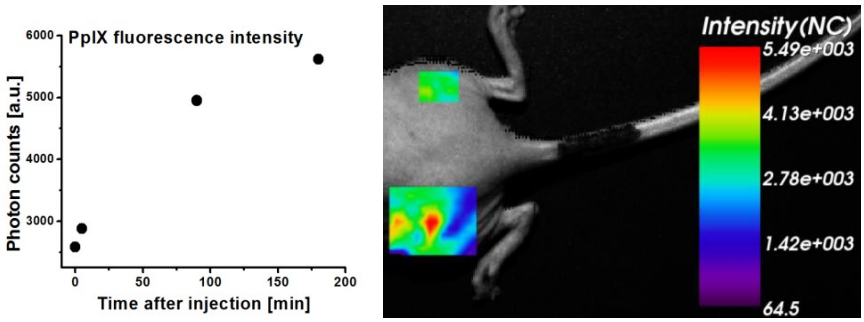

Fig. 2: Left, PpIX autofluorescence intensity with time after δ-ALA injection. Average values of fluorescence intensity were obtained from regions of interest in respect to tumor topographic location. Right, intensity scan of PpIX fluorescence performed 1.5 hour after injection of δ-ALA.

Moreover, using time-resolved scan, fluorescence lifetime (τ < 0.5 ns) of PpIX in tumor region showed to be shorter than in healthy tissue (Fig. 3 left). This observation is in agreement with PpIX lifetimes estimated *in vitro* (Fig. 3 right), and can significantly improve the ability to distinguish tumorous tissues from healthy ones.

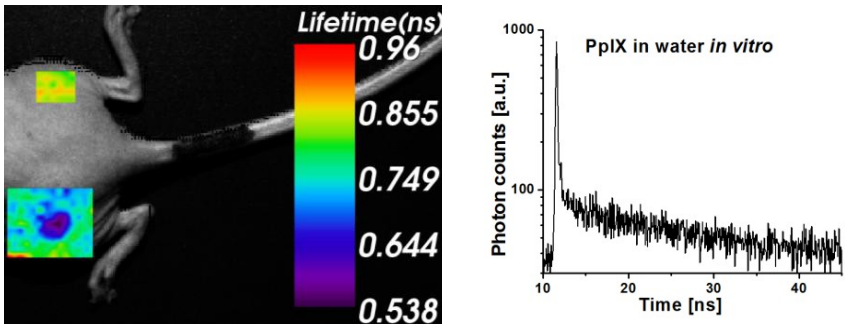

Fig. 3: Left, example of PPIX fluorescence lifetime image scanned 1.5 hour after δ-ALA injection. Right, PPIX fluorescence decay recorded in pure water.

Conclusion. δ-ALA-induced time-resolved fluorescence of PpIX in U87-MG tumor was recorded using the MX3 system in living mice. Despite the fact, that MX3 is not originally optimized for autofluorescence detection, we were able to record the *in vivo* autofluorescence and even fluorescence lifetimes with acceptable goodness of fit (χ^2<1.2). Increase of PpIX fluorescence intensity in time was observed reaching its maximal concentration in approximately 180 minutes after injection of δ-ALA. Shorter fluorescence lifetime of PpIX in tumor was detected. Combination of steady-state spectroscopy of δ-ALA – induced PpIX autofluorescence with time-resolved detection showed to be an useful tool for detection of cancerous changes in tissues and is also a perspective tool in the clinical diagnostics and treatment.

Acknowledgements
This work was supported by: Slovak Research and Development Agency under the contract APVV-0242-11, the European Social Fund's Doctoral Studies and Internationalisation Programme DoRa5. We would like to thank Miriam Ann Hickey for technical help with the MX3 system and Kent Langel for kindly providing homozygous female nude mice from University of Tartu, Estonia.

References

[1] Berezin MY & Achilefu S (2010). Fluorescence Lifetime Measurements and Biological Imaging. *Chemical Reviews* 110, 2641-2684
[2] Ajioka RS, Phillips JD, & Kushner JP (2006). Biosynthesis of heme in mammals. *Biochim Biophys Acta* 1763, 723-736

[3] Smolka J, Mateasik, Cunderlikova B, Sanislo L, Mlkvy P (2006) In vivo fluorescence diagnostics and photodynamic therapy of gastrointestinal superficial polyps with aminolevulinic acid. A clinical and spectroscopic study, *Neoplasma* 53, 418-23

Simulated manifold learning for image analysis and visualization -exploration of the potential of Langevin dynamics

D. Horváth, J. Uličný

Center of Interdisciplinary Biosciences, P. J. Šafárik University, Košice, Slovakia,
email: denis.horvath@upjs.sk

One of the main tasks in exploratory data analysis is to crate appropriaterepresentation for complex and high-dimensional data. Such data collection can becreated, for example, in the case of non-crystalline diffractive techniques. To achievehigh resolution one must solve a phase-retrieval inverse problem by including many subimages or high-dimensional structured signal from many photon counting pixel detectors[1]. Because of the low number of degrees of freedom expected, such numerical dataclouds may be viewed as low-dimensional manifolds.

A wide range of manifold learning (ML) methods [2] has been employed with theultimate goal to find nonlinear dimensionality reduction of multi-dimensional datasetsinto 2D or 3D space. Mathematically these problems may be termed as NP complete.However, living most most restrictive assumptions, various heuristic and approximatealgorithms have been suggested. Examples are: Principal component analysis (PCA),Multidimensional scaling (MDS), ISOMAP, generalized topological mapping (GTM),Local Linear Embedding (LLE), Laplacian Eigenmaps, Hessian-based LLE, LocalTangent Space Alignment (LTSA). While such techniques produce near-optimumsolutions, there is therefore requirement for suffciently robust and powerfuloptimization.

Here we revisit the problem of ML from two main perspectives. First, we will focuson the construction of Langevin/Brownian dynamics of translational motions of virtualparticles in 2D. Their configuration consists of the coordinates acquiring the meaning ofthe 2D projection of the original data. Second, we are dealing with the accuracy anduniqueness attained by means of stochastic search metaheuristics - simulated annealing[3] in the presence slowly decaying diffusion noise term.

The key "physical terms" which specify the dynamics and also properties of thetarget mapping are inter-particle potential forces. Their form is designed so as to reacton the discrepancies caused by the numerous conditions placed on the mapping. Morespecifically, the interaction force can be assumed to be proportional to disparities (ordistances) of the original data and distances in low dimensions.

References

[1] D. Giannakis, P. Schwander, A. Ourmazd, Optics Express, 20 (2012) 12799-12826
[2] L.J.P van der Maaten, E.O.Postma, H.J. van den Herik, Dimensionality Reduction: AComparative Review, Tilburg University Technical Report, TiCC TR 2009-005
[3] L. Ingber, Mathl. Comput. Modelling, 18 (1993) 29-57

Effect of cell electromotive potential on cell impedance in cardiac myocytes.

M. Hoťka [1, 2], I. Zahradník [1]

[1] Institute of Molecular Physiology and Genetics, Slovak Academy of Science, Bratislava, Slovakia
[2]Department of Biophysics, Faculty of Science, Pavol Jozef Šafárik University, Košice, Slovakia.

A typical model of the passive cell membrane impedance is represented by a capacitance C_M in parallel with a conductance G_M. In contrast to their typical physical equivalents, the cell impedance is not stable but varies due to various cell activities. Changes in the membrane capacitance reflect changes in the cell surface membrane area and the membrane conductance reflects activity of its ion channels. We studied the impedance of isolated cardiac myocytes to reveal relations between impedance variation and physiological states of myocytes. Cardiac muscle cells are large cells with the typical capacitance of 100 – 200 pF given by high spatial dynamics of its surface membrane (sarcolemma). This membrane is rich in ion channels that are often collocated with specific sarcolemmal structures. Simultaneous changes of C_M and G_M may thus reflect, for instance, dynamics of coupling of transverse tubules to the surface sarcolemma. Conventional methods used for monitoring impedance parameters rely on assumptions that the cell current response to a voltage step pulse is represented by a single time constant [1] [2]. This is not the case in cardiac myocytes. These cells often exhibit large conductance changes due to changes in activity of various ion selective channels, which may result in variation in an effective value of the reversal potential of the membrane current. Such changes in membrane conductance may also cause the false changes in membrane capacitance due to cross-correlations between values of measured impedance components. We focused here on identification of contributions of various types of cell conductances to the time constant of the cell equivalent electrical circuit. Our method is based on stimulating the cell by bipolar square-wave voltage stimuli that elicit exponential current responses, I_M. We developed a new algorithm for separation of the electrical charge charging the cell membrane capacitance and the charge flowing through the conductive branch of the membrane. This allowed us to observe how the impedance parameters and the reversal potential of the cell change in time. We found that changes in membrane conductance affect behavior of the equivalent circuit in dual way. The first, nonselective, type of change of membrane conductance does not alter the membrane capacitance estimate and it does not alter the reversal potential of the membrane current. The second, ion-selective type of change of membrane conductance affects the C_M estimate due to the positive cross-correlation to Gm and changes the reversal potential that adds to the imposed membrane potential. By integration of I_M response for calculation of membrane capacitance, we could track the amount of charge transferred during charging of the membrane. As the time constant of the current response remains unchanged, the transferred electrical charge stays the same as well and results in false estimate of the membrane capacitance. Thus the equivalent circuit with only nonselective conductive path is not sufficient to describe such a change. Therefore, we propose to use the equivalent circuit shown in *Figure 1* with one conductive branch representing the basal nonselective conductance G_M and the additional conductive branch with a source of the electromotive force representing a dis-balance in ion-selective conductances G_S. In the case that the conductance of this branch is zero no current flows through this branch and the cell can be represented by a standard equivalent circuit. When conductance of this branch rises, the battery becomes connected to the circuit and alters the voltage through the conductive branch, so the cell would be better represented by the proposed extended circuit.

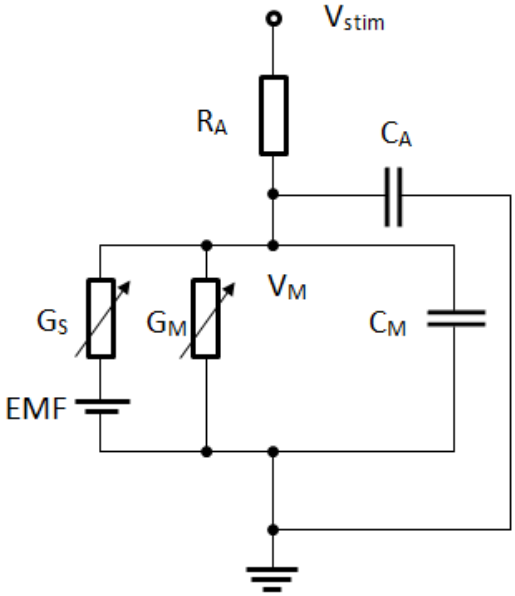

Figure 1: *Extended equivalent circuit of cell impedance in whole-cell configuration*
The cell impedance is represented by the membrane capacitance C_M, by the non-selective membrane conductance G_M and by the ion-selective membrane conductance G_S in series with electromotive force EMF generated by ion concentration gradient. Access resistance R_A and the pipette capacitance $C_P$represents the cell-pipette interface. As the ion-selective conductance G_S raises the battery representing the electromotive force EMF alters the membrane voltage V_M.

Acknowledgement
This work was supported by the Slovak Grant Agency VEGA, project No. *2/0203/11,* VEGA, project No. *2/0147/14*

References
[1] Novák, P., Zahradník, I., Ann Biomed Eng. 34, 2006, 1201-1212.
[2] Lindau M, Neher E., Pflugers Arch. 1988 Feb;411(2):137-46.

Temperature and voltage dependence of membrane capacitance in cardiac myocytes

M. Hoťka[1,2], I. Zahradník[1]

[1]Institute of Molecular Physiology and Genetics, SAS, Vlárska 5, 833 34 Bratislava, Slovakia, e-mail: ivan.zahradnik@savba.sk, [2]Department of Biophysics, Faculty of Science, UPJŠ, Košice, Slovakia.

Brief irradiation of a spot of neuronal tissue by an infrared laser pulse causes activation of an action potential and excitation of the tissue. The effect of laser stimulation was explained by a local rise of temperature that increases the cell membrane capacitance [1]. The abrupt change in capacitance causes fast redistribution of membrane charge that depolarizes the membrane and triggers an action potential. Here we study the temperature dependence of the membrane capacitance of cardiac myocytes, which also form an excitable tissue, with the aim to verify the general application of the theory of laser stimulated tissue excitation.

The relationship between membrane capacitance and temperature in cardiac myocytes is not known. Therefore, we studied the dependence of membrane capacitance on the bath temperature in isolated myocytes obtained from left ventricular and atrial tissue of rat myocardium. An isolated myocyte was whole-cell patch clamped and its membrane capacitance was measured by means of the high-resolution square wave stimulation method [2] using an improved algorhitm [3] with a resolution of about 10 fF at 20 Hz. The temperature of the bath (Tyrode solution) was increased by 3 to 10 ºC using a home-made temperature controller from starting temperatures ranging from 14 to 25 ºC to final temperatures of 17ºC – 33ºC at a rate of 0.1ºC/s. The temperature increase caused no mechanical activity and no change in the shape of myocytes. Experiments at -50 mV provided an increase of the cell capacitance by 0.29 ± 0.01 %/ºC. The temperature-dependent increase of membrane capacitance was the higher, the higher was the cell capacitance (R=0.81). The effect of temperature on membrane capacitance was reversible and reproducible on the same cell. The membrane capacitance was voltage dependent. At 0 mV it was by 4.0 ± 0.01 % less than at -50 mV, however, the temperature dependent increase was 0.4 ± 0.02 %/ºC, slightly higher than at -50 mV. There were no significant differences between data obtained on atrial and ventricular myocytes.

The presented data are in quantitative agreement with published data obtained in HEK cells and in bilayers [1]. Therefore, we may conclude that the effect of temperature on cell capacitance in cardiac myocytes is similar to that in other tissues. This study provides an independent confirmation of the theory of laser stimulation of excitable tissue.

This work was supported by the Slovak Research and Development Agency under the contract No. APVV-0721-10 and by the Slovak Grant Agency VEGA 2/0203/11 and VEGA 2/0147/14.

References

[1] Shapiro et al., Nat. Commun. 3:736, 2012A.
[2] Novák and Zahradník, Ann. Biomed. Eng. 34:1201, 2006
[3] Hoťkaand Zahradník, Fluctuation Analyzer, SourceForge, 2013

Highly sensitive *in vivo* pO_2 detection by luminescence lifetime of photosensitive probes

V. Huntošová[1], P. Miškovský[1,2], G. Wagnières[3]

[1]Centre of Interdisciplinary Biosciences (CIB), PF UPJS, Jesenná 5, 041 01 Košice, Slovakia.
[2]Department of Biophysics, PF UPJS, Jesenná 5, 041 01 Košice, Slovakia.
[3]ISIC-LCOM, EPFL, Batiment CH, Station 6, CH-1015 Lausanne, Switzerland.
e-mail: veronika.huntosova@upjs.sk

The non-invasive measurement of tissue oxygenation is challenging and has been addressed by numerous research groups for decades. Tissue hypoxia can be caused by a number of factors [1]. Besides photodiagnostics and phototherapy, a measurement of oxygen partial pressure (pO_2) provides valuable fundamental information regarding the tissue respiration [2].

Generally two main methods are used for pO_2 measurement in tissue: Eppendorf polarographic needle electrodes and optical fiber-based sensors [3]. Both methods are based on the use of needles or interstitial catheters with diameters in the order of several hundreds of microns. Consequently, in vivo measurements with these methods induce tissue damage or modification. Following the development of sensitive and non-invasive time-resolved optical spectroscopic techniques based on the oxygen-dependent luminescence quenching of molecular probes, a third methods is now available, whereby the level of oxygenation can be measured quantitatively and minimally invasively at selected sites. Time-resolved luminescence detection techniques to measure pO_2 are in general more reliable than luminescence intensity-based methods, because luminescence lifetime does not depend on the concentration of a probe. Unfortunately, most of these luminescent oxygen probes are phototoxic, due to the production of singlet oxygen in the quenching process of their triplet state [4]. This phototoxicity leads to tissue damage, including vascular damage, during the pO_2 measurements.

In this work we demonstrate a variety of *in vivo* application and detection of hydrophobic (Protoporphyrin IX) or hydrophilic (dichlorotris(1,10-phenanthroline)-ruthenium(II) hydrate) probes in the chicken embryo chorioallantoic membrane model. The relation between the tissue pO_2 and the probes' luminescence lifetime is governed by the Stern-Volmer equation. In our approach the luminescence lifetimes of the probes were measured with a highly sensitive dedicated optical fiber-based, time-resolved spectrometer [5] without photo-damage of examined tissue.

Acknowledgement
This work was supported by the SCIEX-NMS^{ch} project N° 10.142 and by the project CELIM316310 funded by EU 7FP.

References
[1] JB. West, Respiratory physiology-the essentials, Blackwell Scientific, Oxford, etc. (1974)
[2] EG. Mik, J. Stap, M. Sinaasappel, JF. Beek, JA. Aten, TG. van Leeuwen and C. Ince, Nat Methods 3 (2006) 939-945
[3] DR. Collingridge, WK. Young, B. Vojnovic, P. Wardman, EM. Lynch, SA. Hill and DJ. Chaplin, Radiat Res. 147 (1997) 329-334
[4] TK. Stepinac, SR. Chamot, E. Rungger-Brandle at al., Invest Ophthalmol Vis Sci. 46 (2005) 956-966.

[5] F. Piffaretti, K. Santhakumar, E. Forte et al., J Biomed Opt. 16 (2011) 037005

Perspectives of nonlinear optical imaging in cardiovascular research

D. Chorvát[1,2], M. Uherek[1,2] A. Mateašík[1], A. Marček Chorvátová[1]

[1]International Laser Centre, Ilkovičova 3, 84104 Bratislava, Slovakia.
[2] Department of Nuclear Physics and Biophysics, FMFI UK, Mlynská dolina F1, 842 48 Bratislava, Slovakia, e-mail: chorvat@ilc.sk

Introduction

Since the discovery of confocal laser scanning microscopy (CLSM), a number of new approaches for imaging of unstained cells and tissues have been developed. Examples of such techniques [1,2] include second-harmonic generation (SHG) imaging, or fluorescence lifetime imaging (FLIM). In this study we utilized SHG and FLIM with the aim to visualize structural and functional changes in rat aorta, accompanying cardiovascular disease development (CVDD).

SHG imaging is an emerging microscopy technique, particularly well suited to visualize collagen fibers in unstained tissue due to its high second order nonlinear susceptibility. Its intrinsically noninvasive nature offers great advantage over other histological methods (e.g. Sirius Red staining) and potential for clinical use as *in-vivo* / *ex-vivo* biopsy. This approach is also promising for evaluation of pharmaceutical drugs for future functional cure of CVD.

Materials and Methods

Segments of aorta (ranged from 1 to 3 cm) were isolated from i) healthy (control) adult male Wistar rats (10 weeks), ii) hypercholesterolemic animals on 4% cholesterol and 10% pork unguent diet (10 weeks), and iii) rats with Diabetes mellitus, induced by streptozotocin (8 weeks). Samples were transferred in a physiological buffer solution (max. 2hours at 4 ºC), stored in formaldehyde, protected from light and measured *in vitro*. Sample preparations and measurements were carried out at room temperature. All animals were weighted and monitored for blood glucose and triacylglycerol (TAG) concentration during the experiment. Spatial distribution of SHG and 2P-excited fluorescence was imaged by microscopy workstation based on femtosecond mode-locked ytterbium laser (1038nm, t-pulse 20, Amplitude Systemes), coupled to LSM 510 META NLO microscope (Zeiss) and TCSPC electronics (SPC 830, Becker-Hickl) at ILC, Bratislava, or using a proprietary CLSM microscope with Ti:Sa excitation (Chameleon, Coherent), SHG detection and TCSPC detector subsystem (Becker-Hickl) at LENS, Firenze.

Results

We investigated structural changes induced in the rat aorta wall by cholesterol-rich diet or by diabetes. We tested the potential of simultaneous SHG and 2-photon excited FLIM to study distribution of metabolic markers (NADH, flavins) together with structure of collagen fibers.

SHG imaging

In the aorta wall of rats fed with the cholesterol-rich diet we observed increased thickness of tunica intima and not significant differences in structural organization of collagen. The aortas from diabetic rats show the opposite - decreased SHG signal and increased disorganizationof collagen fibers. For semiquantitative comparison of image properties we used 2D FFT plots and numerical analysis of intensity distribution (kurtosis and skewness). 3D confocal datasets

were first deconvolved according to [3]. Gathered preliminary results are given at Fig.1. Rats fed with the cholesterol-rich diet show increased thickness of tunica intima in the aorta wall, slight increase of SHG signal and certain degree of structural reorganization of collagen. Diabetic rats show decrease of SHG signal amplitude (related to collagen mass and/or structure) and less apparent structural reorganization of collagen fibers.

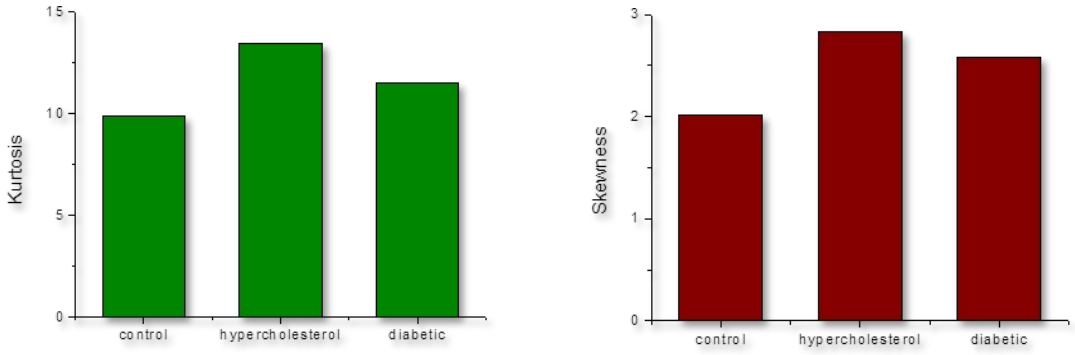

Figure 1. Analysis of intensity distribution in the SHG images (Left - Excess kurtosis, right - sample skewness).

Fluorescence lifetime imaging

In addition to SHG we recorded fluorescence lifetime images of the rat aortas after 2-photon excitation by femtosecond laser. Fluorescence lifetime histogram show distinct difference between diabetic vs. control animals with a shift of mean fluorescence lifetime to lower values, while the high-cholesterol samples show only slight broadening and no significant change of the lifetime distribution centre.

Summary

In this study we showed feasibility of quasi-simultaneous recording of SHG and AF-FLIM images of *in vitro* samples from rat aorta, allowing to detect spatial distribution of collagen and NADH / flavin molecules. We tested dedicated computational algorithms to increase resolution and quantitatively characterize recorded images. The developed approaches can significantly advance our understanding of changes in collagen organization and functional changes in rat aorta wall, accompanying development of cardiovascular diseases.

Acknowledgement

Supported by projects APVV-0242-11, LASERLAB-EUROPE III (7FP n°284464) and NanoNet2 (OPRD-RFRD fund, ITMS n°26240120018). Authors acknowledge collaboration with Dr. Riccardo Cicchi and prof. Francesco Pavone, European Laboratory for Non-linear Spectroscopy (LENS) Florence, Italy, within the frames of EuroBioImaging Proof-of-concept studies. The sample preparation and animal handling was done in collaboration and uder supervision of Comenius University in Bratislava, Faculty of Mathematics, Physics and Informatics.

References

[1] Wallace S.J. et al., J Biomed Opt 13:064018; 2008
[2] Chorvat D. jr. and Chorvatova A., Laser Physics Letters 6(3): 175-193; 2009
[3] Topor et al., J.Microscopy 243(3):293, 2011

EPR detection of radical(s) in cytochrome c oxidase

D. Jancura[1,2], M. Fabian[2,3]

[1] Department of Biophysics, Faculty of Science, Safarik University, Kosice, Slovakia
[2]Center for Interdisciplinary Biosciences, Faculty of Science, Safarik University, Kosice, Slovakia
[3]Department of Biochemistry & Cell Biology, Rice University, Houston, USA
e-mail: daniel.jancura@upjs.sk

Cytochrome c oxidase (CcO) is an integral membrane protein which catalyzes the reduction of oxygen to water and additionally pumps protons across the mitochondrial inner membrane. The net reaction can be written as follows:

$$4\ c^{+2} + 8H^{+}_{i} + O_2 \rightarrow 4\ c^{+3} + 2\ H_2O + 4\ H^{+}_{o}$$

where c^{+2} and c^{+3} represents reduced and oxidized form of cytochrome c, respectively, H^{+}_{i} denotes protons taken up from the matrix phase and H^{+}_{o} is referring to protons released into cytosolic phase of mitochondria [for recent reviews see 1-3].

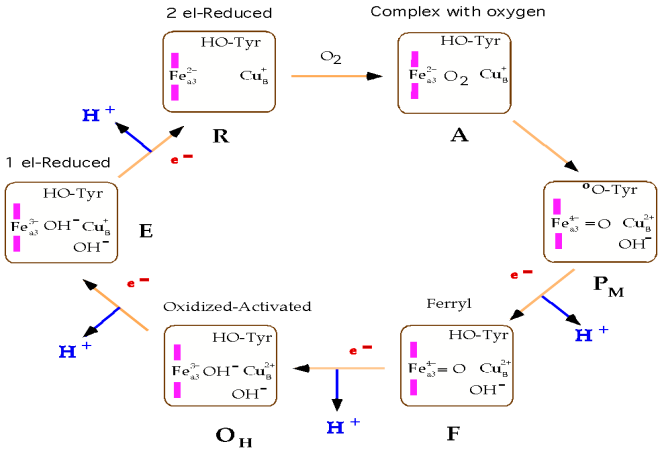

Fig. 1.Catalytic mechanism of CcO. The binuclear Fe_{a3}-Cu_B center reduced by two electrons (**R**) makes complex with oxygen (**A**). This biding step is followed by sequence of electron donations to oxygen with a formation of 'peroxy' (**P**) and ferryl (**F**) intermediates, and oxidized enzyme ($\mathbf{O_H}$). Tyr244 is oxidized to neutral radical (Tyr-O') in the **P** state. Blue arrows represent the coupling of redox reactions with a proton pumping.

Catalytic mechanism of CcO (Fig. 1) involves formation of the intermediates **P** (peroxy) and **F** (ferryl). The production of these intermediates is accompanied by a generation of protein-based radical(s). Additionally, some models of proton pumping predict the participation of protein-based radical(s) either in proton translocation or in the gating of protons through the protein matrix [4, 5]. The reaction of the oxidized CcO with hydrogen peroxide [6, 7] as well as mixed-valence (MV.CO) complex with the oxygen [8, 9] also lead to a formation of **P** (and **F**) and corresponding radical species. However, the application of electron paramagnetic spectroscopy (EPR) to detect such radical(s) has resulted only in the observation of low amounts of radical relative to the concentration of the **P** intermediate (no more than 10 %) [6, 7]. A possible reason for this fact is a coupling of the unpaired electron of radical with the paramagnetic metal center(s) within the catalytic site of CcO.

We have developed a new approach, a moderate destabilization of the enzyme structure by protein denaturant, guanidinium chloride (Gnd.Cl), to detect stoichiometric amount of the radical in CcO. In this situation, a coupling between protein-based radical and a metal center(s) is broken. As our results show, the yield of the free radical EPR signal (g=2.0023) observed in **P** form(prepared by the reaction of the 2-electron reduced CcO with O_2 as well as by the interaction of the oxidized enzyme with H_2O_2)is significantly increased in the presence of Gnd.Cl relative to that in the absence of denaturant. In a sample with 2 M Gnd.Cl, the yield of the detected radical reached ~50% of the **P** population. The origin of EPR detected radical(s) and their possible roles in the catalytic cycle of CcO is discussed.

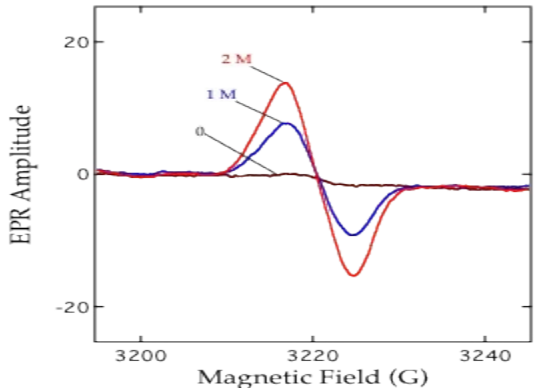

Fig. 2. An enhancement of the g= 2.0023 EPR radical signal in the **P** state of CcO in the presence of 0, 1 and 2 M guanidinium chloride.

Acknowledgement
This work was supported by the Agency of the Ministry of Education of Slovak Republic for the Structural funds of the European Union, Operational program Research and Development (NanoBioSens, ITMS code: 26220220107, SEPO II, ITMS code: 26220120039, and CEVA II, ITMS code: 26220120040 and the project CELIM (316310) funded by7FP EU (REGPOT).

References
[1] M. Wikstrom, Biochim. Biophys. Acta 1817(2012) 468-475.
[2] S.A. Siletsky, A.A. Konstantinov, Biochim. Biophys. Acta 1817 (2012) 476-488.
[3]. S. Ferguson-Miller, C. Hiser, J. Liu, Biochim. Biophys. Acta 1817 (2012) 489-494.
[4] S. de Vries, Biochem. Biophys. Acta 1777 (2008) 925-928.
[5] F.G. Wiertz, O.M.H. Richter, B. Ludwig, S. de Vries, J. Biol. Chem. 282 (2007) 31580-31591.
[6] F. MacMillan, A. Kannt, J. Behr, T. Prisner, H. Michel, Biochemistry 38 (1999) 9179-9184.
[7] P.R. Rich, S.E.J. Rigby, P. Heathcote, Biochim. Biophys. Acta 1554 (2002) 137-146.
[8] P. Nicholls, Biochem. J. 175 (1978) 1147-1150.
[9] P. Nicholls, P. Chanady, Biochim. Biophys. Acta 634 (1981) 256-265.

Across the world with Raman spectroscopy: From the research laboratory to the museum exposition, from the artworks to the organic molecules

Z. Jurašeková[1]

[1] Department of Biophysics, Faculty of Sciences, University of P. J. Safarik, Jesenna 5, 041 54 Kosice, Slovakia
e-mail: zuzana.jurasekova@upjs.sk

Raman spectroscopy, discovered in 1928 by Chandrasekhara Venkata Raman, is the inelastic scattering of light by matter, from molecules to crystals. The effect is highly sensitive to the physical and chemical properties of the scattering material as well as to any environmental effect. Since the technique is relatively simple to perform and require relatively simple or no specific sample preparation, as well as only low amount of sample is required and the sample form can be solid, liquid, gel, *etc.*; it has been long routinely used to study especially vibrational modes which are specific to the chemical bonds and symmetry of molecules. Therefore, Raman spectra show characteristic fingerprints by which the molecule can be identified. However, there also are some disadvantages of the technique, perhaps the most significant is the interference it suffers from fluorescence.

Raman spectroscopy is commonly used in chemistry, but it also shows strong potential for providing non-invasive information from various samples important in biology and medicine. In addition, it has reached a relevant position among the non-destructive materials characterization techniques employed in the Conservation and Restoration laboratories. Generally, Raman spectroscopy is being successfully applied to the analysis of a wide-ranging number of materials and systems.

In the present work, we induct a brief summary of our main results obtained by means of Raman spectroscopy. To the best of our knowledge, we have registered the first Raman and SERS spectra of some flavonoid molecules at trace concentrations. Surface-enhanced Raman scattering (SERS) is a surface-sensitive technique that allows achieving significant enhancements of the Raman signal for molecules adsorbed on or present in close proximity to nanostructured metal surfaces. In addition, flavonoid pigments were also detected for the first time *in situ* by SERS spectroscopy on textiles' fibres dyed according original old recipes without their previous extraction. This was possible thanks to the fabrication of silver nanoparticles *in situ* by photoreduction. The reproducibility and suitability of the method was also successfully examined by *in situ* analysis of other flavonoid compounds detected on wool fibres dyed by different flavonoid-containing dyestuffs according the dyeing recipes range from traditional Mediterran methods to pre-Columbian Central and South America ones. Finally, a real archeological Coptic textile (6^{th}-8^{th} AD) from Egyptian origin was also inspected, and the anthraquinone alizarin has been clearly identified. In recent years, the potential of SERS for the ultrasensitive detection of organic molecules used as artists' colorants has been widely appreciated and exploited. The introduction of this analytical tool in the field of cultural heritage investigations has significantly improved the chances of successfully identifying dyes. However, there is still a large interest to find and define an appropriate non-destructive analytical technique. Until that time, Raman spectroscopy can be further evolved as en efficient non-destructive or micro-destructive, and even *in situ*, technique for identification of different materials in artworks. Nowadays, we are trying to transfer our knowledge and experience to Slovak Cultural Heritage Analysis.

Study of physic-chemical characteristics of flavonoids and their interactions with different (bio)molecules, for example with proteins, is highly required, not only because to carry out correct diagnosis and to define optimum conditions for the conservation of the studied artefacts, but also because these molecules possess significant preventive and

therapeutic effect. Flavonoids have aroused considerable interest because of their potential beneficial effects on human health – they have been reported to have antiviral, antiallergic, antiplatelet, anti-inflammatory, antitumor and antioxidant activities. The antioxidant activity of flavonoids is related to their ability to chelate metal ions and to scavenge free radicals. We have conducted an extensive and detail vibrational study of several flavonoids, with a primary focus on the quercetin molecule, in order to identify and define the relationship between their structure and activity since the antioxidant-activity of a flavonoid is closely related to its chemical structure. On the other side, radical-induced changes to proteins can lead to adverse functional consequences including reduced protein enzymatic and binding activities, increased susceptibility to aggregation and proteolysis and changes to their uptake by cells. As a result, radical-mediated modifications of proteins have been implicated in both diseases and aging. Thus, we have also used Raman spectroscopy to study damages induced by free radicals on human serum albumin (HSA), the most prominent protein in plasma. The degradation of HSA was studied under different stress conditions in order to assess the main sites of radical attack and their consequences on protein folding. Model stress conditions were obtained by using gamma-radiolysis of aqueous solutions as source of free radicals. Raman spectroscopy was shown to be a useful tool in identifying conformational changes of protein structure and specific damages occurring at sensitive amino acid sites.

In conclusion, the present work would like be a simple review showing some of the potential applications of Raman spectroscopy.

Acknowledgement

The author would like to express her sincere appreciation and gratitude to Dr. Santiago Sánchez-Cortés (IEM CSIC in Madrid), Dr. Armida Torreggiani (ISOF CNR in Bologna), Dr. Silvia Centeno (Metropolitan Museum of Art in New York) and prof. Pavol Miškovský (University of P. J. Safarik in Kosice). The author would also like to thank all the people that have worked with her and it is not possible to mention all of them personally.

This work was supported by European Community's Sixth Framework Programme (contract No. MEST-CT-2004-513915), by COST CM0603 program (COST-STSM-CM0603-5337; COST-STSM-CM0603-06063), by the Structural funds of the EU (contract: NanoBioSens, ITMS code: 26220220107), by the contract APVV-0242-11, and the EU 7FP project CELIM 316310. We also acknowledge MINECO (grant FIS2010-15405) and *Comunidad de Madrid* through the MICROSERES II network (grant S2009/TIC-1476).

References

Jurasekova Z, Garcia-Ramos JV, Domingo C, Sanchez-Cortes S: Surface-enhanced Raman scattering of flavonoids *J. Raman Spectrosc.*, *37* (2006) 1239-1241.

Jurasekova Z, Domingo C, García-Ramos JV, Sánchez-Cortés S: Vibrational Spectroscopy as an Analytical Tool in the Identification and Characterization of Natural Dyes employed in the Cultural Heritage *COALITION*, *14* (2007) 14-21.

Torreggiani A, Jurasekova Z, Sanchez-Cortes S, Tamba M: Spectroscopic and pulse radiolysis studies of the antioxidant properties of (+)catechin: metal chelation and oxidizing radical scavenging *J. Raman Spectrosc.*, *39* (2008) 265-275.

Jurasekova Z, Domingo C, Garcia-Ramos JV, Sanchez-Cortes S: In situ detection of flavonoids in weld-dyed wool and silk textiles by surface-enhanced Raman scattering *J. Raman Spectrosc.*, *39* (2008) 1309-1312.

Jurasekova Z, Marconi G, Sanchez-Cortes S, Torreggiani A: Spectroscopic and Molecular Modeling Studies on the Binding of the Flavonoid Luteolin and Human Serum Albumin *Biopolymers*, *91* (2009) 917-927.

Jurasekova Z, Torreggiani A, Tamba M, Sanchez-Cortes S, Garcia-Ramos JV: Raman and surface-enhanced Raman scattering (SERS) investigation of the quercetin interaction with metals: Evidence of structural changing processes in aqueous solution and on metal nanoparticles *J. Mol. Struct.*, *918* (2009) 129-137.

Jurasekova Z, del Puerto E, Bruno G, García-Ramos JV, Sanchez-Cortes S, Domingo C: Extractionless non-hydrolysis surface-enhanced Raman spectroscopic detection of historical mordant dyes on textile fibers *J. Raman Spectrosc.*, *41* (2010) 1455-1461.

Jurasekova Z, Domingo C, Garcia-Ramos JV, Sanchez-Cortes S: Adsorption and catalysis of flavonoid quercetin on different plasmonic metal nanoparticles monitored by SERS *J. Raman Spectrosc.*, *43* (2012) 1913-1919.

Jurasekova Z, Domingo C, Garcia-Ramos JV, Sanchez-Cortes S: Effect of pH on the chemical modification of quercetin and structurally related flavonoids characterized by optical (UV-visible and Raman) spectroscopy *PCCP* (submitted).

What do we know about quercetin and other flavonoids from their Raman spectra?

Z. Jurašeková[1], S. Sánchez-Cortés[2], P. Miškovský[1,3]

[1] Department of Biophysics, Faculty of Sciences, University of P. J. Safarik, Jesenna 5, 041 54 Kosice, Slovakia
e-mail: zuzana.jurasekova@upjs.sk
[2] Instituto de Estructura de la Materia, CSIC, Serrano 121, 280 06 Madrid, Spain
[3] Centre for Interdisciplinary Biosciences, Faculty of Sciences, University of P. J. Safarik, Jesenna 5, 041 54 Kosice, Slovakia

Quercetin (QUC), 3,3‘,4‘,5,7-pentahydroxyflavone (Fig. 1), is one of the most common flavonols widely distributed in the plant kingdom. It has attracted the attention of many researchers because of its biological and pharmaceutical applications, including anticancer therapy. Many of beneficial effects of QUC are related to its antioxidant properties which result from the ability to scavenge free radicals and chelate metal ions [1,2]. Further, QUC and its glycoside quercitrin are the main components of the natural dyestuff quercitron, extracted from the quercitron bark or black oak (*Quercus velutina* Lam.). QUC is also found in Persian berries, a dye derived from the berries of shrubs of the *Rhammus genus* [3]. Thus QUC is of interest both as a dye andbiologically active molecule.

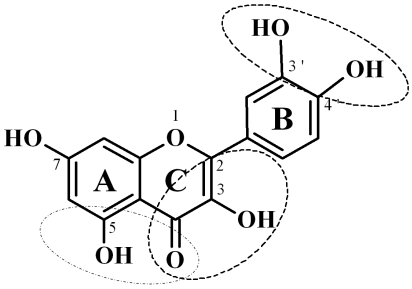

Figure 1. *Molecular structure and atomic numbering of quercetin (QUC). The marked parts design labile chemical sites identified in the QUC structure.*

Among the studied flavonoids, QUC deserves a special attention because of its chemical structure and unique properties. In fact, QUC is one of the most studied flavonoids. However, despite the enormous importance, only few Raman studies are devoted to the study of this flavonoid molecule (Fig. 2).

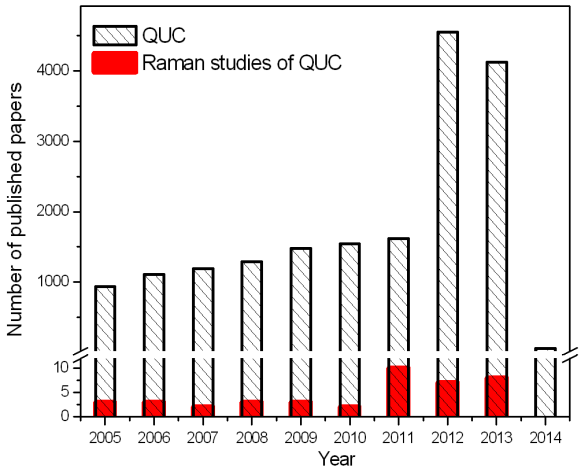

Figure 2. *Number of scientific papers concerning QUC and Raman studies of QUC published over the last decade (source: Web of Science).*

In the present work we have performed Raman studies of QUC and other related flavonoids. The chelation property of flavonoids towards metal ions have been attributed to the presence of 3- or 5-hydroxypyran-4-one, rather than the 3’,4’-dihydroxy group on B-ring [4].However, depending on pH and metal-to-ligand ratio, various chelating sites of QUC have been observed with different metal-chelating ability [5]. In addition, a study of the interaction of QUC with metal nanoparticles (NPs) followed by surface-enhanced Raman spectroscopy (SERS) reveals (Fig. 3A) that QUC undergoes a large chemical modifications at this interaction due to the existence ofseveral labile chemical sites (Fig. 1),which are subjectedto thefollowing processes: condensation, metal complexation, and a possible degradation. From SERS spectra obtained at different QUC concentrations (Fig. 3C),in the presence of chloride (Fig. 3D) and usingvarious excitation wavelengths it was deduced thatthe interaction of QUC with the silversurface mainly takes place throughC5-

OH/C4=O and C4=O/C3-OH groups placed in A- and C-rings. We have also suggested that a chemical change takes place through formation of C-C and C-O-C bondsbetween rings.At alkaline pH (Fig. 3B), the SERSspectra revealed a change in the condensation mechanismof QUC with a possible key role of the B-ring. Thus, the QUC condensation products may differ depending on pH because of the existence of different reaction pathways. Comparison of Raman spectra of different flavonoids indicates that there are several important structural features which determine the reactivity of the molecule under different experimental conditions. This analysis can facilitate to find some specific spectral/structural markers for the possible detection and identification of the flavonoids. [6-9]

In conclusions, the study of QUC modifications can be interesting for controlling the chemical degradation of this compound, and consequently for avoiding of undesirable effects, such as browning of QUC-containing mixtures. Moreover, the antioxidant activity of flavonoids is closely related to their tendency to undergo deep chemical changes. This work can contribute to the knowledge pool about the chemical properties of these compounds in order to improve their beneficial properties for the application in medicine and in the field of the cultural heritage.

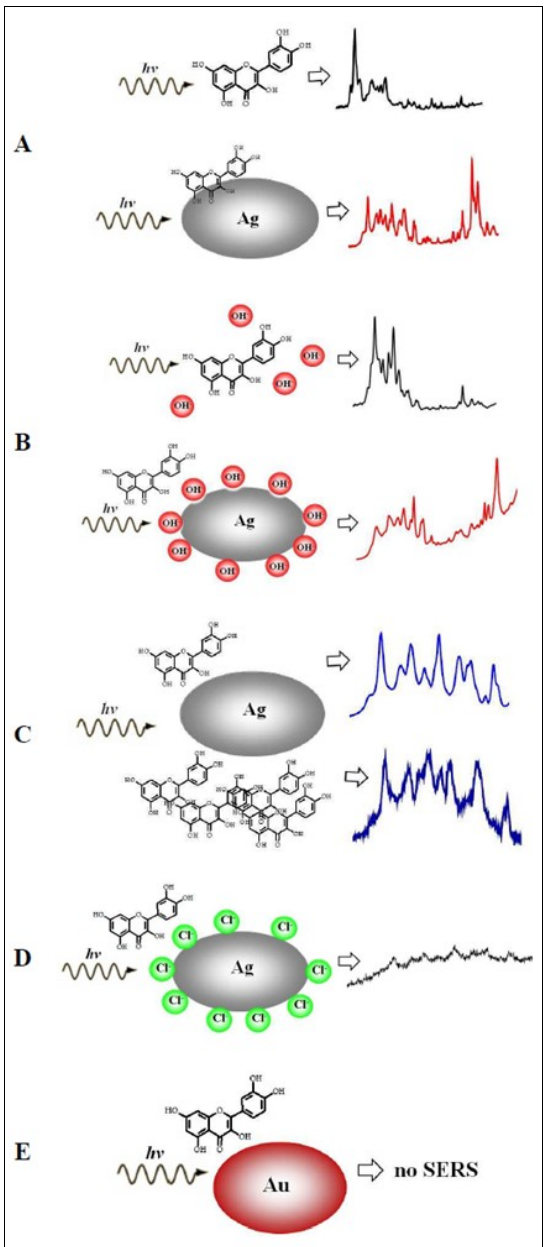

Figure 3. *Schematic representation of Raman/SERS studies of QUC: (A) at neutral and (B) alkaline pH; (C) at different QUC concentrations; (D) in the presence of chloride; carried out using silver and (E) gold nanoparticles.*

Acknowledgement
This work was supported by the Structural funds of the EU (contract: NanoBioSens, ITMS code: 26220220107), by the contract APVV-0242-11, and the EU 7FP project CELIM 316310. We also acknowledge MINECO (grant FIS2010-15405) and *Comunidad de Madrid* through the MICROSERES II network (grant S2009/TIC-1476).

References

[1] Middelton E, Kandaswami C In *The Flavonoids: Advances in Research since 1986*; Harborne JB, Ed.; Chapman and Hall: London, (1994), p 619-652.
[2] Hollman PCH, Katan MB. *Food Chem. Toxicol.*, *37* (1999) 937-942.
[3] Hofenk de Graaff JH *The colourful past - Origins, Chemistry and Identification of Natural Dyestuffs*; Archetype Publications: London, (2004).
[4] Mira L, Fernandez MT, Santos M, Rocha R, Florencio MH, Jennings KR. *Free Radical Research*, *36* (2002) 1199-1208.
[5] Torreggiani A, Trinchero A, Tamba M, Taddei P. *J. Raman Spectrosc.*, *36* (2005) 380-388.
[6] Jurasekova Z, Garcia-Ramos JV, Domingo C, Sanchez-Cortes S. *J. Raman Spectrosc.*, *37* (2006) 1239-1241.
[7] Jurasekova Z, Torreggiani A, Tamba M, Sanchez-Cortes S, Garcia-Ramos JV. *J. Mol. Struct.*, *918* (2009) 129-137.
[8] Jurasekova Z, Domingo C, Garcia-Ramos JV, Sanchez-Cortes S. *J. Raman Spectrosc.*, *43* (2012) 1913-1919.
[9] Jurasekova Z, Domingo C, Garcia-Ramos JV, Sanchez-Cortes S: Effect of pH on the chemical modification of quercetin and structurally related flavonoids characterized by optical (UV-visible and Raman) spectroscopy *Anal. Bioanal. Chem.* (submitted).

Temperature study of the DOPE+DOPC+alkanol system

M. Klacsová[1], J. Karlovská[1], D. Uhríková[1], S.S. Funari[2], P. Balgavý[1]

[1] Department of Physical Chemistry of Drugs, Faculty of Pharmacy, Odbojárov 10, 832 32 Bratislava, Slovakia
e-mail: klacsova@fpharm.uniba.sk
[2] HASYLAB at DESY, 22603 Hamburg, Germany.

Many biological membranes contain substantial amounts of phospholipids, like unsaturated phosphatidylethanolamines (PEs), which destabilize the lamellar L_α phase of the bilayer and promote the formation of inverse hexagonal H_{II} phase. PEs are abundant in presynaptic nerve terminals, which might be one of the active sites of anesthetics. Alkanols (CnOH, n is the even number of carbons in the alkyl chain) are also known as general anesthetic – in the homologous series the anesthetic potency increases up to C11OH, for longer CnOHs the anesthetic potency suddenly disappears [1,2]. It was suggested [3] that the anesthetic action might be coupled to membrane protein function via alteration of the tensions leading to the spontaneous curvature of lipid monolayers. Using ^{31}P-NMR, CnOHs up to n=4 were found to increase the $L_\alpha \rightarrow H_{II}$ transition temperature of egg phosphatidylethanolamine, whereas longer CnOHs induced a preference for the H_{II} phase organization [4,5]. Moreover, with increasing CnOH chain length lower amounts were needed to produce equivalent bilayer destabilization.

We have studied the $L_\alpha \rightarrow H_{II}$ phase transition of the dioleoylphosphatidylethanolamine (DOPE) : dioleoylphosphatidycholine (DOPC) = 3:1 mol:mol system in presence of long CnOHs (n = 8 – 16) at CnOH:(DOPE+DOPC) = r = 0-0.5 mol:mol using small-angle X-ray diffraction (SAXD).

Synthetic DOPE and DOPC were purchased from Avanti Polar Lipids (USA), CnOHs were from Sigma (USA) and the organic solvents from Slavus (Slovakia). Stock solutions of DOPE, DOPC and CnOHs, respectively, were prepared in methanol+chloroform mixture. Samples were prepared at required (DOPE+DOPC) : CnOH molar ratios, the solvent was then evaporated under a stream of gaseous nitrogen and its traces removed by an oil vacuum pump. Finally, redistilled water was added at H_2O : (DOPE+DOPC) = 210:1 (mol:mol). SAXD experiments were performed at beamline A2 in HASYLAB at DESY using a monochromatic radiation of wavelength 0.15 nm. The heating rate during temperature scans was 1°C/min. The diffraction peaks were fitted with Lorentzian functions and positions of maxima and intensities were estimated with a non-linear least-squares program.

The $L_\alpha \rightarrow H_{II}$ phase transition temperature t_{LH} decreases linearly withC10OH: (DOPE+DOPC) molar ratio r, reaching t_{LH} = 20°C at r = 0.5 (Left figure). C10OH is thus suggested to lessen the packing energy of the lipid system leading to a decrease of spontaneous radius of curvature R_0 and concomitant decrease of t_{LH}. The lattice parameter d of the L_α phase obtained at 5°C linearly decreases in presence of C10OH down to d = 5.80 nm at r = 0.3. The lattice parameter of the H_{II} phase also decreases with r in presence of C10OH, reaching a = 6.89 nm at r = 0.5. The observed decreases may arise from changes in either the lipid-water interfacial area A or lipid monolayer thickness.

With CnOH chain length the $L_\alpha \rightarrow H_{II}$ phase transition temperature of DOPE+DOPC system systematically decreases (Right figure). This result is in accordance with study of Cullis and coworkers [4,5] and our previous turbidimetric study [7]. The lattice parameter d of the DOPE+DOPC system is decreased in presence of C8OH and C10OH, however it is slightly increased when longer of studied CnOHs are intercalated. This effect of CnOHs can be explained simply by the mismatch between CnOH and lipid hydrocarbon chain lengths. The lattice parameter of the H_{II} phaseis, within experimental error, decreased up to C12OH by the same level, further decrease of parameter *a* is observed for longer CnOHs. The CnOH chain length dependent decrease of *a* and t_{LH} may be explained in terms of relieving hydrocarbon stress due to effect of CnOHs on lipid monolayer curvature and hydrocarbon chain packing.

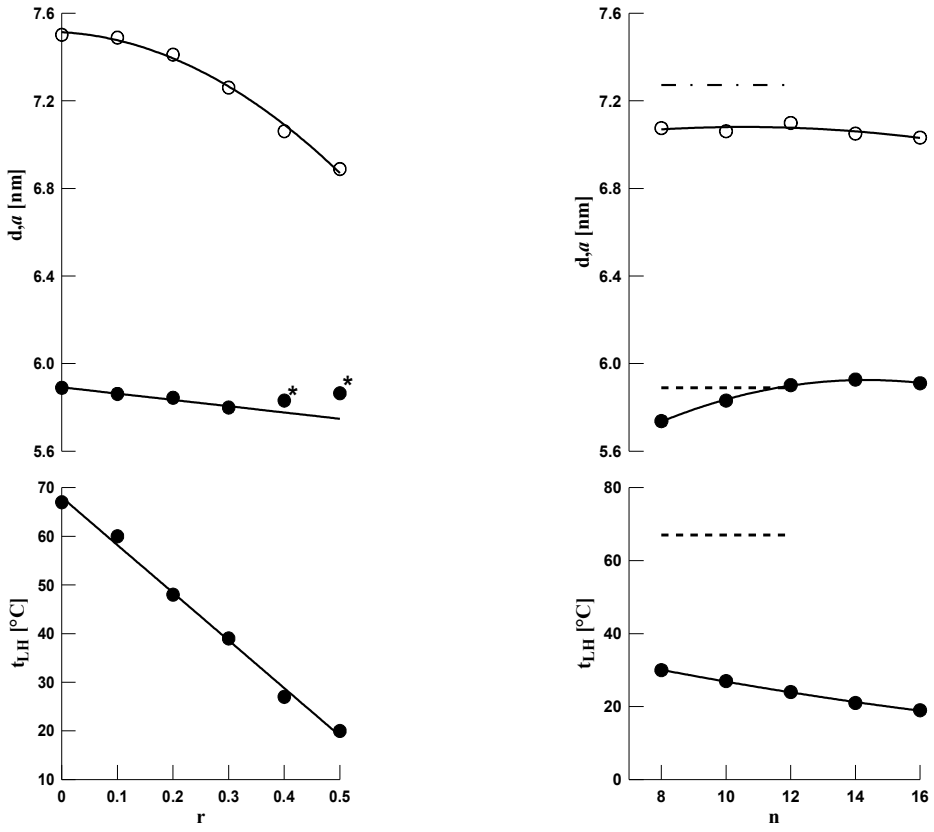

Figure. End-point temperatures of the $L_\alpha \rightarrow H_{II}$ phase transition and lattice parameters d (filled symbols) and a (open symbols) of the L_α and H_{II} phase at 5°C and 50°C, respectively, as a function of C10OH:(DOPE+DOPC) molar ratio (left) and of CnOH chain length (right). Dashed and dash-dotted lines denote the corresponding transition temperature and lattice parameters of the pure DOPE+DOPC. Solid lines are the best fits of corresponding data points. Stars denote data points obtained in the region of the L_α and H_{II} phase superposition.

Acknowledgement
This work was supported under the FP6 "Structuring the European Research Area" Programme, Contract RII3-CT-2004-506088 (HASYLAB project II-20052018 EC), by the VEGA 1/0159/11 grant and by the JINR project 04-4-1069-2009/2014.

References

[1] K. H. Meyer, H. Hemmi, Biochem Z 277 (1935) 39-72.
[2] M. J. Pringle, K. B. Brown, K. W. Miller, Mol Pharmacol 19 (1981) 49-55.
[3] S. M. Gruner, E. Shyamsunder, Ann NY Acad Sci 625 (1991) 685-697.
[4] A. P. Hornby, P. R. Cullis, Biochim Biophys Acta 647 (1981) 285-292.
[5] C. P. Tilcock, P. R. Cullis, Ann NY Acad Sci 492 (1987) 88-102.

[6] R. H. Templer, S. J. Castle, A. R. Curran, G. Rumbles, D. R. Klug, Faraday Discuss 111 (1998) 41-53.
[7] M. Klacsová, E. Surovcová, E. Ondrušová, J. Karlovská, P. Balgavý, Acta Facult Pharm Univ Com 56 (2009) 85-92.

Hematite particles in human globus pallidus

M. Kopáni[1], M. Čaplovičová[2]

[1]Institute of Pathology, School of Medicine, Comenius University, Sasinkova 2, 813 72 Bratislava, Slovakia, martin.kopani@fmed.uniba.sk,
[2]Department of Geology of Mineral Deposits, Faculty of Natural Sciences, Comenius University, Mlynská dolina, 842 15 Bratislava, Slovakia

Introduction

Iron is essential element used for fundamental cell functions, and as catalyst for chemical reactions. It can be found in human body mainly in the form of ferritin [1]. It is primary an iron storage protein situated in the cytoplasm of the cells and in small amounts in the blood circulation. This protein shows spherical morphology with a diameter of 12 nm. The core of ferritin consists of 6 nm Fe(III)-oxide particle stored in the form of ferrihydrite (5 $Fe_2O_3 \cdot 9H_2O$). Several studies show that the core physiological ferritin is composed of ferrihydrite, magnetite (Fe_3O_4) or maghemite (γ-Fe_2O_3) and hematite (α-Fe_2O_3) [2]. Under some unknown conditions mineralization to bigger aggregates can occur. Magnetite Fe_3O_4 and/or maghemite (γ-Fe_2O_3) particles are the dominant iron oxide components in human brain tissue under physiological and pathological conditions [3]. It is suggested that iron oxide particles may grow from ferritin iron cores [4].

Material and methods

Postmortem tissues were taken from globus pallidus externus of ten male and female human brains without any clinic-pathological findings on a disease of central nervous system. Investigation with transmission electron microscope (TEM) was done.

Results

All investigated samples reveal isolated, 6 nm sized ferritin-like particles. Corresponding diffraction pattern reveals amorphous material. TEM investigation of all samples reveals sometimes aggregates of nanometer-sized oval ferritin-like particles. The shape of these aggregates is irregular. TEM dark field mode images reveal aggregate of ferritin-like particles with the size around 9 nm. Selective electron diffraction in TEM shows the presence of crystalline ferrihydrite. Selective electron diffraction in TEM shows the presence of well crystalline material with hexagonal structure with lattice parameters a = 0.503 nm, c = 1.375 nm corresponding to hematite. The shape of larger bumpy particles is more irregular. Sometimes the bumpy particles exhibit less ordered structure (Fig.1). The size of these particles is up to 6 μm. On the surface of some particles are seen small deposits of unknown origin.

Discussion

Biomineralization process in the brain is the interaction between metabolic processes products and the surrounding environment. It takes place in the environment at ambient temperature, pressure and pH. The final product of biomineralization depends on many other factors such as temperature, pH, presence of reactive oxygen radicals (ROS), ions of inorganic chemical elements (S, Al, Cu) and time [5]. Iron/ferritin is physiologically found in glial cells of globus pallidus [6]. Under some conditions biologically mineralization of iron results in different size, shape, structure, composition and organization of iron oxides particles. We suggest internal dehydration and rearrangement within the ferrihydrite aggregates with strong influence of reactive oxygen species, mainly OH radicals and organic compounds. But the absence of other (intermediate) iron oxides, mainly goethite, is still unclear. Since the size of hematite particles can not be explained as the impact of temperature and pH we should consider other factors such as chemical elements and organic compounds as a important component of hematite particles formation. Our findings show that conditions (temperature, pH and –OH presence) in globus pallidus of human brain favor hematite formation over other iron oxides, mainly goethite. The findings of crystalline, well defined solid structure support view of biologically partly controlled mineralization.

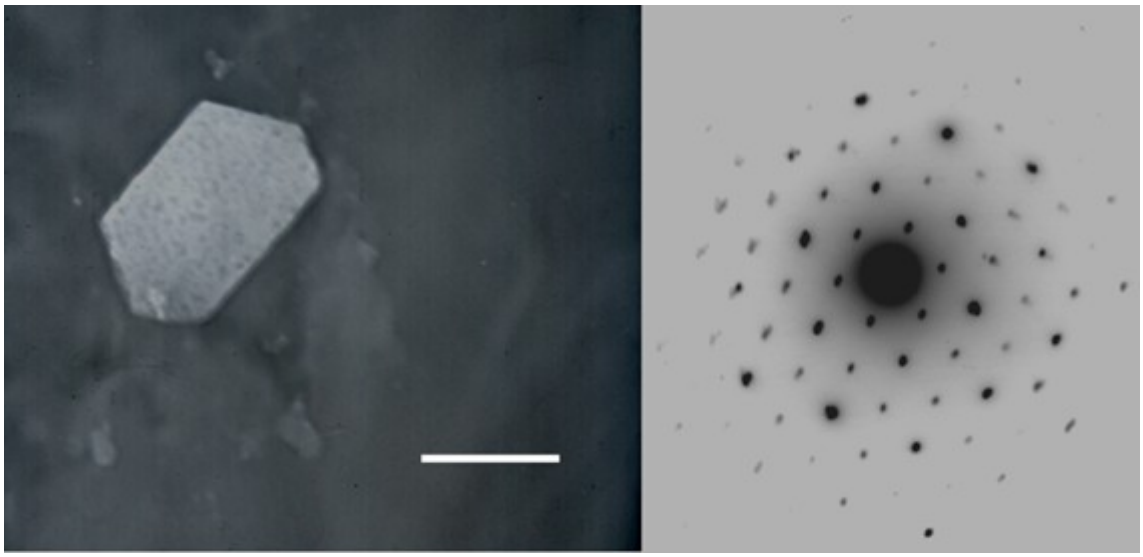

Fig.1 Human brain, glubus pallidus, sample no. 5. Hexagonal micrometer-sized particle (left) with diffraction pattern corresponding to hematite - α-Fe_2O_3. On the surface of some particles are seen small deposits of unknown origin. Scale bar 1 µm.

Acknowledgement
This work was supported by the grants VEGA No. 1/0220/12.

References

[1] J. Dobson, FEBS Lett. 496 (2001) 1-5.
[2] J.M. Cowley, D.E. Janney, R.C. Gerkin, P.R. Buseck, J. Struct. Biol. 131 (2000) 210-216.
[3] J.L. Kirschvink, A. Kobayashi-Kirschvink, B.J. Woodford, Proc. Natl. Acad. Sci. USA. 89 (1992) 7683–7687.
[4] D. Hautot, Q.A. Pankhurst, C.M. Morris, A. Curtis, J. Burn, J. Dobson, Biochim. Biophys. Acta 1772 (2007) 21-25.
[5] K. A Baltpurvins, R.C. Burns, G.A. Lawrance, A.D. Stuart, Environ. Sci. Technol. 30 (1996) 939-944.
[6] R. Meguro, Y. Asano, S. Odagiri, C. Li, K. Shoumura, Arch. Histol. Cytol. 71 (2008) 205-222.

Histochemical, immunohistochemical, electron microscopy, Mössbauer spectroscopy and SQUID magnetometry study of iron biomineralization in human *globus pallidus*

M. Kopani[1], R. Boca[2,3], M. Miglierini[4],M. Caplovicova[5], R. Fiala[6], N. Zilka[7], T. Smolek[7], V. Sisovsky[8], S. Galbavy[9],
J. Jakubovsky[10]

Institute of Medical Physics, Biophysics, Informatics and Telemedicine, Faculty of Medicine, Comenius University, Bratislava, Slovakia, martin.kopani@fmed.uniba.sk
[2]Department of Chemistry, Faculty of Natural Sciences, University of SS Cyril and Methodius, Trnava, Slovakia
[3]Institute of Inorganic Chemistry, Faculty of Chemical and Food Technology, Slovak University of Technology, Bratislava, Slovakia
[4]Institute of Nuclear and Physical Engineering, FEI, Slovak University of Technology, Bratislava, Slovakia
[5]Department of Geology of Mineral Deposits, Faculty of Natural Sciences, Comenius University, Bratislava, Slovakia
[6]Institute of Botany, Slovak Academy of Sciences, Bratislava, Slovakia
[7]Institute of Neuroimmunology, Slovak Academy of Sciences, Bratislava, Slovakia
[8]Institute of Pathology, Faculty of Medicine, Comenius University, Bratislava, Slovakia
[9]Institute of Forensic medicine, Faculty of Medicine, Comenius University, Bratislava, Slovakia
[10]Institute of Histology and Embryology, Faculty of Medicine, Comenius University, Bratislava, Slovakia

Introduction

Iron in human tissues can be found in the form of ferritin and/or hemosiderin (ferritin breakdown product). Its structure depends greatly on its ligand-based environment. Ferritin is an iron storage nonheme-protein comprised of a protein shell, which contains 24 polypeptide subunits surrounding a single crystal of ferrihydrite; which is about 8 nm diameter. Its crystal size is controlled by the amount of iron in the cell and the corresponding microenvironment.

The localization and distribution of iron (ferritin/hemosiderin) and their relation to saccharide sulfate/hydroxyl/carboxylate microenvironment (Alcian blue positivity) and saccharide hydroxyl microenvironment (PAS - Periodic acid–Schiff positivity) in human *globus pallidus* is investigated. To determine their effect on iron structure, transmission electron microscopy (TEM) and the superconducting quantum interference device (SQUID) and Mössbauer spectroscopy measurements were performed.

Results

Accumulation of Fe(III) and ferritin reveals two different structures with distinctive foci. The first structure is the accumulation of regular shapes around glial cells in the globus pallidus of human brain. The second structure is associated with the presence of neutral and acidic deposits of glycoconjugates. TEM investigation shows micrometer-sized particles of hematite. Spacial correlation between ferritin and iron oxyhydroxides was unable to be demonstrated in this study. Measurements performed by Mössbauer spectroscopy and SQUID indicate the presence of various iron oxyhydroxides in human *globus pallidus* – free ferritin, aggregated ferritin and various (not only Fe(III)) structures.

Discussion

Our findings of iron depositions near glial cells and spheroid structures in *globus pallidus* agree with results of other studies [1]. Macroenvironment (extracellular matrix) influences microenvironment (cells) in both animals and plants. Aquino et al. [2] found that carboxylated polysaccharides biosynthesis in macroenvironment with higher salinity was higher than sulphated ones. They concluded that negatively charged cell wall polysaccharides might play a role in coping with salt stress. Formation of hematite particles is strongly influenced by pH, temperature and the presence of oxygen radicals from ferrihydrite [3]. Conditions prevailing in globus pallidus of human brain (temperature, pH and the presence of oxygen radicals) may favor hematite formation over other iron oxides compounds. The Mössbauer spectra show that high-spin iron(III) centers dominate over

small admixture of low-spin Fe(II). A number of iron-oxide minerals has been detected in the samples extracted from the human brain. Measurements performed by SQUID indicate the presence of various iron oxyhydroxides in human *globus pallidus* – free ferritin, aggregated ferritin and various (not only Fe(III)) structures.

Conclusion

The experimental data collected by the scanning/transmission electron microscopy, SQUID magnetometry and the Mössbauer spectroscopy show that the samples extracted from the *basal ganglia* of the human brain contain a number of iron-oxide minerals. The deposits are not only of different composition but also of different size/shape and count and such a distribution is unknown. Iron oxyhydroxides can be the result of interaction between iron and the microenvironment in the form of polysaccharides of glycoconjugates or other biomolecules.

Acknowledgement

This work was supported by the Slovak Grant Agency VEGA, projects 1/0220/12, 1/0073/13 and COST 4120/11, CM1103.

References

[1] M.F. Casanova, J.M. Araque, Psych. Res. 121 (2003) 59-87
[2] R.S. Aquino, C. Grativol, P.A. Mourão, PLoS One. 6 (2011) e18862
[3] U. Schwertmann, E. Murad, Clays Clay Miner. 31 (1983) 277-284

Analysis of the Electrical Activity of the Heart Atria Using Autocorrelation Maps at Time Normalization.

K. Kozlíková, M. Trnka

Institute of Medical Physics, Biophysics, Informatics and Telemedicine, Faculty of Medicine in Bratislava, Comenius University, Sasinkova 2, 813 72 Bratislava, Slovak Republic, katarina.kozlikova@fmed.uniba.sk

The electrical activity of the heart atria is represented by the P wave that can be recorded using different procedures. Most information obtained non-invasively offers the multi-lead recording - the body surface potential mapping. Voltage distributions over the whole surface of the chest can be displayed in form of a set of isopotential maps that can be analysed quantitatively in different ways [1]. One of them uses the Pearson´s correlation coefficient that allows the construction of autocorrelation maps (ACM) [2].

The aim of this retrospective study was to analyse the autocorrelation maps in young adults when using time normalisation of the P wave.

The P wave duration of each subjects was time normalised, i.e. the P wave was divided into 20 equal parts. We constructed 21 isopotential maps from 24-lead system after Barr [3-5] in 88 controls (48 women, 40 men) without cardiovascular diseases, aged (18.5 ± 0.4) years. For each P wave, every isopotential map was compared with every isopotential map using Pearson's correlation coefficient r [6]. The values of the coefficients were displayed in form of autocorrelation maps, squared graphs with values $r = 1.000$ on the main diagonal [2] and symmetrical according to it. We analyzed the regions with high positive correlation $r \geq 0.900$ where the potential distributions changed slowly.

The mean of the P wave duration (± standard deviation) was (84 ± 10) ms (men: (86 ± 9) ms; women: (82 ± 10) ms; $p < 0.05$ according to the t-test [6]). The mean correlation coefficients of single autocorrelation maps were 0.666 ± 0.093 ranging from 0.353 to 0.845. The high positive correlation covered in average (32 ± 7) % of the whole autocorrelation map ranging from 20 % to 66 % with the mean correlation coefficients 0.968 ± 0.002 (almost 5 % correspond always to $r = 1.000$). Negative correlation occurred in 67 of 88 autocorrelation maps covering in average less than 8 % of these maps and occurring mainly at the borders with the mean value -0.192 ± 0.109.

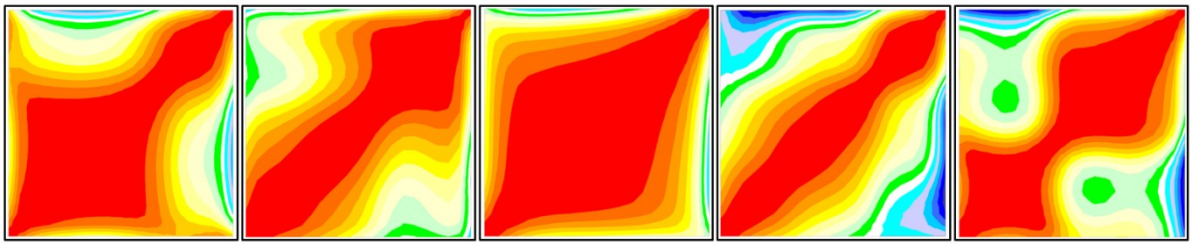

Figure 1: Examples of autocorrelation maps of women.

The beginning of the P wave corresponds to the lower left corner of the autocorrelation map, the end of the P wave to the right upper corner. The step between different colours representing correlation coefficient values is $\Delta r = 0.100$. Blue tints correspond to negative values. From left to right: types A, B, C, D, and E.

We identified five types of autocorrelation maps according to the form of the region with high positive correlation (Figure 1). In the type A (12 men, 4 women), the broadest area appeared at beginning of the P wave, in the type B (3 men, 10 women) at the end of the P wave, and in the type C (6 men, 10 women) approximately in the middle of the P wave. This broadening was always connected with narrow parts at its borders. The region of $r \geq 0.9$ had approximately uniform broadness along the main diagonal in the type D (15 men, 18 women). In the remaining 10 cases (4 men, 6 women – the type E), the broader parts in the beginning and the end of the P wave were separated by clear narrowing in the middle.

We assume that different types of the autocorrelation maps probably display atrial activation represented by circular isochrones (slow changes) or preferential paths (quick changes). The narrowing of the region with high positive correlation after or before the broader part corresponds probably to the moment when the activation spreads form the right atrium to the left one. This hypothesis has to be proved in further studies.

Acknowledgements
The work is dedicated to the 60th birthday of Professor JánJakuš, MD, DSC.
This work was partially supported by the VEGA project No. 1/0727/14 from the Ministry of Education, Science, Research and Sport, SlovakRepublic.

References

[1] K. Kozlíková, Bratisl. lek. Listy 91 (1990) 815 – 823 (in Slovak).
[2] J. A. Abildskov et al. Circulation 54 (1976) 901 – 906.
[3] R. C. Barr, M. S. Spach, G. S. Herman-Giddens, IEEE Trans. Biomed. Eng. 18 (1971) 125 – 138.
[4] V. Rosík, M. Tyšler, M. Turzová., in Proceedings of International Conference of Measurement, I. Frollo, A. Plačková (Eds.) SAV, Bratislava, 1997.
[5] K. Kozlíková, Physiol. Res. 56 (2007) S123 – S128.
[6] K. Kozlíková, J. Martinka, The Essentials of Biomedical Measurement Processing II, Asklepios, Bratislava, 2009 (in Slovak).

The application of the isointegral QRST maps

K. Kozlíková

Institute of Medical Physics, Biophysics, Informatics and Telemedicine, Faculty of Medicine in Bratislava, Comenius University, Sasinkova 2, 813 72 Bratislava, Slovak Republic, katarina.kozlikova@fmed.uniba.sk

The differences in cardiac depolarisation and repolarisation properties can be quantified by the ventricular gradient. If recovery were simply the reverse of depolarisation, the ST-T wave would cover the same area as the QRS complex, but of opposite polarity, and the sum of the QRS area and the ST-T area would equal zero. If there is variability in local repolarisation properties, this sum differs from zero. This difference is usually represented in vectorial form as the vectorial sum of the QRS vector and the ST-T vector. The three-dimensional analogue of the ventricular gradient is the isointegral map of the QT interval (IIM QRST), displaying the distribution of QRST voltage-time integrals on the whole chest surface obtained using multi-lead recordings (body surface potential mapping [1]). It is also expected that the ventricular gradient is independent from the ventricular activation sequence in the sense that the repolarisation changes are linked to the activation sequence changes in such a way that the relation between them remains constant [2].

The aim of this study is to review our application of the IIM QRST in controls, in hypertensive patients and patients with left ventricular hypertrophy, and for evaluation of vulnerability to ventricular arrhythmias in a longitudinal study after myocardial infarction.

In a group of 23 healthy young men (18-19 years old) we found that the IIM QRST do not change significantly if we use a linear zero baseline (the isoelectric points set before the P waves) and a 3-point baseline (additional isoelectric point in the PQ segment) [3] although the QT interval was significantly longer when using the 3-point baseline [4]. When comparing comparing IIM QRST between 9-10 years old boys and 13-14 years old boys, we found decreased values of IIM QRST maxima, minima, and peak-to-peak values in older boys while the time integral distributions remained similar [5]. The comparison of IIM QRST extrema between 18 young men and 25 young women revealed non-significantly higher extrema in men [6].

Left ventricular hypertrophy (increased mass of the left ventricle) may either increase or decrease the values of time integrals in IIM QRST. We found significantly decreased mean maxima and peak-to-peak values in 23 patients with left ventricular hypertrophy and hypertension compared to 12 controls matched by age [7]. Any significant changes were found neither in map extrema values nor between hypertensive patients with and without left ventricular hypertrophy nor between “pure” hypertensives and controls.

Vulnerability index is a quantitative parameter evaluating the risk of arrhythmia development derived from isointegral maps by comparing the patient’s IIM QRST with the IIM QRS and IIM ST-T of a control. We studied various properties of the vulnerability index. We found that its value does not change significantly between different control groups of the same age [8]. The value of vulnerability index does not change significantly between controls of different age [9]. The vulnerability index increases slightly with increasing RR interval

[10]. The vulnerability index was applied in longitudinal evaluation of patients with myocardial infarction. In a 4-year lasting study with repeated body surface examinations we found that the vulnerability index values of patients with myocardial infarction are higher than in controls during the first 4 months after myocardial infarction and that the vulnerability index values are higher in patients with inferior myocardial infarction than in patients with anterior myocardial infarction [11].

These results indicate that body surface potential mapping and especially IIM QRST could be a useful tool for clinical medicine.

Acknowledgements
The work is dedicated to the 60th birthday of Professor Ján Jakuš, MD, DSC.
This work was partially supported by the VEGA project No. 1/0727/14 from the Ministry of Education, Science, Research and Sport, Slovak Republic.

References

[7] K. Kozlíková, Bratisl. lek. Listy 91 (1990) 815 – 823 (in Slovak).
[8] D. M. Mirvis, Electrocardiography: A Physiologic Approach, Mosby-Year Book Inc., St. Louis, 1993.
[9] Z. Balázsiová, K. Kozlíková, E. Kráľová, in Proceedings 2nd International Workshop Applied Informatics in Biomedicine and Medical Engineering, K. Čápová, I. Čáp, M. Hrianka (Eds.). EDIS, Žilina, 1998.
[10] Z. Balázsiová, K. Kozlíková, in Bionika a biomedicínske inžinierstvo. Zborník referátov. STU, Bratislava, 2001 (in Slovak).
[11] K. Kozlíková et al., Bratisl. lek. Listy 89 (1988) 694 – 705 (in Slovak).
[12] E. Popperová et al., in Současné směry v patologické fysiologii. Univerzita Karlova, Praha, 1989 (in Slovak).
[13] K. Kozlíková, J. Martinka, J. Bulas, Measurement Science Review 6 (2006) 28 – 31.
[14] J. Martinka, K. Kozlíková, Scripta Medica 78 (2005) 299 – 304.
[15] J. Martinka, K. Kozlíková, Measurement Science Review 6 (2006) 20 – 23.
[16] J. Martinka, K. Kozlíková, Physiol. Res. 56 (2007) S129 – S132.
[17] K. Kozlíková et al., in Biomedical Measurement and Instrumentation, Dubrovnik, 1998.

Anti- and pro-apoptotic Bcl2 proteins distribution and metabolic profile in human aorta endothelial cells before and after HypPDT.

M. Maslaňáková, L. Balogová, P. Miškovský, R. Tkáčová, K. Štroffeková

Deregulation of apoptosis can contribute to diverse pathologic processes. Understanding its regulatory mechanisms in endothelial cells (ECs) has great importance for the development of novel therapy strategies for cancer and cardiovascular pathologies. An oxidative stress with the generation of radical oxygen species (ROS) is a common mechanism causing ECs' dysfunction and apoptosis. The generation of ROS can be triggered by various stimuli including photodynamic therapy (PDT). The molecular mechanisms underlying PDT, and specifically Hypericin PDT (HypPDT), are not completely understood, although it has been shown that the sub-cellular Hyp localization and distribution determine which signaling pathway will lead to cell death. Cell responses to HypPDT are highly dependent on the Hyp intracellular localization and accumulation. The mechanisms by which ROS cause or regulate ECs apoptosis typically include receptor activation, caspase activation, Bcl-2 family proteins, and mitochondrial dysfunction. We were particularly interested in Bcl-2 family proteins and investigated their role in apoptosis of ECs triggered by HypPDT. In the present work, we show that the presence of Hyp itself has an effect on the distribution of Bcl2 family members, without affecting the mitochondria function. Presence of Hyp triggers translocation of Bax into mitochondria, and translocation of Bax and Bcl2 into nuclei in ECs. Further, HypPDT abolishes mitochondria function and results primarily in necrotic type of death in HAEC cells.

Carbosilane dendrimers complexes with HIV-derived peptides and their interactions with lipid monolayers and vesicles

S. Melikishvili[1], K. Ciepluch[2], M. Ionov[2], Z. Garaiová[1], I. Waczulíková[1], T. Hianik[1], M.A. Muñoz-Fernandez[3], J.F. de la Mata[4], R. Gomez-Ramirez[4], M. Bryszewska[2]

[1] Department of Nuclear Physics and Biophysics, FMFI UK, Mlynska dolina F1, 842 48 Bratislava, Slovakia, e-mail: s.melikishvili@gmail.com
[2] Department of General Biophysics, Faculty of Biology and Environmental Protection, University of Lodz, Pomorska 141/143, 90-236 Lodz, Poland
[3] Immunomolecular Biology Laboratory, Hospital Gregorio Marañon, Dr. Esquerdo 46, 28007 Madrid, Spain
[4] Inorganic Chemistry Department, University Alcala de Henares, 28871 Alcala de Henares, Spain

The aim of this work was to study interactions between carbosilane dendrimers complexed with HIV-derived peptides (dendriplexes) and lipid monolayers and vesicles that model plasma membrane of dendritic cells. The model membranes were composed of zwitterionic dimyristoylphosphatidylcholine (DMPC) and negatively charged dipalmitoylphosphatidyl glycerol (DPPG). Three HIV-derived peptides: Gp160, Nef and P24 and two carbosilane dendrimers of second generation: BDBR11 and NN16 were used for dedriplexes formation.The complexes were characterized by measuring the size and Zeta potential using dynamic light scattering and Doppler laser velocimetry methods. The mechanisms of interaction of dendriplexes with lipid monolayers were characterized by measuring the surface pressure using Wilhelmy method. Dendriplexes induced increase of the surface pressure, which is probably due to repulsive forces between cationic complexes inserted into the monolayers.

To analyze possible changes in membrane fluidity, we studied the steady-state fluorescence anisotropy of the probes embedded at different depths within the lipid bilayer of vesicles. For this reason, the probes diphenylhexatriene (DPH) and its cationic derivative (TMA-DPH) were used. The increased concentration of dendriplexes resulted in decrease of fluorescence anisotropy of DPH, which is evidence on increased fluidity of hydrophobic part of the lipid bilayer. The changes in anisotropy depended on the type of dendrimers and peptides. However, no significant changes were observed in the fluorescence anisotropy of TMA-DPH probe. The obtained results suggest that dendriplexes strongly interact with negatively charged lipid membranes. The results are discussed in respect of the structure of dendrimers and peptides.

Acknowledgement
This work was supported by Slovak Research and Development Agency, projects No. SK-PL-0070-12, APVV-0410-10, by Science Grant Agency VEGA (project No. 1/0785/12) and Polish Ministry of Science and Higher Education (Polish-Slovak bilateral grant).

Correlation between polymorphism of amyloid fibrils and cytotoxicity in renal cells

M.-M. Mocanu[1], C. Ganea[1], K. Siposova[2], A. Filippi[1], E. Demjen[2], J. Marek[2], Z. Bednarikova[2,3], A. Antosova[2], I. Baran[1], Z. Gazova[2,4]*

[1]Department of Biophysics, "Carol Davila" University of Medicine and Pharmacy, Bucharest, Romania
[2]Department of Biophysics, Institute of Experimental Physics, Slovak Academy of Sciences, Kosice, Slovakia
[3]Department of Biochemistry, Faculty of Science, Safarik University, Kosice, Slovakia
[4]Department of Medical and Clinical Biochemistry and LABMED, Faculty of Medicine, Safarik University, Kosice, Slovakia
e-mail: gazova@saske.sk

The deposition of extra- or intra-cellular misfolded proteins is responsible for the development of a group of generic diseases which are known as amyloidoses. Although the proteins associated with amyloidosis do not appear to demonstrate any type of sequence or structural homology, amyloid aggregates employ a similar nucleation-dependent pathway of fibrillization [1] which involves the formation of nuclei, dimers, oligomers, protofilaments and fibrils with characteristic morphology, immunogenicity and cytotoxicity.

More recently, it has become generally accepted that protein amyloid aggregates are involved in cell death and cumulative tissue degradation. A large number of reports have shown that oligomer amyloid species can induce cell death through the direct interaction of soluble aggregates with the membrane that lead to membrane permeabilization, the formation of ion channels and oxidative stress [2]. In contrast, a recent study has warned against the oversimplification of the mechanisms involved in amyloid pathology and has suggested that it may be incorrect to ascribe the entire process to oligomer causality. It has been reported that amyloid fibrils can produce a cytotoxic effect via the deposition of huge fibril assemblies into the tissues causing organ failure and act as infectious particles in the case of prion diseases [3]. Bucciantini et al. demonstrated that amyloid fibrils could induce lipid rafts clustering leading to the activation of death receptors triggering the apopototic pathway [4]. These findings have triggered a great deal of intensive research aimed at establishing a relationship between the structure of amyloid aggregates and their cytotoxic activity.

Despite the strikingly similar natures of the fibrillar amyloid structures the formed fibrils differ in morphology, stability, and cytotoxicity depending on factors utilized during fibrillization [5]. This polymorphism underscores the complexity of the peptide conformational landscape that encompasses the structural differences in the molecular packing of the polypeptide chains.

We studied polymorphism of lysozyme amyloid fibrils formed under two different experimental conditions: at acidic pH (LAF2) and neutral pH (LAF6) and the implications of morphological differences of both types of lysozyme amyloid fibrils on the cytotoxic effect on the LLC-PK1 renal cells. The structural characteristics and morphology of the formed fibrils were evaluated using spectroscopic methods, atomic force microscopy and image analysis. The cytotoxic effect of both types of lysozyme amyloid fibrils on the LLC-PK1 renal cells was evaluated with growth curves and apoptotic/necrotic assays.

Atomic force microscopy showed the significant differences in morphological appearance of fibrils and their tendency to associate laterally (Figure 1). Further analysis of the fibril morphology using image analysis of AFM topographies confirmed the structural diversity of the formed assemblies, specifically in the diameter and length of fibrils and the

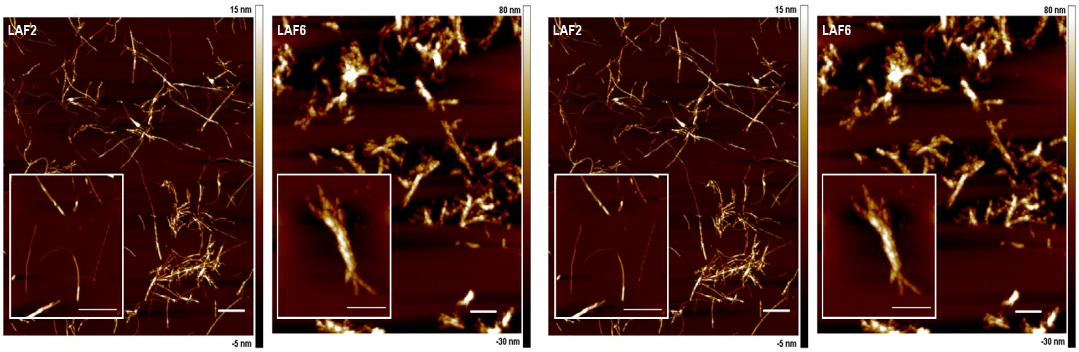

height of

Figure 1. AFM image of lysozyme amyloid fibrils prepared at pH 2.7 (A) and pH 6.0; the bars represent 1 μm.

assembled bundles. We suggest that polymorphism of fibrils is caused by different alignments of lysozyme molecules within amyloid structure and content of β–sheets in mature fibrils.

Our study showed that both types of mature lysozyme fibrils with a different morphology are cytotoxic in a model of non-neuropathic amyloidosis. Thus, our results support the hypothesis that mature amyloid fibrils are actively involved in the process of cell death. The lysozyme fibrils prepared at acid pH (LAF2) affect cell growth in a dose dependent manner while inhibition by fibrils prepared at neutral pH (LAF6) requires a certain threshold. Experiments clarifying the mechanism of the cell death support the involvement of both types of mature lysozyme fibrils in triggering the late apoptosis/necrosis which was observed at different fibril concentrations for each type of fibril.

Our findings clearly indicate that protein aggregation can give rise to fibrillar species with different degrees of cytotoxicity due to intrinsic differences in their physicochemical and structural characteristics. The inhibition of cell growth and the accumulation of late apoptotic/necrotic cells depended significantly on the structural properties of the studied fibrils. We suggest that the observed differences in cytotoxicity are related to the polymorphism of the fibrils.

Acknowledgement
This work was supported by the following projects: VEGA 2/0181/13 and 2/0175/14, APVV SK-RO-0016-12, APVV- 0171-10 and 0526-11, ESF 26220120021, 26220220005, and a grant from the Romanian National Authority for Scientific Research CNCS – UEFISCDI, project number PN-II-RU-TE-2011-3-0204.

References
[1] J. D. Sipe, Amyloid Proteins, Wiley-VCH Verlag GmbH and Co. KgaA, Weinheim Germany, 2005.
[2] A. A. Meratan, A. Ghasemi, M. Nemat-Gorgani, Membrane integrity and amyloid cytotoxicity: a model study involving mitochondria and lysozyme fibrillation products, in J. Mol. Biol. 409 (2011) 826-838.
[3] M. Stefani, Structural features and cytotoxicity of amyloid oligomers: Implications in Alzheimer's disease and other diseases with amyloid deposits. Prog. Neurobilogy 99 (2012) 226 – 245.
[4] M. Bucciantini, D. Nosi, M. Forzan et al. Toxic effects of amyloid fibrils on cell membranes: the importance of ganglioside GM1, in The FASEB Journal 26 (2012) 818 – 831.
[5] A. T. Petkova, R. D. Leapman, Z. Guo, W. M. Yau, M. P. Mattson, R. Tycko, Selfpropagating, molecular-level polymorphism in Alzheimer's β-amyloid fibrils, in Science 307 (2005) 262–265.

Contribution of Oxidatively Modified Cardiolipin to Mitochondrial Oxidative Stress

A. Musatov

Department of Biophysics, Institute of Experimental Physics, Slovak Academy of Sciences, Watsonova 47, 04001 Kosice, Slovakia.
e-mail: musatov@saske.sk

Cardiolipin (diphosphatidylglycerol, CL) is a unique phospholipid with in essence a dimeric structure, having four acyl groups and carrying two negative charges. In eukaryotes, CL is the only lipid synthesized in the mitochondrion and found exclusively in the mitochondrial inner membrane and in bacterial plasma membranes. CL contains a much higher percentage of unsaturated to saturated fatty acid residues than do other mitochondrial phospholipids (80-90% linoleic acid) making CL much more susceptible to oxidative damage than mitochondrial phosphatidylcholine or phosphatidylethanolamine. The initial product of linoleic acid peroxidation is formation of conjugated dienes followed by the generation of hydroperoxy octadecadienoic acid, a lipid peroxide, and a number of secondary lipid peroxidation products, including very toxic aldehydes 4-hydroxy-2-nonenal (HNE) and malondialdehyde (MDA). Two populations of CL exist within the inner mitochondrial

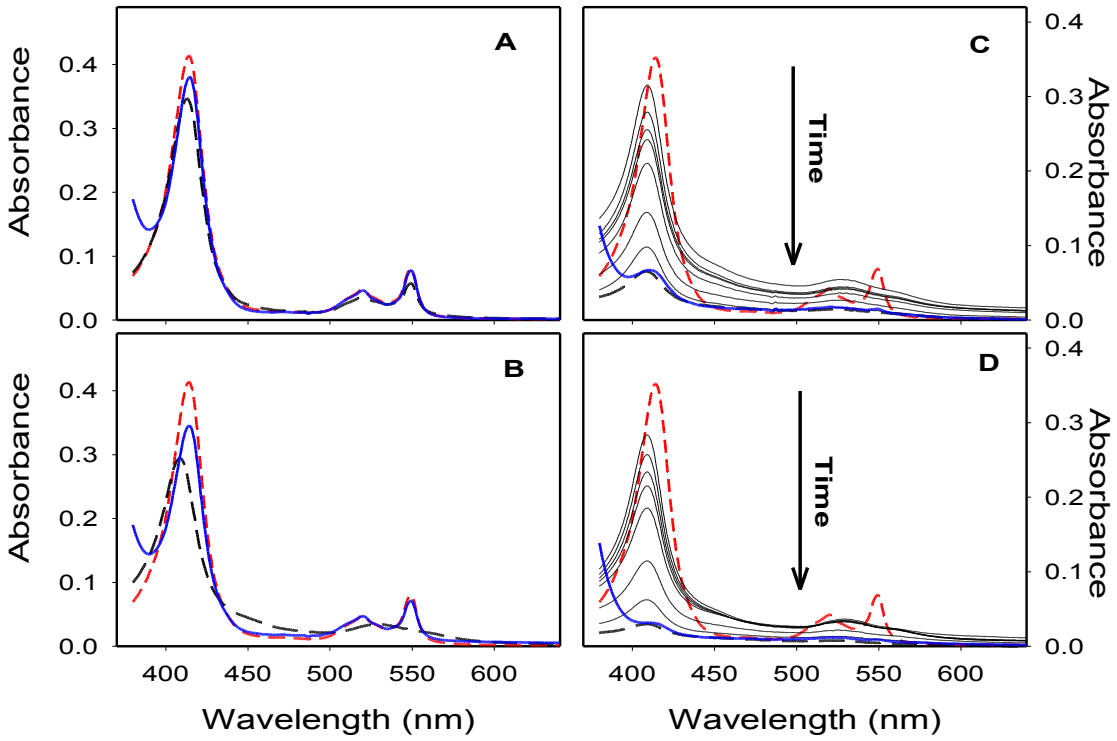

Figure 1. Concentration– and time–dependent effect of peroxidized cardiolipin on ferrocytochrome *c* heme disruption. Absolute spectra of ferrocytochrome *c* were taken before incubation (red dotted lines), after incubation with peroxidized cardiolipin for 30 min at room temperature (black dashed lines), and after addition of 5 mM Na-ascorbate (blue solid lines). Panels (C) and (D) also demonstrate spectra taken 0.25, 1, 2, 3, 5, 10 and 15 min after an addition of peroxidized CL to ferrocytochrome *c* (thin black lines). The initial concentration of cytochrome c^{2+} was 2.9 µM (panel (A) and (B)) and 2.3 µM (panel (C) and (D)). The concentrations of peroxidized cardiolipin were 5, 10, 25, and 50 µM in panels (A), (B), (C), and (D), respectively. Base lines were taken on peroxidized cardiolipin in 20 mM Tris-Cl, 1 mM EDTA, buffer pH 7.4.

membrane: 1) CL that is tightly bound to mitochondrial inner membrane proteins; and 2) bilayer CL that is not protein bound and is presumably free to diffuse within the mitochondrial inner membrane.

The main objective of our research has been to provide a detailed understanding of how modified CL affects mitochondrial electron transfer proteins. We now have evidence that oxidatively modified CL and CL derived products can react with hemes, producing damaging free radicals or can directly react with specific amino acids, destabilizing important subunit interactions within multisubunits complexes [1-4]. Although the mechanism in each case is different, the end result is quite similar – structural and functional alterations of proteins. For example, the reaction of ferrocytochrome *c* with peroxidized CL results in a two-phase process: first, the oxidation of ferrocytochrome *c*, and second, heme *c* rupture (Figure 1). The interaction of peroxidized CL with cytochrome *c* generates hydroxyl radicals as demonstrated by the EPR data. Good correlation of the rates of hydroxyl radical production and heme *c* rupture suggests that hydroxyl radicals are mostly responsible for heme destruction. In addition, heme *c* degradation causes significant changes in the aggregation state of cytochrome *c*. The effectiveness of peroxidized CL can be explained by the exceptionally specific nature of interaction with cytochrome *c* (Figure 2). We also demonstrated that ROS-induced damage to CL bound to mitochondrial Complex IV is associated with irreversible loss of enzymatic activity [2,4]. Therefore, based on our studies it is clear that oxidative modification of either, protein bound or bilayer CL, significantly contributes to mitochondrial oxidative stress.

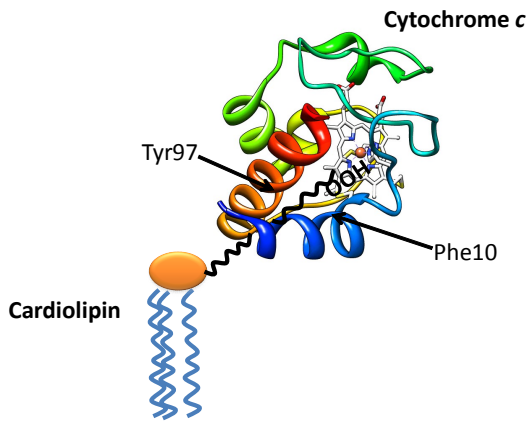

Figure2.Model of the cytochrome *c*–peroxidized CL complex. Insertion of a monohydroperoxide cardiolipin acyl chain (black) into the hydrophobic pocket of cytochrome *c* surrounded by Tyr97 and Phe10. The heme is in white, and the iron ion is shown as a dark-orange sphere. The protein structure was visualized with Protein Data Bank entry 1CRC.

Acknowledgements
The research was supported by GM024795 grant from the National Institutes of Health and by the grant from the Slovak Grant Agency VEGA 2/0176/14.

References

[1] Musatov, A., Carroll, C.A., Liu, Y-C., Henderson, G. I., Weintraub, S.T., & Robinson, N.C. Biochemistry 41 (2002), 8212-8220
[2] Musatov, A. Free Radic. Biol. Med. 41 (2006), 238-246
[3] Musatov, A., Fabian, M., Varhač, R. J. Biol. Inorg. Chem. 18 (2013), 137-144
[4] Musatov, A. J. Biol. Inorg. Chem. 18 (2013), 729-737

The role of PKCα in cell death induced by photo-activated hypericin

Z. Nadova[1,2], J. Joniova[1,3], M. Misuth[1], F. Sureau[3], P. Miskovsky[1,2]

[1]Department of Biophysics, Faculty of Science, P. J. Safarik University, Jesenna 5, 04001 Kosice, Slovakia (zuzana.nadova@upjs.sk)
[2]Centre for Interdisciplinary Biosciences, Faculty of Science, P. J. Safarik University, Jesenna 5, 04001 Kosice, Slovakia
[3]Laboratoire Jean Perrin, Pierre et Marie Curie University, Paris, France

We have previously shown that in human glioma cells (U87 MG) hypericin (Hyp) is mostly localized in endoplasmic reticulum and partially in mitochondria, lysosomes and Golgi apparatus [1]. Photo-activation of Hyp affects mitochondrial function and induces apoptosis via mitochondrial apoptotic pathway [2, 3]. We have also described an interaction between Hyp and "anti-apoptotic" PKCα and its activation and trans-localization after Hyp photo-activation [3]. PKCα is likely Bcl-2 kinase in U87 MG cells and modulation of its activity may be important for cell response to Hyp PDT treatment.

A potential role of PKCα in cell death pathway induced by photo-activated Hyp is presented in this work.

Small interfering RNA (siRNA) was used to post-transcriptional silencingof *pkcα* gene expression (Fig.1). U87 MG cells were pre-incubated with siRNA prior to addition of Hyp and its photo-activation. Cell survival, cell death pattern, mitochondrial membrane potential depolarization ($\Delta\Psi_m$) and reactive oxygen species (ROS) generation were assessed by flow cytometry. Sub-cellular distribution of Bcl-2 family protein members and PKCα were monitored by confocal fluorescence microscopy.

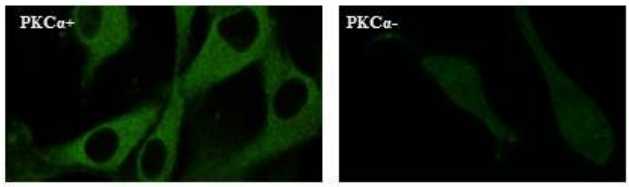

Fig.1 Detection of PKCα in U87 MG cells

Results:

Post-transcriptional silencing of *pkcα* ge
changes in type of cell death induced by photo-activa

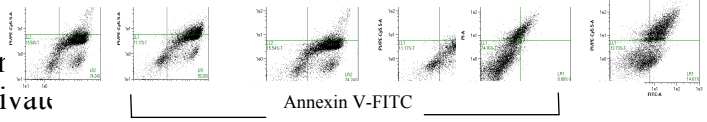

Fig.2Cell detah induced by photo-activated Hyp in U87 cells MG cells

The externalization of phosphatidylserine (PS) int
sign of apoptosis was detected by a green fluorescence of bounded Annexin V to PS. The dead cells were identified by a red fluorescence of PI marker (bound to DNA in nucleus) Annexin V^-/PI^- are defined as live cells, Annexin V^+/PI^- cells are defined as early apoptotic cells, and Annexin V^+/PI^+ are defi
as late apoptotic/ necroticce
Photo-activation of H
preferentially induces apoptosis
U87 MG cells (Fig.2B).

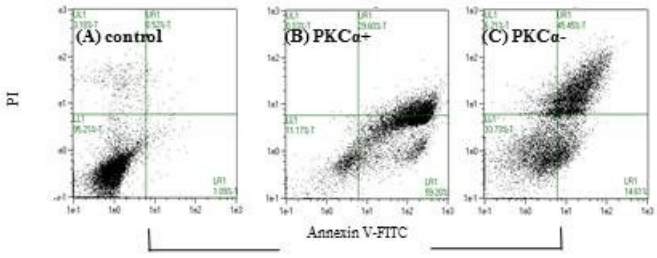

Fig.2 Cell detah induced by photo-activated Hyp in U87 cells MG cells

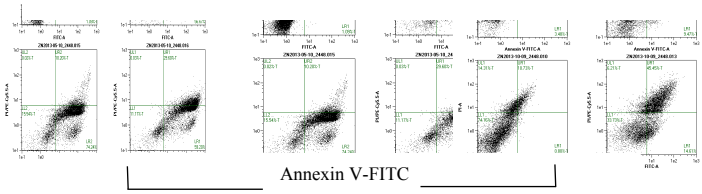

Fig.2Cell detah induced by photo-activated Hyp in U87 cells MG cells

Our results show that ROS production is significantly increased in PKCα- cells treated with photo-activated Hyp which consequently leads to necrosis (Fig.2C, Fig.3 B,C).

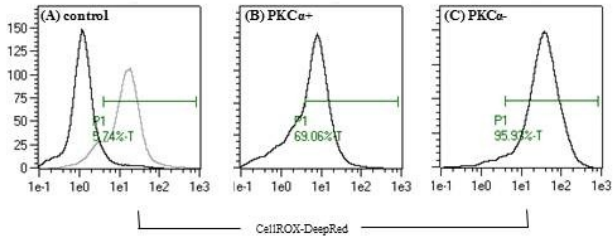

Fig.3 Production of ROS after Hyp photo-activation in U87 cells MG cells

Conclusions:

PKCα, as Bcl-2 kinase, supports stabilization of Bcl-2 in membranes and its antioxidant function and indirectly protects mitochondria/cells against oxidative stress and subsequent cell death.

Acknowledgement:
This work was supported by the FP7 EU (CELIM 316310) and by Slovak Res. and Dev. Agency (APVV-0242-11)

References:

[1] Huntosova V, Nadova Z, Dzurova L, Jakusova V, Sureau F, Miskovsky P. Photochem. Photobiol. Sci. 2012 Sep;11(9):1428-36
[2] Petrovajova D, Jancura D, Miskovsky P, Chorvat jr D, Chorvatova A, Ragas X, García-Díaz M, Nonell S., Nadova Z: Monitoring of singlet oxygen luminescence and mitochondrial autofluorescence after illumination of hypericin/mitochondria complex: a time-resolved study, Laser Phys. Lett. 2013, 10; 7
[3] Kocanova S, Hornakova T, Hritz J, Jancura D, Chorvat D, Mateasik A, Ulicny J, Refregiers M, Maurizot JC, Miskovsky P. Photochem. Photobiol. 2006 May-Jun;82(3):720-8

Effects of H_2S donor AP39 on rat blood pressure and membrane channels

K. Ondrias[1], F.Kristek[2] , L. Tomasova[1], L. Malekova[1], A. Misak[1], M. Tomasek[1], M. Whiteman[3]

[1] Institute of Molecular Physiology and Genetics SAS, Vlarska 5, 83334 Bratislava, e-mail: karol.ondrias@savba.sk
[2] Institute of Normal and Pathological Physiology SAS, Sienkiewiczova 1, 813 71 Bratislava,
[3] University of Exeter Medical School, University of Exeter, Exeter, United Kingdom

H_2S is important in the homeostasis of the cardiovascular system and the pathogenesis of cardiovascular diseases. H_2S donors have the viable to be effective therapeutic agents. The aim of our work was to study a potential of novel slow H_2S donors AP39 and AP67 to influence rat haemodynamic parameters when NO deficiency was induced by inhibition of endogenous NO synthesis using L-NAME. Drugs were administered into the right jugular vein (i.v.) as bolus and blood pressure (BP) pulse waveform (PW) was detected by fiber-optic pressure transducer (Samba Preclin) in cannulated left carotid artery of anaesthetized Wistar rat. In control experiments, without L-NAME, bolus i.v. administration of AP39 (250 and 500 nM/kg body weight) influenced PW, transiently decreased BP, heart rate and significantly influenced $\pm dP/dt_{max}$ and a position of dicrotic notch. AP67 and Na_2S, had similar effects at 3-30 μM/kg concentrations. L-NAME (i.v., 30 mg/kg) significantly influenced PW and increased BP. In the presence of L-NAME, AP39 (250-500 nM/kg), AP67 (15-30 μM/kg) and Na_2S (4-30 μM/kg) significantly decreased systolic BP, but were less efficient on diastolic BP. This effect was more prolonged in the presence of L-NAME.To investigate an involvement of membrane channels in these AP39-mediated vascular effects, we investigated the effects of AP39 on calcium ryandodine (RyR2) and intracellular chloride channels.RyR2 channels were derived from rat heart sarcoplasmic reticulum (SR) and single calcium channels were measured in bilayer lipid membrane. AP39 (10-20 μM) decreased open probability of RyR2 channels from the cytoplasmic side, but not from the luminal side. AP39 increased conductance of mitochondrial single chloride channels derived from rat heart SR, suggesting the compound may induce channel pore dilation. These results suggest that slow release H_2S donors such as AP39 and AP67 may offer a novel therapeutic opportunity in conditions whereby NO bioavailability is deficient, such as heart failure, hypertension, atherosclerosis and other pathologies.

Acknowledgement
This work was supported by the Slovak Research and Development Agency under the contract No. APVV-0074-11

Display technologies in evolving of new protein therapeutics

E. Sedlák

Centre for Interdisciplinary Biosciences, P.J. Šafárik University, Jesenná 5, 040 01 Košice, Slovakia.
Department of Biochemistry, P.J. Šafárik University, Moyzesova 11, 040 01 Košice, Slovakia.
e-mail: erik.sedlak@upjs.sk

Recognition of molecular diversity of cell surface proteomes in disease is essential for the development of targeted therapies. Progress in targeted therapeutics requires establishing effective approaches for high-throughput identification of agents specific for clinically relevant cell surface markers. Over the past ~15 years, a number of platform strategies have been developed to screen polypeptide libraries for ligands targeting specific receptors. These so called display technologies are indispensable part of directed evolution methods and include such methods as phage display, yeast display, and ribosome display [1, 2] (Fig. 1). In this talk I will shortly describe the principles of the ribosome and yeast displays: (i) Ribosome display is a potent in vitro method to select and evolve proteins or peptides from a naïve library with very high diversity (up to 10^{12}) to bind to any chosen target of interest [3]. Using ribosomedisplay, proteins, such as designed ankyrin repeat proteins (DARPins), have been evolved to bind various targets with affinities all the way down to the picomolar range [4, 5]. (ii) The expression of recombinant proteins incorporated into the cell wall of *Saccharomyces cerevisiae*, termed yeast display, offers selected advantages relative to other display technologies, most notably eukaryotic expression of the heterologous target protein, making it an outstanding tool for display and engineering of many proteins, including dimeric, that are difficult to produce in other display formats [6]. Successful application of yeast display include affinity maturation (that enables to evolve an antibody with femtomolar affinity [7]), protein engineering for improved production and stability, as well as novel applications in cell-based selections, epitope mapping, cDNA library screening, cell adhesion molecule engineering, and selection against non-biological targets [6].

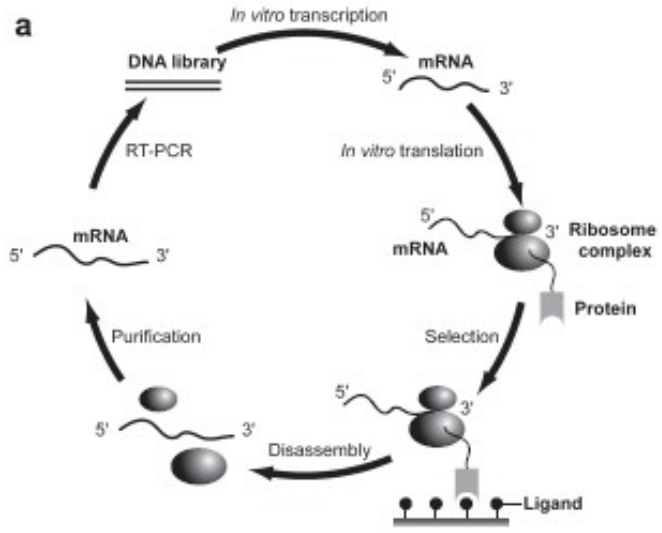

Figure 1. *Schematic representation of ribosome display cycle. In general, analogous scheme can be drawn for all display methods – of course, with different component involved, e.g. yeast cells instead of ribosome in yeast display .*

Taken from Matsuura & Yomo,J. Biosci. Bioeng. 101(2006) 449-456.

Antibodies are, currently, a major driver of the pharmaceutical industry with several blockbuster drugs on the market and many more in clinical development. The key for this success is that antibodies can be selected to bind to virtually any given target with high affinity and specificity, thereby displaying neutralizing or cytotoxic functions with very limited side effects [8]. Antibodies, however, suffer from clear limitations: they are expensive to produce, difficult to formulate, show low tissue penetration, feature a complex architecture, bind their target bivalently, and their commercial use is often blocked by intellectual property restrictions. To address some of the shortcomings of antibodies, several alternative non-

immunoglobulin based scaffolds have been brought intoattention of researchers [9] (Fig.2). Arguably, the most promising group of proteins with alternative scaffold is DARPins (Fig. 2D).

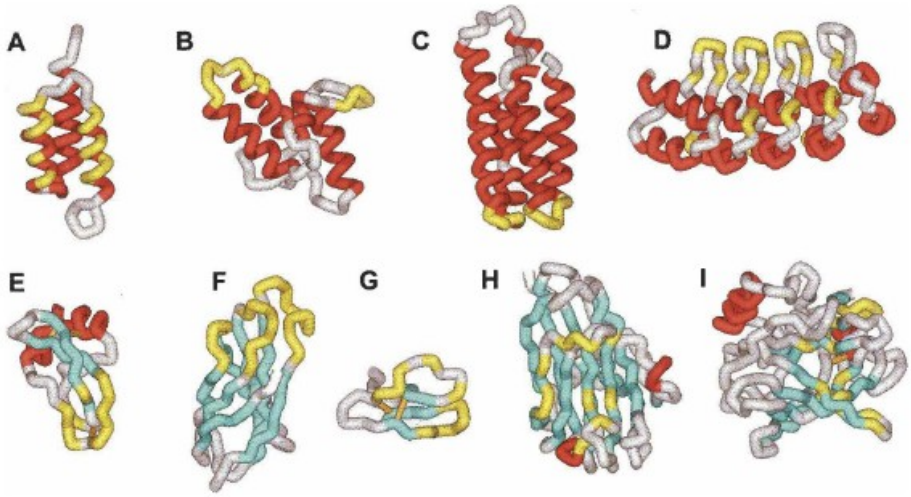

Figure2. Representative protein display scaffolds selected for novel molecular recognition by library construction or grafting experiments. α-helices aredepicted in red; β-sheets, in blue; disulfide bonds, in orange; and positions subjected to random or restricted substitutions, inyellow. The PDB IDs used to generate this figure are given in parentheses: (A) Affibody: Z-domain of protein A (1Q2N), (B)immunity protein: ImmE7 (1CEI), (C) cytochrome b562 (1M6T), (D) repeat-motif protein: ankyrin repeat protein (1SVX), (E)kunitz-domain inhibitor: Alzheimer's amyloid β-protein precursor inhibitor (1AAP), (F) 10th fibronectin type III domain(1FNA), (G) knottin: cellulose binding domain from cellobiohydrolase Cel7A (1CBH), (H) carbohydrate binding moduleCBM4-2 (1K45); and (I) anticalin FluA: bilin-binding protein (1T0V) with cavity randomization for fluorescein binding.

Taken from Hosse et al. Protein Sci. 15 (2006)14-17

DARPins are successful example of protein therapeutics evolved by display technologies with extreme potential for numerous therapeutic applications [10]. Advantages of DARPins in comparison with antibodies are: (i) high tissue penetration, (ii) absence of effector function, (iii) adjustable pharmacokinetics, (iv) allosteric inhibitions, and (v) new administration routes.

Acknowledgement
This work was supported by CELIM (316310) funded by 7FP EU (REGPOT).

References

[1] A. Sergeeva, M. G. Kolonin, J. J. Molldrem, R. Pasqualini, W. Arap, Adv. Drug Deliv. Rev. 58 (2006) 1622-1654.
[2] K. Hida, J. Hanes, M. Ostermeier, Adv. Drug Deliv. Rev. 59 (2007) 1562-1578.
[3] J. Hanes, A. Plückthun, Proc. Natl. Acad. Sci. U.S.A. 94 (1997) 4937-4942.
[4] P. Amstutz, H. K. Binz, P. Parizek, M. T. Stumpp, A. Kohl, M. G. Grütter, P. Forrer, A. Plückthun, J. Biol. Chem. 280 (2005) 24715–24722.
[5] B. Dreier, A. Plückthun, Methods Mol. Biol. 687 (2011) 283–306.
[6] L. R. Pepper, Y. K. Cho, E. T. Boder, E. V. Shusta, Comb. Chem. High Throughput Screen. 11 (2008) 127-134.
[7] E. T. Boder, K. S. Midelfort, K. D. Wittrup, Proc. Natl. Acad. Sci. U.S.A. 97 (2000) 10701-10705.
[8] D. Schrama, R. A. Reisfeld, J. C. Becker, Nat. Rev. Drug Discov. 5 (2006) 147-159.
[9] Y. L. Boersma, A. Plückthun, Curr. Opin. Biotechnol. 22 (2011) 849-857.
[10] R. Tamaskovic, M. Simon, N. Stefan, M. Schwill, A. Plückthun, Methods Enzymol. 503 (2012) 101-134.

Implementation of computer technology into biophysical lessons at University of Veterinary Medicine and Pharmacy

J. Staničová, V. Verebová

Institute of Biophysics, University of Veterinary Medicine and Pharmacy, Komenského 73, 041 81 Košice, Slovakia, jana.stanicova@uvlf.sk, valeria.verebova@uvlf.sk

Biophysics integrally participates in curriculum of human medicine, veterinary medicine and pharmacy. It grants inevitable basic knowledge necessary for understanding these laws, phenomena and processes proceeding in the living organisms, which have physical base. Medical biophysics also gives the information about experimental methods, which are used in human and veterinary diagnostics, therapy, pharmaceutical practice and research as well. As a basic subject, it stands between mathematics, physics, physical chemistry and biological sciences on the other hand. This subject also gives physical bases necessary for managing subsequent subjects in the medicine training such as chemistry, biochemistry, physiology, surgery, X-ray diagnostics, orthopedics, pharmacology.

With concern of biophysical education at University of Veterinary Medicine and Pharmacy in Košice (UVMP) we try granting to students of UVMP the logical and apt explanation of biophysical processes in lectures and teaching them to obtain practical skills in practical lessons. This year, we started a new managing of practical exercises by implementation of computer technology. Students have a possibility to evaluate their experimental results by computers directly situated in laboratory room. We have also created share pages on university intranet to communicate with students electronically. Beside that some new experiments in biophysical laboratory were realized. They serve for demonstration of the physical principles of diagnostics methods such as electrocardiography and ultrasound imaging. On the other hand, some biophysical exercises especially for students of pharmacy were arranged, too.

In our contribution we will aim to describe above mentioned activities serving for innovations of pedagogical process at UVMP.

Acknowledgment:
This work was supported by the Slovak Grant Agency KEGA, project No. 014UVLF-4/2013

Cough and sneeze, differences and their mutual interactions

M. Šimera[1], I. Poliaček[1], B. Dobrolubov[1], M. Veterník[1], J. Plevková[2], J. Jakuš[1]

[1] Department of Medical Biophysics, Jessenius Faculty of Medicine in Martin, Comenius University in Bratislava, Malá hora 4, 036 01 Martin
[2] Department of Pathophysiology, Jessenius Faculty of Medicine in Martin, Comenius University in Bratislava, Sklabinska 26, 037 53 Martin

Coughing and sneezing are important airway defensive reflexes each with some common and different characteristic in generation and modulation. During coughing, foreign bodies are expelled from the throat, larynx, and trachea through the oral cavity while during sneezing, they are expelled from the nasal cavity. In order to expel foreign bodies efficiently, both reflexes exhibit three common phases: inspiratory, compression, and expulsion, each of which can be identified experimentally by a stereotypical pattern of activation of neural discharges [1]. The afferent pathways for cough comprise vagus nerve fibers arising from two main groups of sensory nerve endings [2,3]: rapidly adapting mechano- and acid sensing cough receptors, represented by Aδ nodose fibers, and nociceptive-like free endings of jugular C-fibers. While afferent pathway of sneeze reflex comprise free nerve endings of trigeminal origin (anterior ethmoidal and posterior nasal nerves) [4,5]. Sneezing expiratory nasal airflow, that does not occur in coughing [6], is caused by activation of additional auxiliary muscles, e.g. the elevator of the back of the tongue- styloglossus (SG) muscle, which is explosively activated during the sneeze expulsion [7]. Although neural mechanisms of coughing has been systematically studied for last few decades, the differences between coughing and sneezing as well as neuronal mechanisms of sneeze reflex in general are still poorly understood [8,7] Our study on 12 anesthetized spontaneously breathing cats investigates mutual interactions of mechanically induced cough and sneeze as well as respiratory motor output during these behaviors induced simultaneously or sequentially. Mechanical stimulation of the tracheobronchial mucosa resulted in repetitive coughing while nasal stimulation produced exclusively sneezing. Reflexes were classified (coughs vs. sneezes) based on area of stimulation (tracheobronchial vs. nasal). The amplitude of SG integrated EMG during sneeze expulsion was 1630±320 % of that during cough ($p<0.001$; 10 cats) (Fig.1). This activity became main differentiation criterion for cough and sneeze during combined stimuli (Fig.1). Other differences in parameters of control coughing and sneezing were: weaker sneeze than cough inspiratory effort amplitudes of diaphragm (DIA EMGs) during sneeze were 72±8 % of that during cough; $p<0.01$; peak inspiratory esophageal pressure (EP) EP -0.98±0.15 kPa and -1.44±0.15 kPa, respectively; $p<0.01$) and longer inspiratory cough/sneeze phase (1.35±0.17 s vs. 1.01±0.12 s, $p<0.05$) and the duration of DIA activation (1.60±0.17 s vs. 1.27 ± 0.15 s, $p<0.05$) in sneeze.

Mechanical nasal stimulation that induced no sneeze reflex (and started at least 10 s before cough stimulus) had no effect on parameters of coughing elicited by tracheobronchial stimulation (7 cats). When both reflexes were executed (cough and sneeze; 8 cats) during combined stimuli the responses were classified as either sneeze or cough (no hybrid responses occurred) and they were potentiated comparing to control reflexes (Fig. 1). DIA EMG moving average maxima and peak inspiratory EP (Fig. 2) were increased in sneezes induced during combined trials compared to control sneezing ($p<0.05$). Expiratory maxima of EP (Fig. 2) and amplitudes of abdominal EMG moving average were increased in coughs and sneezes induced during combined trials compared to control coughs and sneezes (both $p<0.05$). In coughs consistent with higher expiratory efforts during dual stimulation also amplitudes of SG EMG activity in the active expiratory cough/sneeze phase reached 150% of that in control

coughs ($p<0.05$). The number of reflexes during combined trials (either coughs or sneezes) was not altered significantly compared to controls ($p>0.05$).

Complex temporal analysis of cough and sneeze revealed no other differences in temporal features of cough and sneeze than longer inspiratory cough/sneeze phase and DIA activation in sneeze (already reported in the 1st paragraph) including those during combined stimuli.

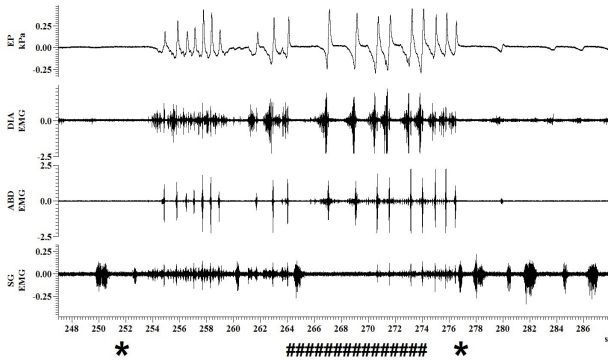

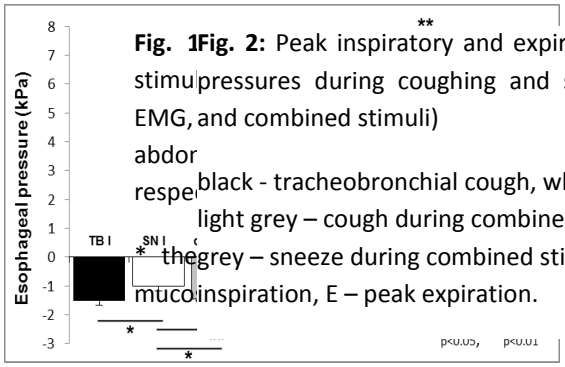

Fig. 1Fig. 2: Peak inspiratory and expiratory esophageal stimu pressures during coughing and sneezing (control EMG, and combined stimuli)
abdor
respe black - tracheobronchial cough, white – sneeze, light grey – cough during combined stimuli, dark the grey – sneeze during combined stimuli, I – peak muco inspiration, E – peak expiration.

The main finding of our study is that in anaesthetized cats the patterns of sneezes and coughs are not disrupted in dual upper/lower airway mechanical stimulation, but rather the strength of the efforts is significantly increased. We conclude that mechanosensitive nasal afferents have limited effect on the tracheobronchial cough response. However, co-expression of coughing and sneezing results in a variety of enhanced cough and sneeze responses supposedly representing improved airway defense and depicting mutual behavioral (not sensory afferents) modulation of reflex behaviors.

Acknowledgements: We gratefully acknowledge Iveta Najslova and Ing. Peter Machac for the excellent technical assistance. This work was supported by the VEGA 1/0126/12. The project is co-financed from EU sources“ – ERDF – European Regional Developmental Fund. „This work was supported by the Slovak Research and Development Agency under the contract No. APVV-0189-11" (prof. Jakus)

References

[1] Ono K, Shen TY, Chun HH, Solomon IC. Upper airway and abdominal motor output during sneezing: is the in vivo decererate rat an adequate model? Adv Exp Med Biol. 2010;669:173-6.
[2] Widdicombe JG.: Neurophysiology of the cough reflex. Eur Respir J. 1995 Jul;8(7):1193-202. Review.
[3] Canning BJ, Mori N, Mazzone SB. Vagal afferent nerves regulating the cough reflex. Respir Physiol Neurobiol. 2006 Jul 28;152(3):223-42.
[4] Cauna N, Hinderer KH, Wentges RT. Sensory receptor organs of the human nasal respiratory mucosa. Am J Anat. 1969 Feb;124(2):187-209.
[5] Wallois, F., Macron, J.M., Jounieaux, V., Duron, B., 1991. Trigeminal afferences implied in the triggering or inhibition of sneezing in cats. Neurosci. Lett. 122(2):145-7.
[6] Korpas and Tomori, 1979. Cough and Other Respiratory Reflexes. Kager, Basel, 356 p.
[7] Satoh, I., Shiba, K., Kobayashi, N., Nakajima, Y., Konno, A., 1998. Upper airway motor outputs during sneezing and coughing in decerebrate cats. Neurosci. Res. Oct;32(2):131-5.
[8] Shannon, R., Bolser, D. C., Lindsey, B. G., 1996. Neural control of coughing and sneezing. In: Miller. A. D., Bianchi, A. L., Bishop, B.P. (Eds.), Neural control of breathing. Boca Raton: CRC Press. 215-224.

Institute of Medical Biophysics, – yesterday and nowadays

M. Šimera, I. Poliaček, N. Višňovcová, M. Veterník, I. Najšlová, P. Macháč, M. Somorová

Institute of Medical Biophysics, Jessenius Faculty of Medicine, Comenius University in Bratislava, Slovakia, Malá hora 4 , 03601 Martin.
e-mail: simera@jfmed.uniba.sk

Institute of Medical Biophysics at Jessenous faculty of Medicine, Comenius University in Martin started its activity in academic year 1966/67 as a common Institute of Physics and Nuclear Medicine with head MUDr. Jozef Holan, CSc. In the academic year 1982/83 the intitute has changed its name to Institute of Medical Biophysics and in 1984 its leadership took over prof. MUDr. Albert Stránsky, CSc. In 2007 until now prof. MUDr. Ján Jakuš, DrSc became a new head of Institute of Medical Biophysics. Research work is focused to Biophysics and Physiology of respiratory system, particularly analysing the mechanisms of neuronal regulation of breathing, protective reflexes of airways and the motion of laryngeal muscles. Electrophysiological laboratory at our institute is currently the only electrophysiological lab in the Slovak Republic which deals with questions concerning the neurophysiology of breathing, coughing and other breathing related reflexes. The institute has a long-lasting scientific co-operation with the Veterinary College, University of Florida, U.S.A., Department of Normal and Pathological Physiology SAV in Bratislava, Department of Medical Biophysics UPJŠ Košice and departments and institutes of medical biophysics in Czech Republic.

Excellent leading and research skills of prof. MUDr. Ján Jakuš, DrSc. resulted in acquisition of several international and domestic grants such as: The study of brainstem area and neuronal essential for coughing, expiration and aspiration reflexes in anaesthetized cats and rabbits. *Project VEGA No.1/2274/05*, The study of brainstem neuronal area and mechanism essential for coughing, expiration and aspiration reflexes in anaesthetized cats and rabbits. Project *VEGA No.1/0038/09* and Study of central mechanisms of vital functions after the brainstem lesions, local administration of antitussives and exposure to HF electromagnetic fields, *Project No. APVV-0189-11.*

His authentic research experiences and results have been summarized in scientific monograph: *Jakuš J., Tomori Z., Stránsky A.: Neuronal Determinants of Breathing, Coughing and Related Motor Behaviours. Wist, Martin, 2004* as well as in several international indexed publications with wide-world scientific acceptance.

To prof. Jakuš`s 60th birthday we would like to say "big thank you" for your enthusiastic work, we wish you a good health and happiness in professional and family life.

The staff of the Institute of Medical Biophysics

Study of protein amyloid aggregation: focus on inhibitors

K. Siposova
Department of Biophysics, Institute of Experimental Physics, Slovak Academy of Sciences, Kosice, Slovakia
e-mail: siposova@saske.sk

The conversion of normally soluble protein into fibrillar aggregates is of central importance for several diseases, including Alzheimer's and Parkinson's diseases or type II diabetes. The common feature of amyloid diseases is presence of amyloid deposits consisting mainly of aggregated poly/peptide typical for given disease. Although polypeptides associated with amyloidosis do not show particular similarity in the structure, size or function, the resulting self-assembled amyloids have similar morphological characteristics. Amyloid fibrils are usually 60–130 Å wide, 1–6 μm long and consist of protofilaments that are twisted around each other in unique compact structure. X-ray diffraction techniques demonstrated that the organized core of fibrils has a "cross-beta" structure in which β-sheets are assembled from beta-strands that run perpendicular to the fibrillar axis [1]. Once formed, amyloid fibrils are very stable and essentially unbreakable under physiological conditions.

Currently, there is no treatment for amyloid-related diseases. However, experimental data suggest that reduction and/or prevention of amyloid aggregates is beneficial [2]. Therefore, the therapeutic approaches for amyloidogenic disorders are either preventing of formation of amyloid fibrils or disrupting of amyloid structures.

In our work we identified the conditions leading to formation of protein amyloid aggregates and studied morphological features of amyloid structures. We have also investigated the interference of protein amyloid aggregation with low-molecular weight compounds (derivatives of acridine, phytoalexin and polyphenol), peptides (tripeptides) and various magnetic fluids (such as Fe_3O_4-based magnetic nanoparticles).

We have studied their ability to destroy amyloid aggregates as well as to inhibit amyloid self- assembly. Particular attention has been paid to structural-functional aspects of "anti-amyloid" active compounds. For example, in case of acridine compounds our data suggest that planarity of the acridine core ring is important but not the sole parameter of the effectiveness of the inhibitory activity of the derivatives of acridine. The linker and the saccharide type are also important (for glyco-acridines).

Intensive study of the effect of magnetic fluids containing magnetite nanoparticles showed that magnetic Fe_3O_4-based magnetic fluids (MF) are able to inhibit formation of amyloid aggregates and have a potential to affect amyloid aggregation. The results demonstrated that magnetic component of magnetic fluids is important for their anti-amyloid activity; however, the physical properties of nanoparticles-coating determine the extent of inhibition/depolymerization activity. Thus, for BSA-modified magnetic fluids (MFBSAs) we have found, that physical–chemical features of studied MFBSAs, such as hydrodynamic diameter, zeta potential and isoelectric point, significantly affected the extent of MFBSA depolymerizing activity.

We concluded that studied compounds can potentially be used as therapeutic agents targeting amyloidosis due to their ability to reduce amount of amyloid aggregates, extent of reduction amyloid aggregates dependent significantly on the structural and physical-chemical properties of studied compounds.

Acknowledgement: This work was supported by the research grant projects 26110230097 in frame of SF EU, VEGA 0181, 0176 and APVV 0171-10, No 2011/01/B/NZ1/01622.

References:

[1] Bucciantini M., Giannoni E., Chiti F., Barni F., Formigli L., Zurdo J., Taddei N., Ramponi G., Dobson C.M., Stefani M. In: Nature, 416 (2002) 507-511
[2] Cohen F. E, Kelly J. W. In: Nature, 426, (2003), p. 905-909

Anti-amyloid activity of indole-based compounds

K. Siposova[1], T. Kozar[1,2], P. Kutschy[3], Z. Kristofikova[4], A. Bartos[4], D. Ripova[4], A. Antosova[1], Z. Bednarikova[1,5], D. Fedunova[1], Z. Gazova[1]

[1]Department of Biophysics, Institute of Experimental Physics, Slovak Academy of Sciences, Kosice, Slovakia
[2]Department of Biophysics, Faculty of Science, Safarik University, Kosice, Slovakia
[3]Department of Organic Chemistry, Faculty of Science, Safarik University, Kosice, Slovakia
[4]Prague Psychiatric Centre, Alzheimer Disease Centre, Prague, Czech Republic
[5]Department of Biochemistry, Faculty of Science, Safarik University, Kosice, Slovakia
e-mail: siposova@saske.sk

More than twenty human proteins can fold abnormally to pathological amyloidal aggregates that are associated with a number of amyloid-related pathological conditions including Alzheimer's disease, type II diabetes, Parkinson- and Creutzfeld–Jacob diseases. The common feature of amyloid diseases is presence of amyloid deposits consisting mainly of aggregated poly/peptide typical for given disease.Insulin belongs to the group of globular proteins that may self-assembly into β-sheet-rich amyloid aggregates. Insulin amyloid deposits have been found in the sites of subcutaneous insulin application in patients with prolonged diabetes treatment by insulin. However, it should be noted, that no evidence of *in vivo* formation of pathogenic fibrillar aggregates by endogenous insulin was presented.

No real cure is currently directed toward the amyloid-related diseases and still remains unclear which step in the cascade of amyloid formation is the most toxic.The current approaches, however, suggest that reduction of the amyloid aggregation by direct inhibition of amyloid fibrillization or clearance of amyloid aggregates are beneficial [1]. Many efforts are expended to screen compounds interfering with amyloid formation as potential drugs to treat amyloid-related disorders.

Our goal was to investigate the interference of insulin amyloid aggregation with low-molecular weight compounds – phytoalexins. Phytoalexins are indole-based compounds naturally occurring in cruciferous vegetables. These secondary metabolites, which are synthesized *de novo* in response to diverse forms of stress, are part of the plant chemical and biochemical defense mechanisms [2].

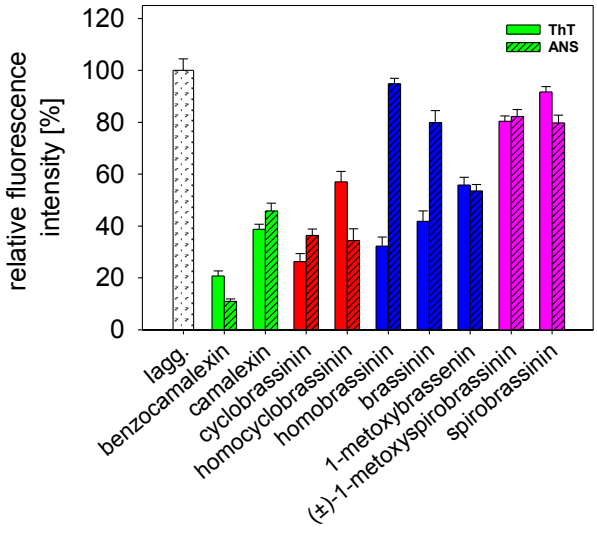

Figure 1 - Inhibition of insulin amyloid aggregation by phytoalexins observed by ThT assay. The fluorescence was normalized to the signal detected for insulin amyloid aggregates alone (Iagg).

Insulin amyloid fibrils were created by incubation of soluble protein at acidic pH and high temperature with additional intensive stirring. Formation of amyloid fibrils was then verified through some specific methods of amyloid detection such as thioflavin T (ThT) and 1-anilinonaphyhalene-8-sulfonic acid (ANS) fluorescence; Congo red absorbance assays, circular dichroism and transmission electron microscopy (TEM).

The effects of nine indole-based phytoalexins on the amyloid fibrillization of insulin were examined through the use of ThT/ANS fluorescence measurements. According to

structural similarities, phytoalexins were divided into four groups – camalexins, cyclobrassinins, brassinins and spirobrassinins. Results indicate that inhibition of insulin amyloid fibrillization strongly depends on the type of phytoalexin derivative (Fig 1).

We were interested to investigate effect of phytoalexins structure in more details; therefore, we studied the kinetics of the fibril formation in presence of phytoalexins derivatives belonging to each structural group. By ThT fluorescence assay the time dependencies of the extent of amyloid aggregation in the presence of phytoalexins derivatives were investigated. Time-dependent measurements indicated that benzocamalexin and cyclobrassinin were able to inhibit insulin amyloid fibrillar species, while the effect of spirobrassinin was comparable to insulin fibril growth in the absence of inhibition by phytoalexins. For the most effective compounds – benzocamalexin and cyclobrassinin the inhibiting ability of these compounds was studied at a concentration range (from 10pM to 1mM) and fixed protein concentration (10μM) by ThT and ANS assays to determine the IC_{50} values. Transmission electron microscopy (TEM) was used to visually the inhibitory effect of the phytoalexins. In addition, molecular modeling tools were used in order to shed light into the possible binding modes of the studied phytoalexins.

We have evaluated also *in vitro* effect of selected phytoalexins in the cerebrospinal fluid of patients with multiple sclerosis and Alzheimer's disease. We have found significant differences in fluorescence (λ excitation = 440 nm, λ emission = 485 nm) of samples among particular groups, namely young controls < multiple sclerosis, Alzheimer's disease < old controls. Differences among groups were observed also in thioflavin-T-based fluorescence, i.e. young controls = multiple sclerosis < Alzheimer's disease < old controls and the most marked change from native to thioflavin-T-based fluorescence was found in young controls. Phytoalexins evoked drops in thioflavin-T-based fluorescence and was more efficient in in multiple sclerosis patients compared to young controls.

It can be concluded that phytoalexins have ability to inhibit amyloid fibrillization of insulin with different efficiency in dependence on the compound properties. The structure-activity relationship analysis suggested that structural and conformational features of compounds under study are of key importance for affecting their anti-amyloid activities. The intensive reduction of amyloid formation in presence of the most effective phytoalexin inhibitors suggests their potential to diminish the problems associated with protein amyloid aggregation.

Acknowledgement: This work was supported by the research grant projects 26110230097 in frame of SF EU, VEGA 0181, 0176 and APVV 0171-10; in the Czech Republic - IGA NT 13183 grant and by MH CZ - DRO (PCP, 00023752) project.

References:

[1] Cohen F. E, Kelly J. W. In: Nature, 426, (2003), p. 905-909
[2] Martins, L. O., Huber, R., Huber, H., Stetter, K. O., Da Costa, M. S. & Santos, H. In: Appl Environ Microbiol 63, (1997), p. 896-902

Mobile Phone and Adolescents - Knowledge and Efficiency of Their Education

Špigúthová D.[1], Jakušová V.[2], Habiňáková H.[1], Jakuš J.[1]

[1] Institute of Medical Biophysics , Jessenius Faculty of Medicine in Martin, Slovakia
[2] Institute of Public Health , Jessenius Faculty of Medicine in Martin, Slovakia

The emphasis on prevention of serious diseases among citizens pointed us to study the effects of electromagnetic (elmg.) radiation on a human body. From a view of health protection, an overproduction of electric smog is caused also by rapid increase in a numberof mobile phones. In 2013 the Slovak Ministry of Transport and Regional Development stated that in our country there were about 6 million active SIM cards and around 2.8 million of mobile internet connections. Health hazards which may result from an increase in the number of users of mobile technologies require education, particularly among young people. Here we present the results of research and education of adolescents studying at one high school in the Turiec area.

The sample consisted of 58 adolescents aged 16-17 studying at the Grammar School of William Pauliny-Toth in Martin in 2012/2013. Out of 58 students, 34 (58.6 %) were women and 24 (41.4 %) men. The aim of the study was to determine the knowledge of students on elmg. radiation from mobile phones and to determine the effectiveness of their education. The level of knowledge was determine by questionnaire of our provenance. Based on our former findings, we developed five educational topics (Electromagnetic fields , How does a cell phone work, Specific Absorption Rate, Effects of electromagnetic radiation, Negative effects of elmg. radiation from mobil phones - preventive recommendations). Education of students lasted three months and was incorporated in accordance with the State educational programs for high schools.

In 58respondents before the education an average percentage of successful responses in students was 40.9 % (23.75 ± 20.91) and after the education was found 94.8 % (55.00 ± 3.02). In women, average percentage of successful responses prior to the education process was 43.4 % (14.75 ± 12.51) and after the education was 96.3 % (32.75 ± 1.49). Before the education in men, we found an average percentage of successful responses 37.5 % (9.00 ± 9.01), whereas after the education it was 92.7 % (22.25 ± 1.98). When calculating the statistical significance of differences before and after the education , the higher level of knowledge was confirmed after the education ($p < 0.001$). As to gender, no higher level of knowledge in women compared to men ($p > 0.05$) was confirmed.

Before the education of high school students we found only a mild level of knowledge on elmg. radiation from mobile phones.Our study proved the high efficiency of our education, since a significant increase of knowledge has been proved after it. We confirmed that mobile phones and mobile Internet connections among the students are popular and used massivelly. Also, our students had a great interest in acquisition of new knowledge in the field of mobile communications .

Acknowledgement
This work was supported " by the Agency for Research and Development under contractNo . APVV- 0189-11 ". (prof. Jakuš)

Anti- and pro-apoptotic Bcl2 proteins distribution and metabolic profile in U87 MG cells before and after HypPDT.

K. Štroffeková[1], L. Balogová[1], M. Maslaňáková[1], P. Miškovský[1,2]

[1] Department of Biophysics, PF UPJS, Jesenná 5, 04001 Košice, Slovakia, email: katarina.stroffekova@upjs.sk.
[2]Center of Interdisciplinary Biosciences, PF UPJS, Jesenná 5, 04001 Košice, Slovakia

Rationale: Apoptosis is an active process of normal cell death in the development and maintenance of tissue. Deregulation of apoptosis can contribute to diverse pathologic processes spanning from cancer to cardiovascular pathologies. A common mechanism causing cell dysfunction and apoptosis is oxidative stress with the generation of radical oxygen species (ROS). The generation of ROS can be triggered by endogenous stimuli such as aging, hypoxia, inflammation, and by artificial stimuli such as chemo- and photodynamic therapy (PDT). Photodynamic therapy (PDT) is based on the concept that the combination of a photosensitizing agent, preferably taken up and retained by tumor cells, with light leads to the formation free radicals (ROS) causing selective damage to the target tissue. ROS can be formed by photosensitization mechanism in the absence (Type I) or in the presence of molecular oxygen (Type II), and the ratio between these two processes depends on the type of photosensitizing agent and the concentrations of substrate and oxygen [1]. Hypericin (Hyp), a naturally occurring photosensitizer, displays antiproliferative and cytotoxic effects in many tumor cell lines [2]. Hyp's photosensitizing properties together with its selective uptake in tumor tissues and its minimal dark cytotoxicity, make it promising for clinical use in PDT [3]. The molecular mechanisms underlying PDT, and specifically Hyp-PDT, are not completely understood, although it has been shown that the sub-cellular Hyp localization and distribution determine which signaling pathway will lead to cell death [2, 4, 5, 6, 7, 8]. Cell responses to HypPDT are highly dependent on the Hyp intracellular localization and accumulation [7, 9, 10, 11]. Thus the initial photodamage can involve different organelles with the consequent activation of specific death pathways, which may be dependent or independent on caspase signaling for their execution. The mechanisms by which PDT triggered ROS cause or regulate apoptosis typically include receptor activation, caspase activation, Bcl-2 family proteins, and mitochondrial dysfunction.

We were particularly interested in Bcl-2 family proteins investigated their role in apoptosis of U87 MG cells triggered by HypPDT. Human malignant glioma cells including U87 MG express proteins of Bcl2 family including Bcl-2, Bcl-$_{XL}$, Bax and Bak [12, 13]. Cells display the specific temporal and spatial patterns of Bcl-2 member expression in a stimulus- and context-specific manner. In the present study, we focused on distribution of two anti-apoptotic Bcl2 and Bcl$_{XL}$ and two pro-apoptotic proteins Bax and Bak in the U87 MG cells. The temporal and spatial expression patterns of Bax and Bak nad their anti-apoptotic partners in the U87 MG cells before and after Hyp-PDT have not been addressed in detail, and because of reported localization of Bax and Bak on the ER and in the nucleus[14, 15], besides their usually assigned cytosol and mitochondria, respectively.

Methods: The molecular mechanisms of signaling pathways at single cell level were assessed by immunocytochemistry and fluorescent confocal microscopy (Zeiss LSM 700, Germany) to monitor the time development in apoptotic signaling pathways. Flow cytometry (MACSQuant Analyzer, Miltenyi Biotec, Germany) was be used to monitor development of apoptosis in intact cells by AnnexinV/PI assay. Further, correlation between temporal development of apoptosis and mitochondrial dysfunction in intact cells [16] was monitored by extracellular flux analyzer (Seahorse XF24, Seahorse Bioscience Co., USA) in combination

with dissipation of mitochondrial membrane potential simultaneously monitored by Rhodamine 123 fluorescence.

Results: We show the distribution of two anti-apoptotic Bcl2 and Bcl_{XL} and two pro-apoptotic proteins Bax and Bak in the U87 MG cells incubated with 500nM Hyp before and after PDT. In control cells, there is a significant co-localization in foci, presumably mitochondria, between Bak and Bcl2 proteins, and significant co-localization between Bax and Bcl_{XL} proteins, suggesting that Bcl2 is a major partner to Bak, and Bcl_{XL} to Bax. 1 hr incubation with Hyp without irradiation resulted in significant changes (decrease in co-localization) in the distribution patterns of anti and pro-apoptotic pairs Bax and Bcl_{XL}, and Bak and Bcl2 proteins. These findings suggest that Hyp may interact with Bcl2 and Bcl_{XL} proteins similarly to Bcl2 inhibitors such as ABT 263 or 787 [17,18]. HypPDT further significantly ($P<0.001$) decreased Bak and Bcl2, and Bax and Bcl_{XL} co-localization, and in the same time we observed significant translocation of Bcl2 into the nuclei. Further we investigated mitochondria function in U87 MG cells in the absence and presence of Hyp, and before and after HypPDT by measurements of metabolic flux rate in intact cells. Presence of Hyp without irradiation resulted in significant ($P<0.04$) decrease in mitochondria function, suggesting that Hyp incorporated into mitochondrial membrane may affect electron transport chain processes. Underlying mechanism is not known and needs further investigation.

Supported by the Slovak Grant Agency VEGA -1-1246-12, by the Slovak Research and Development Agency APVV-0242-11, and by EU 7FP grants (ITMS: 26110230013; PIRG06-GA-2009-256580; CELIM 316310).

References:

[1] Miskovsky, P. (2002) Curr. Drug Targets 3, 55-84.
[2] Kascakova, S., Z. Nadova, A. Mateasik, J. Mikes, V. Huntosova, M. Refregiers, F. Sureau, J.C. Maurizot, P.Miskovsky and D. Jancura (2008) Photochem. Photobiol. 84, 120-127.
[3] Kiesslich, T., B. Krammer and K. Plaetzer (2006) Curr Med Chem 13, 2189-2204.
[4] Agostinis, P., A. Vantieghem, W. Merlevede and P. de Witte (2002) Int. J. Biochem. Cell Biol. 34, 221-241.
[5] Theodossiou, T. A., J. S. Hothersall, P.A. De Witte, A. Pantos and P. Agostinis (2009) Mol. Pharmaceutics 6, 1775-1789.
[6] Vantieghem, A., Y. Xu, Z. Assefa, J. Piette, J.R. Vandenheede, W. Merlevede, P.A.M. de Witte and P. Agostinis (2002) J. Biolog. Chem. 277, 37718-37731.
[7] Buytaert, E., G. Callewaert, N. Hendrickx, L. Scorrano, D. Hartmann, L. Missiaen, J.R. Vandenheede, I. Heirman, J. Grooten and P. Agostinis (2006) FASEB J 20, 756-758.
[8] Krammer, B. and T. Verwanger (2012) Curr. Med. Chem. 19, 793-798.
[9] Kocanova, S., E. Buytaert, J.Y. Matroule, J. Piette, J. Golab, P. de Witte and P. Agostinis (2007) Apoptosis 12, 731-741.
[10] Galanou, M.C., T.A. Theodossiou, D. Tsiourvas, Z. Sideratou and C.M. Paleos (2008) Interactive Transport, Subcellular Relocation and Enhanced Phototoxicity of Hypericin Encapsulated in Guanidinylated Liposomes via Molecular Recognition. Photochem. Photobiol. 84, 1073-1083.
[11] Huntosova, V., Z. Nadova, L. Dzurova, V. Jakusova, F. Sureau and P. Miskovsky (2012) Photochem. Photobiol. Sci. 11, 1428-1436.
[12] Rieger, Bornemann A., Schabet M., Dichgans J., Meyermann R. (1998J. Neurol. Sci. (Amsterdam) **155**(1), 68-75
[13] Wang F., Bhat K., Doucette M., Zhou S., Gu Y., Law B., Liu X., Wong E. T., Kang J. X., Hsieh T.-C., Qian S. Y., Wu E. (2011) Curr. Mol. Med. (Hilversum) **11**(6), 503–511
[14] Annis M. G., Yethon J. A., Leber B., Andrews D. W. (2004) Biochim. Biophys. Acta. (Amsterdam) **1644**, 115–123
[15] Hwang S.-I., Lundgren D. H., Mayya V., Rezaul K., Cowan A. E., Eng J. K., Han D. K. (2006) Mol. Cell Proteomics. (Bethesda) **5**, 1131-1145
[16] Brand M.D. and D.G. Nichols. (2011) Biochem. J. 435, 297–312
[17] Kutuk O. and A. Letai. (2008) *Cancer Res*;68:7985-7994
[18] Vogler M, Hamali H. A., Sun X-M., Bampton E. T. W., Dinsdale D., Snowden R. T., Dyer M. J. S., Goodall A. H. and G. M. Cohen. (2011)BLOOD 117: 7145-7154

Electrodiffusion Kinetics of Ionic Transport in a Simple Model of Membrane Channel

I. Valent

Department of Physical and Theoretical Chemistry, FNS UK, Mlynskádolina CH1, 842 15 Bratislava, Slovakia, e-mail: valent@fns.uniba.sk

Transport of ions plays an important role in many functional mechanisms in biological systems. For example, the identification of potassium and sodium ionic currents in electrical behavior of a nerve fiber was one of the milestones in the development of the field of electrophysiology. Other examples include the signaling role of calcium ions in a variety of biological processes and the essential function of proton transport in the mitochondrial energetics. Transport of ions is usually localized in particular areas of cells, and in many cases it is related to a membrane function. The driving force of such ionic movement is not restricted to the concentration gradient but involves also the electric potential difference. Transport of charged particles driven by gradients of both chemical and electrical (i.e., electrochemical) potentials is termed electrodiffusion. The concept of electrodiffusion based on the Nernst−Planck equations for ionic fluxes coupled to the Poisson equation expressing the relation between the gradient of the electric field and the charge density (hence usually referred to as the NPP or PNP theory) is widely used as a useful theoretical tool for description and modeling of various phenomena and processes in both living and nonliving systems.

Our motivation is a perspective of modeling electrodiffusion dynamics in biological processes. We employed numerical techniques for solving time-dependent full PNP equations in 2D to analyze transient behavior of a simple ion channel subject to a sudden electric potential jump across the membrane (voltage clamp). The ion channel was represented by a rectangle with impermeable uncharged walls filled with water solution of a strong uni-univalent electrolyte. The left and right boundaries of the channel were kept at a constant electrolyte concentration different for each boundary. The left boundary was grounded at zero electric potential the entire time, while the right one was subject to a sudden (at $t = 0$) increase in the potential from zero to a constant value. The following governing equations were solved using the VLUGR2 solver for partial differential equations:

$$\frac{\partial c_1}{\partial t} = D_1\left[\nabla^2 c_1 + \frac{F}{RT}(\nabla c_1 \nabla\varphi + c_1\nabla^2\varphi)\right]$$

$$\frac{\partial c_2}{\partial t} = D_2\left[\nabla^2 c_2 - \frac{F}{RT}(\nabla c_2 \nabla\varphi + c_2\nabla^2\varphi)\right]$$

$$\nabla^2\varphi = -\frac{F}{\varepsilon}(c_1 - c_2)$$

wherec_1 and c_2 are the concentrations of cation and anion, respectively, D_1 and D_2 are the diffusion coefficients, φ represents the electric potential, ε denotes the vacuum permittivity of the medium, R is the universal gas constant, F is the Faraday constant, and T stands for the absolute temperature. In a typical calculation, the parameter values were set to their standard values as follows: $D_1 = 1 \times 10^{-6}$, $D_2 = 5 \times 10^{-7}$ cm^2 s^{-1}, $T = 293$ K, and $\varepsilon_r = 80$. The channel length was usually 10 nm and size of the potential step was normally set to +100 mV.

Standard boundary concentrations for the electrolyte were 50 and 500 mM for the left and right channel end, respectively.

Calculated spatiotemporal profiles of the ion difference concentrations and the electric potential are shown in Figure 1. The results demonstrate that two principal exponential processes can be distinguished in the electrodiffusion kinetics, in agreement with the Planck's theory. The initial fast process corresponds to the Maxwell dielectric relaxation with a typical time constant of 5 ns for the standard conditions. The steady state is approached in a slower exponential process attributed to the nonlinear ionic redistribution with a standard time constant of 160 ns.

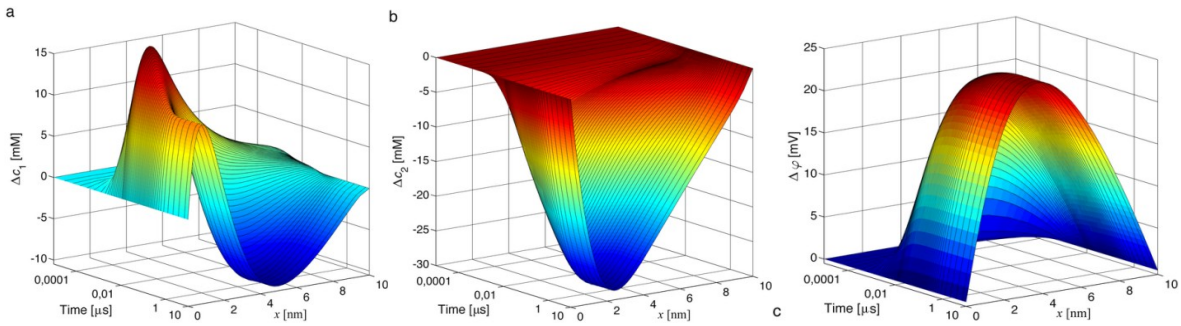

Figure 1. Spatiotemporal profiles of the ionic difference concentrations ((a) for cation, (b) for anion) and the difference electric potential (c). The standard set of parameter values was used in the calculation.

Effects of the model parameters such as the channel length, height of the potential step, boundary concentrations, permittivity of the channel interior, and ionic mobilities on the electrodiffusion kinetics was studied. The obtained results show that neither constant field nor electroneutrality assumption is a sufficiently valid approximation under the constraints reflecting the data known for real membrane channels. Spatiotemporal profiles of the electric field, ionic fluxes, and both the conductive and displacement currents were derived from the obtained solution by means of numerical differentiation. We demonstrate that the displacement current is a significant transient component of the total electric current through the channel. The presented results provide additional data on the classical voltage-clamp problem and offer further physical insight into the mechanism of electrodiffusion. More information can be found in the work [1]. The used numerical approach is applicable to other systems such as synthetic nanopores and nanofluidic devices or nanopipettes. Details on computational methodology were reported in [2].

Acknowledgement
This work was supported by the Slovak Research and Development Agency under the contract No. APVV-0291-11

References
[1] I. Valent, P. Petrovič, P. Neogrády, I. Schreiber, M. Marek, J. Phys. Chem. B 117 (2013) 14283−14293.
[2] I. Valent, P. Neogrády, I. Schreiber, M. Marek, J. Comput. Interdiscip. Sci. 3 (2012) 65−76.

Factors affecting kinetic stability of cytochrome c oxidase

R. Varhač[1], A. Musatov[2], N.C. Robinson[3], E. Sedlák[1,4]

[1] Department of Biochemistry, P.J. Šafárik University, Moyzesova 11, 040 01 Košice, Slovakia.
[2] Department of Biophysics, Institute of Experimental Physics Watsonova 47, 040 01 Košice, Slovakia.
[3] Department of Biochemistry, MSC 7760 The University of Texas Health Science Center at San Antonio 7703 Floyd Curl Drive San Antonio, TX 78229-3900, USA.
[4] Centre for Interdisciplinary Biosciences, P.J. Šafárik University, Jesenná 5, 040 01 Košice, Slovakia.
Slovakia, e-mail: erik.sedlak@upjs.sk

Integral membrane proteins constitute about 30% of all cell proteins, are of fundamental biological importance, and form major targets for drug development. The study of these membrane proteins represents one of the major challenges in contemporary molecular biophysics and structural biology research. Understanding forces that contributes to stability of integral membrane proteins is critical for such processes as purification, crystallization, re-folding and protein engineering of integral membrane proteins. While a considerable amount of literature deals with the structural energetics of water-soluble proteins, relatively little is known about the factors that determine the stability of membrane proteins. Here, we present results of thermal denaturation study of the multisubunit integral membrane protein, cytochrome c oxidase (CcO) isolated from bovine heart. CcO (Complex IV, ferrocytochrome c:O_2 oxidoreductase; EC 1.9.3.1) is the terminal enzyme of the inner mitochondrial electron transport chain that catalyzes electron transfer from reduced cytochrome c to molecular oxygen. The enzyme is composed of 13 nonidentical protein subunits (Fig.1), three of which are products of the mitochondrial genome and ten of which are nuclear encoded. The three mitochondrially encoded subunits (I, II, and III) form the core of the enzyme and contain two heme a moieties and two copper centers as prosthetic groups [1]. The ten nuclear-encoded subunits surround the core and are unique to mitochondrial terminal oxidases. Because the bacterial terminal oxidases function perfectly well without counterparts to the nuclear-encoded subunits, it raises a question regarding the structural and/or functional importance of these subunits.

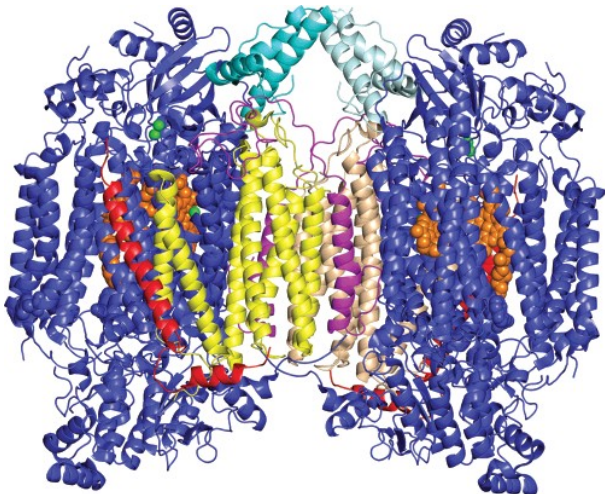

Figure 1. Three-dimensional structure of dimeric CcO illustratingthe location of the four subunits that undergo thermal transition in the first transition: yellow and tan for subunit III, magenta forsubunit VIa, light and dark teal for subunit VIb, red for subunitVIIa, orange for heme a and a3, and green for CuA and CuB. Allother subunits are colored blue.

Taken from Staničová et al., Biochemistry 46 (2007).

We have studied the effect of previously identified factors (tightly-bound phospholipid cardiolipin and detergent sodium cholate) affectingfunctional and oligomeric state of CcO as well as the protein concentration on its thermalstability by means of differential scanning calorimetry (DSC) [2, 3]. So far the analysis of thermal denaturation of CcO has been analyzed mainly in descriptive manner, i.e. the effect of lipid on protein stability has been described by its effect on transition temperature or the thermal denaturation was described as temperature-inducedprecipitation of subunits [reviewed in 4]. DSC thermaldenaturation scan of CcO solubilizedin dodecylmaltoside consists of two distinctive peaks. DSC thermaldenaturation scan of CcO solubilized in dodecylmaltoside consists of two distinctive peaks. DSC thermal denaturation scan of CcO solubilized in dodecylmaltoside consists of two distinctive peaks. The

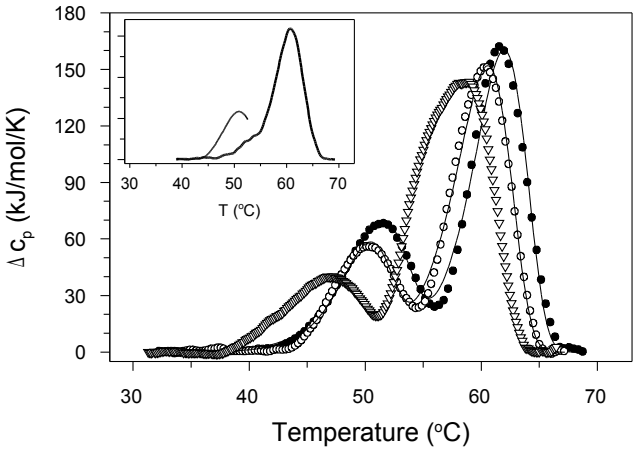

Figure 2. Dependence of DSC scans of nondelipidated CcO on scan rates: 0.5K/min (empty triangle), 1.0K/min (empty circle), 1.5K/min (solid circle). Inset: Rescan of the first transition indicates irreversibility of the transition.

peaks position was highly dependent on scan rate, i.e. the process is under kinetic control and is irreversible (Fig. 2). Therefore, DSC data were analyzed according to the model involving two consecutive irreversible steps as described by Lyubarev and Kurganov [5]. The analysis of thermal transition of intact (nondelipidated) and delipidated CcO led to the following conclusion: (i) kinetic stability of CcO strongly depends on tightly-bound cardiolipin, delipidation destabilizes CcO in terms of so called "shelf-live" (Fig.3), (ii) increasing of protein concentration resulted in protein stabilization, indicating concentration-dependent CcO dimerization, (iii) kinetic stability of dimeric form of CcO is about 2 order of magnitude higher than its monomeric form at physiological temperatures, (iv) CcO activity correlated with the presence of subunits VIIa and III (inset Fig.3),supporting our previous data when CcO structure was perturbed by increased hydrostatic pressure and chemical denaturants [6, 7].

Acknowledgement
This work was supported by the Slovak Grant Agency VEGA, project No. 1/0521/12 and CELIM (316310) funded by 7FP EU (REGPOT).

References

[1] T. Tsukihara, H. Aoyama, E. Yamashita, T. Tomizaki, H. Yamaguchi, K. Shinzawa-Itoh, R. Nakashima, R. Yaono, S. Yoshikawa, Science 272 (1996) 1136–1144.
[2] E. Sedlák, N. C. Robinson, Biochemistry 38 (1999) 14966–14972.
[3] A. Musatov, N. C. Robinson, Biochemistry 41 (2002) 4371-4376.
[4] T. Haltia, E. Freire Biochim. Biophys. Acta 1241 (1995) 295-322.
[5] A. E. Lyubarev, B. I. Kurganov, Biochemistry (Moscow) 63 (1998) 434-440.
[6] J. Staničová, E. Sedlák, A. Musatov, N. C. Robinson, Biochemistry 46 (2007) 7146-7152.
[7] E. Sedlák, N. C. Robinson, Biochemistry 48 (2009) 8143-8150.

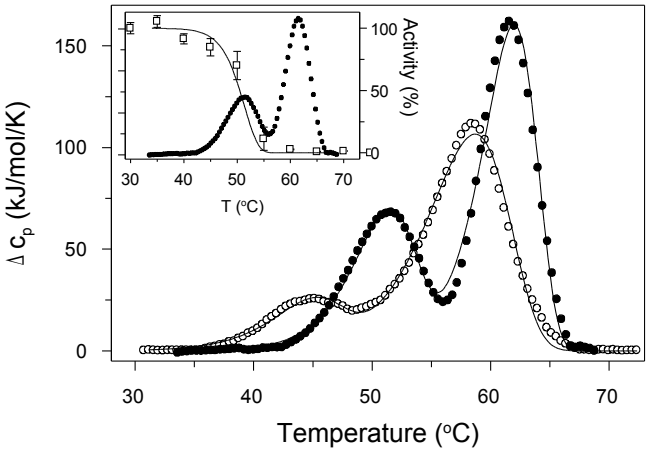

Figure 3. Thermal denaturation of nondelipidated CcO (solid circle) and delipidated CcO (empty circle). Inset: DSC scan of nondelipidated CcO and dependence of CcO activity on temperature. Corresponding fit (solid line) is based on parameters obtained from DSC scan.

Singelt oxygen production by photo-excited RuPhen

J. Varchola[1], V. Huntošová[2], P. Miškovský[1,2], G. Wagnieres[3], G. Bánó[1]

[1]Department of Biophysics, PF UPJS, Jesenná 5, 041 01 Košice, Slovakia.
[2] Centre of Interdisciplinary Biosciences (CIB), PF UPJS, Jesenná 5, 041 01 Košice, Slovakia.
[3]ISIC-LCOM, EPFL, Batiment CH, Station 6, CH-1015 Lausanne, Switzerland.

During the PDT (photodynamic therapy) tumor cells are eliminated via interactions with highly reactive oxygen species (singlet oxygen), which are produced in reactions of photoactivated photosensitizers with triplet oxygen. Monitoring of the tissular oxygenation is essential for PDT optimization. One minimally invasive approach to assess the level of oxygen concentration (pO_2) is based on the measurement of oxygen-sensitive molecule luminescence lifetimes. During our previous work RuPhen has been identified as a very promising compound for pO_2 measurements. Photo-excited RuPhen is known to produce singlet oxygen [1], which can cause unwanted tissue damage when using RuPhen for *in vivo* pO_2 measurements. For non-invasive and non-toxic applications of RuPhen it is essential to know the rate of its singlet oxygen production.

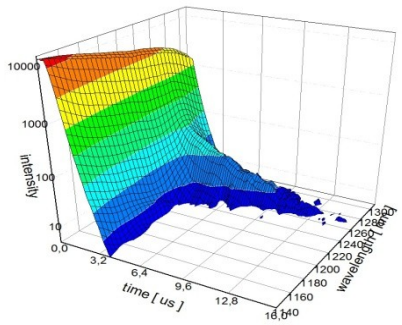

Figure 1. Time resolved spectra showing singlet oxygen emission at 1270 nm combined with a strong phosphorescence background by RuPhen.

In this work we report on singlet oxygen production following pulsed photo-excitation of RuPhen in a cuvette. The phosphorescence of singlet oxygen species at 1270 nm has been measured in a time-resolved experiment. The phosphorescence signal was detected by a NIR PMT working in photon counting mode. Typical emission spectra are shown in Figure 1. The apparatus was calibrated using Rose-Bengal as a reference and the quantum yield of singlet oxygen production by RuPhen was determined at different temperatures.

Acknowledgement
This work was supported by Sciex (Project Code 13.029), by the grants of the Slovak Ministry of Education VEGA 1/1246/12, APVV-0242-11 and by the project CELIM 316310 funded by EU 7FP. This work was also supported by the projects CEVA (26220120040), SEPO-II (26220120039) and NanoBioSens (26220220107) of the Operation Programme Research and Development funded by the European Regional Development Fund.

References
[1] A. A. Abbdel-Shafi, M. D. Ward, R. Schmidt, Dalton Trans. (2007) 2517-2527

Modulation of tonic and phasic activity of respiratory neurons – computer modeling

M. Veterník, M. Šimera, J. Jakuš, I. Poliaček

Institute of Medical Biophysics, Jessenius Faculty of Medicine in Martin, Comenius University in Bratislava, e-mail: veternik@jfmed.uniba.sk

Many research institutes study respiratory system and it´s neural mechanisms. In spite of incereasing amount of knowledge about cellular and subcellular mechanisms, connections within respiratory neural networks included into generation and controlling of breathing, there is still a lack of clarity in these mechanisms. There were described several models of respiratory pattern generator but all of these models contain some importatnt differences. In last years there have been already developed first models of generators of such reflexes as cough, expiratory reflex or swallowing.

The aim of our study was modification of computer model of cough pattern generator and creating of simplified model of breathing. Computer model was created by neuronal developmental environment Newsned and it's graphical user interface. After deep analysis of computer model of respiratory and cough neuronal populations, developed at University of South Florida (Shannon, Lindsey, Morris), we created model of respiratory premotoneurons and motoneurons. Model consisted of 2 populations of motoneurons, one group innervated diaphragm muscle through phrenic nerve and second one innervated expiratory intercostal and abdominal muscles. We added also populations of premotoneurons for modification tonic and phasic activity in output signal. Basic input parameters of neuronal populations were size of population, accommodation, threshold value for resting potential, action potentials firing probability etc. We also modified synaptic connections between populations by changing of number of synaptic terminations and synaptic strength. According to results from simulations we adjusted neuronal parameters in order output waveforms are being consistent with real signals recorded in animal experiments as well as possible.

Our simulations suggest that simplification of USF model is probably opposite way how to reach better and more real output signals but it can be helpful in understanding which neuronal populations are really important for respiration.

Acknowledgement
This work was supported by the Slovak Research and Development Agency under the contract No. APVV-0189-11 and by the Slovak Grant Agency VEGA, project No. 1/0126/12.

Our study of unwanted side effects during radiotherapy treatment

Višňovcová N[1]., Višňovcová N. Jr[2].

[1]*Department of Medical Biophysics, Jessenius Faculty of Medicine in Martin, Comenius University in Bratislava*
[2]*Clinic of Pediatric Surgery, University Hospital Martin*

The aim of our study was to investigate acute post-radiation changes after therapy with ionizing radiation manifested by erythema or dry, squamous and scurfy skin on a breast. We observed 100 female patients suffering from an early stage of breast carcinoma. The entering criteria were: age below 70 years, 100% of the Karnofsky´s Score, no tumor bilaterality, tumor in the stage of T1 or T2. The female patients had finished non-radical surgery consisting from quadrantectomy and deviation of the axilla. Our results showed relationships between the localization and the level of breast skin change as well as between adjuvant chemotherapy and the level of breast skin change and, finally, between the size of the average dose of high energy radiation and the level of breast skin change.

Radiotherapy is, after surgery, the second oldest way of treatment of breast cancer. Historically, radiation therapy (doses and fields) were selected empirically based mainly on experience of empiric guidelines neglecting the underlying anatomy, physiology and dosimetry (1). Over 90% of female patients treated with radiotherapy have suffered in different extent from development of skin reactions, mostly during or shortly after the treatment with ionizing radiation (2). In literature there is not enough information about undesirable effects of ionizing radiation on tissues and organs since they are described more frequently as a part of a treatment schedule (3).

Since there are different responses to ionizing radiation between healthy and malignant tissues the oncologists have endeavoured to classify and explain the core of the pathophysiological mechanism of undesirable post-radiation changes. The work of Stone (1948) was the first to clasify late undesirable side effects on tissues following radiation by fast neutrons. Also Lawrence (1970) decribed scoring criteria for late undesirable side effects caused by fast neutrons. Investigators from the European Organization for Research and Treatment of Cancer (EORTC), headed by William Duncam from Western General Hospital of Edinburgh, created common criteria in anticipation of joint studies. Radiation Therapy Oncology Group (RTOG) protocols were introduced in 1980. Although the RTOG began to use these criteria in reporting toxicity in patients enrolled in all studies from 1981 (beginning with RTOG Protocol 8115), the criteria became a published part of the protocols only in 1983 (4). These criteria were launched into practice in 1995 and are used nowadays for acute and chronic toxic undesirable side effects for all organ systems.

We observed 100 female patients suffering from an early stage of mammary gland carcinoma. The entering criteria were: age below 70 years, 100% of the Karnofsky´s Score, no tumor bilaterality, tumor in the stage of T1 or T2. The female patients had finished non-radical surgery consisting from quadrantectomy and deviation (excentration) of the axilla (at 1$^{st.}$ and 2nd level). In the patients of our experimental group adjuvant chemotherapy and then curative radiotherapy were applied. In the patients there were three phototypes of skin (Tab.No3) which were classified and consulted with the dermatologist. Median of observation of the patients was 5 weeks.

Radiotherapy was applied to all patients by means of high-energy linear accelerator (CONCOR f. Siemens), the high-energy of X-rays was 6 MeV and 18 MeV in an average total dose (TD) of 43.44 ± 1,07 Gy . High-energy electrons were accelerated to 6 and 9 MeV. TD of 11.6 ± 0.33 Gy was applied as " boots". The patients were irradiated by 2 tangential technic fields on the breast area. In our group the patients underwent radiotherapy along with conventional fractionation schedule: 2.0 Gy daily, 5 times in week, 25 fractions within 33 days. The "boots" was applied in all patients (Fig. 1).

Chemotherapeutic treatment started after the surgery and fluorouracil/doxorubicin/ cyclofosfamide (FAC) and fluorouracil/epirubicin/cyclofosfamide (FEC) chemotherapeutic schedule was used within the length of 2 – 4 cycles.

Conclusion :

On the basis of our results we proposed standards for skin care during and after radiotherapy. However , there is still no appropriate skin care standard in clinical practice .We hope that our results will help to make a progress in skin care before, during and after radiotherapy in clinical practice.

Statement:

All procedures were performed in accordance with the laws, rules, and regulations of Slovakian Goverment and EC. the Ethical Committee of JFMED in Martin had approved the protocols. Conflict of interests: None declared.

Acknowledgement: "This work was supported by the Slovak Research and Development Agency under the contract No. APVV-0189-11" (prof. Jakus)

References :

[1] Lawrence, B., Marks, MD., Ellen, D., Jackons, A.: Use normal tissue complication probability modles in clinic. In: Radiation Oncology Biology Physic, 2010, 76, (3)10-19.
[2] D'haese S et al.: Management of skin reactions during radiotherapy in Flanders (Belgium): A study of nursing practice before and after the introduction of a skin care protocol. Eur J Oncol Nurs, 2009. doi: 10.1016/j.ejon.2009.10.006
[3] Hopewell JW.: The skin, its structure and response to ionizing radiation. In: Radiation Oncology Biology, Physic 1990 Apr, 57(4), 751-73.
[4] Hoeller U, Tribius S, Kuhlmey A, Grader K, Fehlauer F, Alberti W.: Increasing the rate of late toxicity by changing the score ? A comparison of RTOG/EORTC toxicity by changing the score ? A comparison of RTOG/EORTC and LENT/SOMA scores. In: Radiation Oncology Biology Physic, 2003, 55, 1013-8.
[5] Steel G.: Basic clinical radiobiology, 3rd edition. Arnold, London 2002, 192-204.
[6] Back, M., Guerrieri, M., et al.: Impact of Radiation Therapy on Acute Toxicity in Breast Conservation Therapy for early Breast cancer. In: Clinic Oncology, 2004, 16, 12-6.
[7] Emami, B., Lyman, J., Brown, A., et al.: Tolerance of normal tissue to therapeutic irradiation. In: Radiation Oncology Biology Physic, 1991, (21), 109-122.
[8] Malkinson, FD., Keane, JT.: Radiobiology of the skin: review of some effects on epidermis and hair. In: Invest Dermatology, 2001, 77(1), 133-8.
[9] Weissberg, MT., Dahmke, L., Schem, C., et al.: In vitro effects of imatinib mesylate on radiosenzitivity and chemosenzitivity of breast cancer cells. In: BMC Cancer, 2010, 9(10), 412-14.

Femtosecond laser use in ophthalmology

P. Žiak[1, 2], K. Lucká[2]

[1] Očná klinika JLF UK v Martine a UN Martin, Slovakia
[2]UVEA Mediklinik, Zelená 10888/1A, Martin- Priekopa, Slovakia, e-mail:lucka.katarina1@gmail.com, lucka@uvea.sk

The eye diseases surgical treatment and refractive defects correction have recently come across the new types of lasers with main characteristic in very short duration laser pulse. They're called femtosecond lasers and represent a significant technological advance in ophthalmology. Safety, accuracy and thrift of surgical interventions assisted by femtosecond laser thus reached a whole new level.

The laser is able to create perfect, extremely accurate and thin cuts in the eye tissues in three dimensions. It is a type of solid-state laser emitting infrared radiation with a 1053 nm wavelength and 100-500 fs length of pulse. It works with high-power short pulses and therefore relatively low energy. Laser works on the principle of fotodisruption, where free electrons transmit their energy to the tissue resulting in emergence of cavitation bubbles. Millions of bubbles form a cut in the tissue as a very thin scalpelm [1].

The ophthalmic femtosecond lasers are mainly used for refractive surgery. Our lecture is an overview of femtosecond lasers applications and also the first clinical experience with femtosecond laser Victus, which is the only one combining functions for cataract surgery, refractive surgery and corneal surgery (keratoplasty, corneal implants).

Laser is used mainly for cataract surgery with an artificial intraocular lens insertion (FEMTO CATARACT). Cataract surgery consists of three laser procedures. First laser creates a regular circular incision in the anterior lens capsule (kapsulorhexa) and splits the lens core clouding (fragmentation). Then the laser replaces scalpel and creates operating incisions in the cornea [1].

The same procedure can also be used in clear and artificial lens exchange in order to achieve the refractive defect correction (CLE, PRELEX).

In terms of refractive surgery, this type of laser is also used to create thin corneal flap in LASIK surgical procedures.

In the lecture, we also present our initial experience with surgical method INTRACOR, femtosecond laser assisted method for correcting presbyopia. Intracor is a new type of intrastromal procedure using mechanism of bulging the center of cornea to correct presbyopia, usually done at non-dominant eye.

Indicating criteria for Intracor are:

- +0.5 to +1.0 D subj . refraction of 0.5 and less Dcyl Max +1.25 Dsph
- pachymetry of 500μm
- Addition of +1.5 Ds and more
- Corneal astigmatism max 2Dcyl
- keratometry min max 39D 48D
- The angle kappa below 10 st.
- Acceptance of a possible drop from a distance

The analysis focuses on eight patients, of which 6 men and 2 women aged 47-58 years diagnosed with hypermetropia leavis, presbyopia.

Patients uncorrected non-dominant eye vision was only 20% of the physiological norm. Procedure is actually painless and well tolerated by patients. It takes less than 90 seconds even with the patient to laser optics fixation. Vision improvement is already noticeable after 2 hours - very quick rehabilitation. Impact on BCVA for distance is minimal and may also improve.

- 7 patients - satisfied (rating objectively - by visus: from 0.1 and 0.2 to 1.0 (J1)
- 1 patient - non respondent, near vision impairment (observing)

The effect is sufficient for daily activities in photopic conditions, at night however, there is a presence of interfering phenomena (circles). The advantage is that the method is suitable for the pseudophakic patient. Intracor represents an absolute novelty and hope in refractive errors removal for the future. With correct patients selection excellent functional results and high patient satisfaction can be achieved while one waits.

Because of laser accuracy and precision, femtosecond lasers have also penetrated into lens surgery so far in an experimental stage. Softening the hardened lens nucleus by millions of tiny laser interventions. The operational method is called LENTOTOMY. The procedure should improve near vision as with surgical method Intracor, where the surgery is performed on the cornea, while the lentotomy is performed on the lens.

References

[1] B. Tullo, Femtosecond Laser Technology in Modern Eye Care

Zoznam účastníkov

RNDr. Andrea Antošová, PhD.
Ústav Experimentálnej fyziky SAV
Watsonova 47
040 01 Košice
e-mail: antosova@saske.sk

Ing. Jaroslava Bágeľová, CSc.
Ústav Experimentálnej fyziky SAV
Watsonova 47
040 01 Košice
e-mail: bagelova@saske.sk

Mgr. Gregor Bánó, PhD.
Katedra biofyziky PF UPJŠ
Jesenná 5
040 01 Košice
e-mail: gregor.bano@upjs.sk

Mgr. Zuzana Bednáriková
Oddelenie Biofyziky
Ústav Experimentálnej fyziky SAV
Bulharská 6
040 01 Košice
e-mail: bednarikova@saske.sk

RNDr. Dominik Belej
Katedra Biofyziky PF UPJŠ
Jesenná 5
040 01 Košice
e-mail: belej.dominik@gmail.com

Mgr. Ľudmila Blaščáková
Katedra Biofyziky PF UPJŠ
Jesenná 5
040 01 Košice
e-mail: ludmilablascakova@gmail.com

Mgr. Ľubomír Borko
Ústav molekulárnej biológie SAV
Dúbravská cesta 21
845 51 Bratislava
e-mail: lubomir.borko@savba.sk

Boris Dobroľubov
Ústav lekárskej biofyziky
Jesseniova lekárska fakulta UK
Malá Hora 4
036 01 Martin
e-mail: borissvk@gmail.com

RNDr. Marian Fabian, CSc.
Centrum Interdisciplinárnych biovied PF UPJŠ
Jesenná 5
041 54 Košice
e-mail: fabian@rice.edu

RNDr. Diana Fedunová, PhD.
Ústav Experimentálnej fyziky SAV
Watsonova 47
040 01 Košice
e-mail: fedunova@saske.sk

Mgr. Zuzana Garaiová, PhD.
Katedra jadrovej fyziky a biofyziky
FMFI UK
Mlynská dolina F1
842 48 Bratislava
e-mail: garaiova.zuzana7@gmail.com

RNDr. Zuzana Gažová, PhD.
Ústav Experimentálnej Fyziky SAV
Watsonova 47
040 01 Košice
e-mail: gazova@saske.sk

Mgr. Marián Grman
Katedra jadrovej fyziky a biofyziky
FMFI UK
Mlynská dolina F1
842 48 Bratislava
e-mail: grman.marian@gmail.com

Mgr. Hana Habiňáková
Ústav lekárskej biofyziky
Jesseniova lekárska fakulta UK
Malá Hora 4
036 01 Martin
e-mail: hhabinakova@gmail.com

Prof. RNDr. Tibor Hianik, DrSc.
Katedra jadrovej fyziky a biofyziky
FMFI UK
Mlynská dolina F1
842 48 Bratislava
e-mail: tibor.hianik@fmph.uniba.sk

Mgr. Júlia Horilová
Katedra biofyziky PF UPJŠ
Šrobárova 2
041 54 Košice
e-mail: j.horilova@gmail.com

Doc. RNDr. Denis Horváth, PhD.
Centrum Interdisciplinárnych biovied UPJŠ
Jesenná 5
041 54 Košice
e-mail: denis.horvath@upjs.sk

Ing. Matej Hoťka
Ústav molekulárnej fyziológie a genetiky SAV
Vlárska 5
833 34 Bratislava
e-mail: matej.hotka@savba.sk

RNDr. Veronika Huntošová, PhD.
Centrum interdisciplinárnych biovied PF UPJŠ
Jesenná 5
040 01 Košice
e-mail: veronika.huntosova@upjs.sk

RNDr. Dušan Chorvát, PhD.
Medzinárodné laserové centrum
Ilkovičova 3
841 04 Bratislava
e-mail: chorvat@ilc.sk

Prof. MUDr. Ján Jakuš, DrSc.
Ústav lekárskej biofyziky
Jesseniova lekárska fakulta UK
Malá Hora 4
036 01 Martin
e-mail: jakus@jfmed.uniba.sk

Doc. Mgr. Daniel Jancura, PhD.
Katedra biofyziky PF UPJŠ
Jesenná 5
041 54 Košice
e-mail: daniel.jancura@upjs.sk

RNDr. Zuzana Jurašeková, PhD.
Katedra biofyziky, ÚFV PF UPJŠ
Jesenná 5
041 54 Košice
e-mail: zuzana.jurasekova@upjs.sk

Mgr. Mária Klacsová, PhD.
Katedra fyzikálnej chémie liečiv
Farmaceutická fakulta UK
Odbojárov 10
832 32 Bratislava
e-mail: klacsova@fpharm.uniba.sk

Doc. RNDr. Martin Kopáni, PhD.
Ústav lekárskej fyziky, biofyziky, informatiky a telemedicíny, Lekárska fakulta UK
Sasinkova 2
813 72 Bratislava
e-mail: martin.kopani@fmed.uniba.sk

doc. RNDr. Katarína Kozlíková, CSc.
Ústav lekárskej fyziky, biofyziky, informatiky a telemedicíny, Lekárska fakulta UK
Sasinkova 2
813 72 Bratislava
e-mail: katarina.kozlikova@fmed.uniba.sk

RNDr. Tibor Kožár, CSc.
Katedra Biofyziky PF UPJŠ
Jesenná 5
040 01 Košice
e-mail: tibor.kozar@upjs.sk

RNDr. Mária Maslaňáková
Katedra Biofyziky PF UPJŠ
Jesenná 5
040 01 Košice
e-mail: maria_maslanakova@yahoo.com

Mgr. Sopio Melikishvili
Katedra jadrovej fyziky a biofyziky
FMFI UK
Mlynska dolina F1
842 48 Bratislava
e-mail: s.melikishvili@gmail.com

Prof. RNDr. Pavol Miškovský, DrSc.
Katedra Biofyziky PF UPJŠ
Jesenná 5
040 01 Košice
e-mail: pavol.miskovsky@upjs.sk

Mgr. Matúš Mišuth
Katedra Biofyziky PF UPJŠ
Jesenná 5
040 01 Košice
e-mail: matus.misuth@gmail.com

MUDr. Andrey Musatov, CSc.
Ústav Experimentálnej fyziky SAV
Watsonova 47
040 01 Košice
e-mail: musatov@saske.sk

RNDr. Zuzana Naďová, PhD.
Katedra biofyziky PF UPJŠ
Jesenná 5
040 01 Košice
e-mail: zuzana.nadova@upjs.sk

RNDr. Karol Ondriaš, DrSc.
Ústav molekulárnej fyziológie a genetiky SAV
Vlárska 5
833 34 Bratislava
e-mail: Karol.Ondrias@savba.sk

Doc. RNDr. Ivan Poliaček, PhD.
Ústav lekárskej biofyziky
Jesseniova lekárska fakulta UK
Malá Hora 4
036 01 Martin
e-mail: poliacek@jfmed.uniba.sk

Doc. RNDr. Erik Sedlák, PhD.
Centrum interdisciplinárnych biovied PF UPJŠ
Jesenná 5
040 01 Košice
e-mail: erik.sedlak@upjs.sk

Doc. RNDr. Jana Staničová PhD.
Ústav biofyziky
Univerzita veterinárskeho lekárstva a farmácie
Komenského 73
040 81 Košice
e-mail: jana.stanicova@uvlf.sk

RNDr. Michal Šimera, PhD.
Ústav lekárskej biofyziky
Jesseniova lekárska fakulta UK
Malá Hora 4
036 01 Martin
e-mail: Michal.Simera@jfmed.uniba.sk

RNDr. Katarína Šipošová, PhD.
Ústav Experimentálnej Fyziky SAV
Watsonova 47
040 01 Košice
e-mail: siposova@saske.sk

RNDr. Daniela Špigúthová
Ústav lekárskej biofyziky
Jesseniova lekárska fakulta UK
Malá Hora 4
036 01 Martin
e-mail: danielaspiguthova@gmail.com

RNDr. Katarína Štroffeková, CSc.
Katedra Biofyziky PF UPJŠ
Jesenná 5
040 01 Košice
e-mail: Katarina.stroffekova@upjs.sk

Doc. MUDr. Ingrid Tonhajzerová, PhD.
Ústav fyziológie
Jesseniova lekárska fakulta UK
Malá Hora 4
036 01 Martin
e-mail: tonhajzerova@jfmed.uniba.sk

PhDr. Michal Trnka, PhD.
Ústav lekárskej fyziky, biofyziky, informatiky
a telemedicíny, Lekárska fakulta UK
Sasinkova 2
813 72 Bratislava
e-mail: michal.trnka@fmed.uniba.sk

Doc. RNDr. Ivan Valent, CSc.
Katedra fyzikálnej a teoretickej chémie
Prírodovedecká fakulta UK
Mlynská dolina CH1-327
842 15 Bratislava
e-mail: valent@fns.uniba.sk

Ing. Marcel Veterník
Ústav lekárskej biofyziky
Jesseniova lekárska fakulta UK
Malá Hora 4
036 01 Martin
e-mail: marcelveternik@gmail.com

Mgr. Nadežda Višňovcová, PhD.
Ústav lekárskej biofyziky
Jesseniova lekárska fakulta UK
Malá Hora 4
036 01 Martin
e-mail: nvisnovcova@jfmed.uniba.sk

RNDr. Ivan Zahradník, CSc.
Ústav molekulárnej fyziológie a genetiky SAV
Vlárska 5
833 34 Bratislava
e-mail: Ivan.Zahradnik@savba.sk

Ing. Alexandra Zahradníková, DrSc.
Ústav molekulárnej fyziológie a genetiky SAV
Vlárska 5
833 34 Bratislava
e-mail: alexandra.zahradnikova@savba.sk

Organizátori VI. Slovenského biofyzikálneho sympózia ďakujú sponzorom:

Jesseniova lekárska fakulta UK v Martine

„Podpora rozvoja ľudských zdrojov s využitím najmodernejších postupov a foriem vzdelávania na JLF UK “

Európska únia
Európsky sociálny fond

Agentúra Ministerstva školstva, vedy, výskumu a športu SR pre štrukturálne fondy EÚ

Operačný program VZDELÁVANIE

Projekt je spolufinancovaný zo zdrojov EU

GRÄPER Europe

Schneider Electric

PEUGEOT

ZOLS s.r.o.